DIFFUSION OF CYCLIC VERSUS LINEAR POLY(OXYETHYLENE) OLIGOMERS IN POLY(METHYL METHACRYLATE) BY ATR - FTIR SPECTROSCOPY

A Dissertation
Presented to
The Academic Faculty

By

MIHAELA PENESCU

In Partial Fulfillment
of the Requirements for the Degree
Doctor of Philosophy in the
School of Chemistry and Biochemistry

Georgia Institute of Technology
August 2009

DIFFUSION OF CYCLIC VERSUS LINEAR POLY(OXYETHYLENE) OLIGOMERS IN POLY(METHYL METHACRYLATE) BY ATR - FTIR SPECTROSCOPY

Approved by:

Dr. Haskell Beckham, Chair
School of Polymer, Textile and Fiber Engineering
Georgia Institute of Technology

Dr. David Bucknall, Co-advisor
School of Polymer, Textile and Fiber Engineering
Georgia Institute of Technology

Dr. Lawrence Bottomley
School of Chemistry and Biochemistry
Georgia Institute of Technology

Dr. Andrew Lyon
School of Chemistry and Biochemistry
Georgia Institute of Technology

Dr. Jiri Janata
School of Chemistry and Biochemistry
Georgia Institute of Technology

Dr. Mohan Srinivasarao
School of Polymer, Textile and Fiber Engineering
Georgia Institute of Technology

Date Approved: May 4, 2009

ACKNOWLEDGEMENTS

I wish to thank my research advisor, Dr. Beckham, for accepting me into his research group, for constantly supporting and directing me, and for his amazing understanding of research which helped me to become a more detailed scientist.

I am deeply indebted to Dr. Bucknall for all his explanations and advices, for all his time dedicated to help me, and for his moral support.

All my committee members, Dr. Bottomley, Dr. Janata, Dr. Lyon and Dr. Srinivasarao, for their guidance into my research, their patience with me, and above all for giving me the opportunity to be part of this great school.

To my colleagues for the inputs into my research and comments in group meetings. To Melissa Wilson and Ryan Kincer for their hard work in helping me with experiments.

My first chemistry professor, Dr. Istrate, from the seventh grade of my middle school in Romania, School number 4, Pucioasa, for offering me valuable knowledge and providing us an interesting research environment.

All my professors from my mother country, Romania, for directing me into the life of chemistry, for their hard work and efforts in making a very valuable school even the times were tough and the resources were limited.

To the companies, Ball Corporation, Consolidated Container Company and The Coca-Cola Company, that I have worked for all these years, during my residency at Georgia Tech, for supporting me through school and accepting me as a part of the "family".

My parents for their affection and love, their support and guidance throughout my studies over the years. I am sorry that they can not be with me, but they need to know that without them a part of my heart is missing. I'll remember all the time my father words "You never must stop to learn as much as you can." I hope they can hear me…

My husband, Horatiu, for loving me, supporting and understanding, and my beautiful boys, Flavius and Octavian, for being a part of my life. None of these would have been possible without my family.

TABLE OF CONTENTS

LIST OF TABLES

Page

LIST OF FIGURES

Page

LIST OF ABBREVIATIONS

ATR - FTIR	Attenuated total reflectance - Fourier transform infrared spectroscopy
DSC	Differential scanning calorimetry
MW	Molecular weight
PMMA	Poly(methyl methacrylate)
POE	Poly(oxyethylene)
PEO	Poly(ethylene oxide)
PEG	Poly(ethylene glycol)
lPOE	Linear poly(oxyethylene)
cPOE	Cyclic poly(oxyethylene)
lPOE500	Linear poly(oxyethylene) with MW = 500 g/mol
cPOE400	Cyclic poly(oxyethylene) with MW = 400 g/mol
cPOE1000	Cyclic poly(oxyethylene) with MW = 1000 g/mol
PMMA120K	Poly(methyl methacrylate) with MW = 120 kg/mol

LIST OF SYMBOLS

M_e Entanglement molecular weight (g/mol)

M_c Critical entanglement molecular weight (g/mol)

χ Flory-Huggins interaction parameter

D Diffusion coefficient (cm^2/s)

D_s Self-diffusion coefficient (cm^2/s)

D_m Mutual (cooperative) diffusion coefficient or interdiffusion coefficient (cm^2/s)

Λ Onsager coefficient

ϕ Volume fraction

N Degree of polymerization

T_g Glass transition temperature (^oC)

n Diffusional exponent

D_e Deborah number

t Time (sec)

v_i Initial velocity (cm/s)

K_{II} Interface velocity (cm/s)

d Thickness of polymer matrix (μm)

z Interface penetration distance (cm)

d_p Depth of penetration (μm)

θ_i Incident angle (^{o})

θ_t Refracted angle (^{o})

θ_c Critical angle (^{o})

N_R Number of reflections

L Crystal length (mm)

l Crystal thickness (mm)

n_1 ATR crystal refractive index

n_2 Sample refractive index

E Electrical field amplitude at penetration depth

E_0 Initial electrical field amplitude at the interface between ATR crystal and polymer

τ Phase factor of transmitted wave

ω Angular frequency (s^{-1})

λ Wavelength (μm)

A Absorbance

I Intensity of transmitted IR light within penetration depth

I_0 Initial intensity of incident light

$c^{'}$ Normalized concentration

ε Extinction coefficient (μm^{-1})

v_c Speed of light (cm/s)

g Number of arms of a star polymer

SUMMARY

Understanding, predicting and controlling diffusion of small or large molecules in polymers still remains a challenging topic for research. Many factors influence this transport behavior of polymers, such as chemical composition, molecular weight, temperature or topology, by which the latter is one of the least understood factors of the diffusion process. The objectives of the research described in this dissertation include an examination of the effects of topology on diffusion of oligomers into a polymeric matrix, in particular the influence of cyclic versus linear topology.

Diffusion of linear and cyclic poly(oxyethylene) (POE) in poly(methyl methacrylate) (PMMA) was investigated in situ using attenuated total reflectance (ATR) infrared (IR) spectroscopy technique at 60 ^{o}C, 85 ^{o}C and 110 ^{o}C. A film of PMMA was solution-cast onto an ATR zinc selenide crystal and POE was added to the surface. The IR peak at 1109 cm^{-1}, characteristic to the ether bond in POE, was used for quantitative analysis. Deconvolution of these peaks from IR spectra along with an absorbance – concentration calibration curve allowed us to determine the normalized concentration of diffusing components as a function of interdiffusion time. Data were fit using appropriate mathematical models from which penetrant velocity and interdiffusion coefficient were extracted and used in diffusion evaluation. An Arrhenius temperature dependence was found for the interdiffusion between linear POE oligomers and PMMA at temperatures below and above the glass transition temperature of the matrix. In addition, gravimetric studies were performed at 60 ^{o}C and 85 ^{o}C from which interface

velocity was computed. The results obtained using ATR-IR spectroscopy and gravimetry were found to be in reasonable agreement. At 60 ^{o}C, the linear POE 500 g/mol moves into PMMA 120kg/mol with an interface velocity of 9.27 ± 0.19 x 10^{-7} cm/s obtained from ATR - FTIR spectroscopy data and 10.83 ± 3.51 x 10^{-7} cm/s from gravimetric studies.

The results indicated that for same molecular weight, cyclic POE moves 1.8 times faster than linear one. A penetrant velocity of 6.43 ± 1.29 x 10^{-6} cm/s and a mutual diffusion coefficient 5.11 ± 1.02 x 10^{-11} cm^2/s were determined for diffusion of cyclic POE 400 g/mol into PMMA120 kg/mol at 110 ^{o}C. In case of linear POE 500 g/mol, a penetrant velocity of 3.67 ± 0.73 x 10^{-6} cm/s and a mutual diffusion coefficient 2.86 ± 0.54 x 10^{-11} cm^2/s were resolved at the same temperature of study.

For the same molecular weight, the data fit Klein's theory, by which the cyclic polymers diffuse into a linear matrix with an interdiffusion coefficient which is two times bigger than that specific to the linear ones.[1] The cyclic polymers act as linear chains with an effective chain length half of the size of the linear one and move into the matrix by following the same dynamics as linear analogous species.

1. Klein, J., Dynamics of entangled linear, branched, and cyclic polymers. *Macromolecules* **1986,** *19*, (1), 105-118.

CHAPTER 1

INTRODUCTION

1.1 MOTIVATION AND OBJECTIVES

Understanding the diffusion of short chain molecules into polymers could provide guidance for a variety of applications, such as designing materials for plastic packaging or drug delivery systems. In general, the majority of the materials used in injection or extrusion blow molding are polymer blends made from a matrix polymer and oligomeric additives such as antistats, processing aids, colorants or plasticizers. For example, plastics have a tendency for dust adhesion due static electricity build-up and so antistat agents are used. As these sometimes diffuse too rapidly to the matrix surface, understanding how molecular shape or topology affect diffusion might be useful for controlling it.

Diffusion of small molecules into polymers is a function of penetrant and matrix. The molecular size, topology and physical state of the penetrant, morphology of the polymer matrix, as well as the compatibility between the two species are only a few factors that are influencing this process, from which the topology is one of the least undefined. A penetrant velocity or matrix relaxation, as well as an interdiffusion coefficient are quantitative measures of that can be extracted from diffusion measurements. These can be determined by applying suitable mathematical models.

The diffusion mechanisms of linear polymer chains into linear entangled polymer melts have been clarified, but the diffusion processes of non-linear polymers are not so

clear. It is well known that the molecular shape of species with the same chemical constitution plays a very critical role in the determination of physical properties.

Different studies have indicated that the properties of star polymers can differ remarkably from those of linear polymers of similar chemical composition and molecular weight. Hence, the research done on star or branched polymers versus linear chains[1] showed that their motion decreases by increasing the number of arms, making them diffuse much slower than the linear species for the same molecular weight.[2]

The limited studies found in literature on interdiffusion of entangled cyclic into linear entangled polymer matrices indicated that rings move faster than linear polymers for the same molecular weight.[3-5] Klein proposed a theoretical model for diffusion of low entangled cyclic polymers into linear matrices, by which the cyclic species move two times faster than linear analogous polymers with identical molecular weight.[4]

Experimental diffusion studies of low molecular weight cyclic oligomers into linear entangled polymers have not been found in literature.

The main goal of this research was to study the diffusion of cyclic and linear poly(oxyethylene) POE oligomers into poly(methyl methacrylate) PMMA and evaluate the influence of penetrant topology (see Figure 1.1). Attenuated total reflectance Fourier transform IR spectroscopy was employed for this purpose. The experimental results have been used to determine how fast the penetrant moves into the matrix.

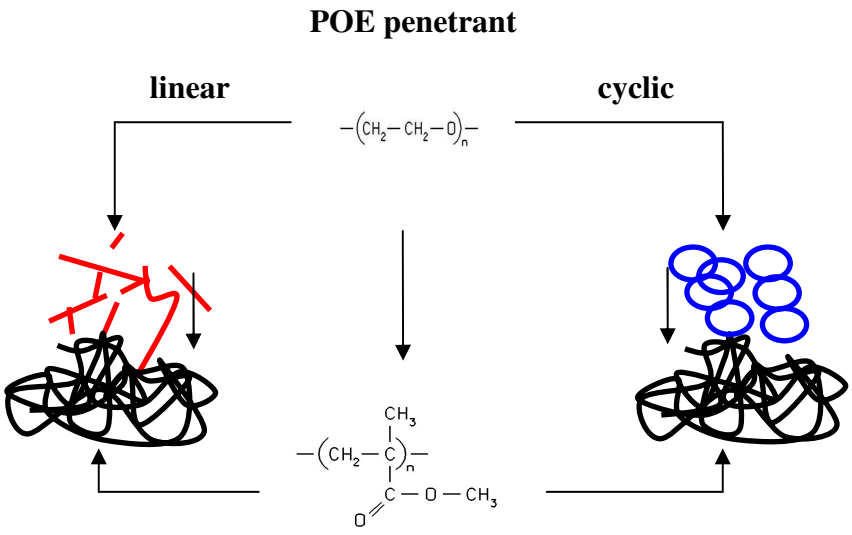

Figure 1.1 - General illustration of poly(oxyethylene) and poly(methyl methacrylate) interdiffusion studied in my research. The penetrant specie is linear or cyclic poly(oxyethylene) POE and the matrix is poly(methyl methacrylate) PMMA.

Evaluation of the diffusion data is facilitated identification by identification of an appropriate mathematical model. *Case I* or *Fickian* diffusion occurs when the rate of diffusion is much lower versus the relaxation rate of polymeric matrix, whereas *Case II* diffusion occurs when the diffusion is very rapid compared to polymer relaxation. Both mathematical models represent highly idealized cases of diffusion, but others also exist, such as anomalous or super-anomalous cases which occur when the diffusion and relaxation rates are comparable or if the penetrant acts as a plasticizer for a polymeric matrix. For the diffusion of POE into PMMA, data were interpreted by a combination of *Fickian* and *Case II* diffusion models, from which the interdiffusion constants were determined.

The results indicated that cyclic POEs move 1.8 times faster than linear POEs of the same molecular weight. An Arrhenius temperature dependence was identified for diffusion of linear POE into PMMA.

To summarize, the main objectives of this research are:

(a) Experimental studies of diffusion at 60 ^{o}C, 85 ^{o}C and 110 ^{o}C of linear POE oligomers into PMMA using attenuated total reflectance IR spectroscopy.

(b) Gravimetric analyses performed at 60 ^{o}C and 85 ^{o}C of linear POE oligomers into PMMA.

(c) Thermal characterization of blends made from linear or cyclic POEs and PMMA using differential scanning calorimetry.

(d) Evaluation of diffusion process and comparison of cyclic/linear sample pair versus linear/linear analogous, by using the same matrix and changing only the topology of penetrants.

(e) Influence of temperature on diffusion.

(f) Influence of penetrant topology on diffusion.

(g) Influence of penetrant molecular weight on diffusion.

(h) Comparison of the results with literature data.

1.2 MATERIALS AND CHARACTERIZATION

The polymer pairs involved in this research have dissimilar properties. Poly(oxyethylene) POE was chosen as penetrant or diffusant specie and poly(methyl methacrylate) PMMA was chosen as the matrix polymer. The molecular weight of POE oligomers used in these diffusion studies was below entanglement molecular weight M_e (M_{ePOE} = 1.6 kg/mol)[6] while the matrix molecular weight was above M_e (M_{ePMMA} = 10 kg/mol).[6] To study the effect of topology on diffusion behavior, linear POE/PMMA samples were compared with cyclic POE/PMMA samples. Cyclic POE oligomers with number average molecular weights of 400 g/mol and 1000 g/mol, linear PMMA matrix with weight average molecular weight of 120 kg/mol and linear POE with number average molecular weight of 500 g/mol were used.

The transport of each component was monitored in situ by attenuated total reflectance Fourier transform infrared (FTIR-ATR) spectroscopy without deuteration or labeling. A film of PMMA was solution-cast onto an ATR zinc selenide crystal and POE was added to the surface. The configuration of the assembly used for in situ oligomer/polymer interdiffusion studies is shown in Figure 1.2.

The IR peak at 1109 cm^{-1}, characteristic to the ether bond in POE, was used for quantitative analysis. Deconvolution of these peaks from IR spectra allowed the determination of the relative concentration of linear or cyclic POE as a function of interdiffusion time, from which the interdiffusion constants were computed and the diffusion evaluated.

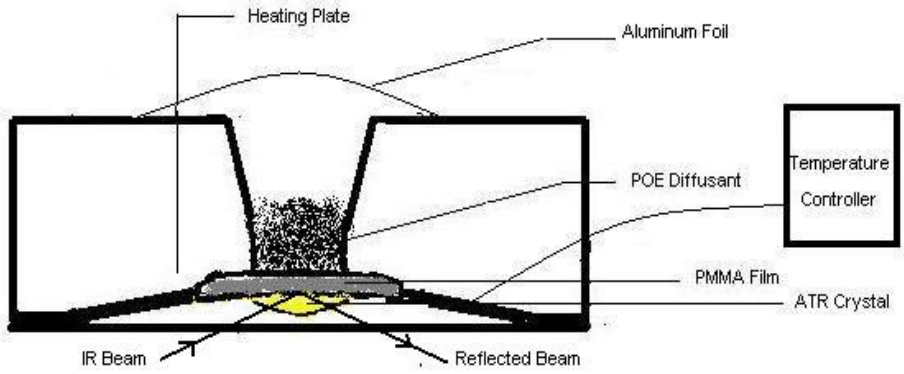

Figure 1.2 - ATR system schematic representation (one single internal reflection) for in situ diffusion measurement between PMMA and POE.

1.3 SCOPE OF DISSERTATION

To address the objectives outlined in the first section, this dissertation is divided into six chapters, including this chapter which represents the introduction.

Chapter 2 is a review of diffusion theory of polymers, where the basics of this transport phenomenon, including the driving factors that are influencing diffusion, are described. The mathematical models used to analyze diffusion are discussed in this chapter. Also, the connection between interdiffusion and self-diffusion is addressed here. A literature review of the limited studies of diffusion of cyclic polymers represents a separate section of this chapter. The last part of Chapter 2 deals with experimental techniques that can be used for interdiffusion evaluation, including a literature review of ATR - FTIR spectroscopy.

A detail description of materials and techniques used in this research is presented in Chapter 3. Main characteristics of diffusant and matrix, experimental set-up, IR

spectra collection and data analysis are explained here. To follow the interdiffusion between linear penetrant oligomers and polymeric matrix at different temperatures, gravimetric experiments were also performed and are described in this chapter. Differential scanning calorimetry used for glass transition temperature measurements on some samples used in this research is discussed at the end of this chapter.

The results obtained from the experimental studies are presented in Chapter 4, where it is shown how the absorbance – time data are used to determine an appropriate diffusion model and further applied to obtain an accurate evaluation of this transport phenomenon. Interpretation of the data in the light of these results is discussed in Chapter 5.

Chapter 6 provides a summary of the results obtained from this research and some recommendations for future work.

The knowledge gained from this study gives us a deeper understanding of transport behavior of low-molecular-weight additives, such as oligomers into polymer matrices and, in particular the influence of topology on diffusion.

1.4 REFERENCES

1. Sikorski, A.; Romiszowski, P., Motion of star-branched vs. linear polymer: A Monte Carlo study. *Journal of Chemical Physics* **1996,** *104*, (21), 8703-8712.

2. Shull, K. R.; Kramer, E. J.; Fetters, L. J., Effect of number of stars on diffusion of star polymers. *Nature* **1990,** *345*, (6278), 790-791.

3. Kawaguchi, D.; Masuoka, K.; Takano, A.; Tanaka, K.; Nagamura, T.; Torikai, N.; Dalgliesh, R.; Langridge, S.; Matsushita, Y., Comparison of interdiffusion behavior between cyclic and linear polystyrenes with high molecular weights. *Macromolecules* **2006,** *39*, (16), 5180-5182.

4. Klein, J., Dynamics of entangled linear, branched, and cyclic polymers. *Macromolecules* **1986,** *19*, (1), 105-118.

5. Tead, S. F.; Kramer, E. J.; Hadziioannou, G., Polymer topology and diffusion - A comparison of diffusion in linear and cyclic macromolecules. *Macromolecules* **1992,** *25*, (15), 3942-3947.

6. Lumma, D.; Borthwick, M. A.; Falus, P., Equilibrium dynamics in the nondiffusive regime of an entangled polymer blend. *Physical Review Letters* **2001,** *86*, (10), 2042-2045.

CHAPTER 2

THEORY OF DIFFUSION IN POLYMERS

In this chapter, an initial introduction to diffusion and different mathematical models that could be applied to describe this process is followed by a literature review. The last part of this chapter concludes with a discussion about diffusion evaluation, by concentrating on interdiffusion and self-diffusion coefficients and theories developed to connect those parameters.

2.1 FACTORS INFLUENCING DIFFUSION IN POLYMERS

Diffusion is defined as a process related to movement of matter due to random molecular motion[1] and chemical potential difference. In fluids, diffusion processes are fast and corresponding coefficients can be successfully predicted by a number of theories. In solids where diffusion is much slower, application of theoretical models is more difficult because of a higher variance in the values of diffusion coefficients.[2] The complexity of this transport process in polymers arises from the fact that these macromolecules are an intermediate case between liquids and solids. A lot of research has been done to identify diffusion mechanisms that occur in polymeric systems, but no single model can explain the observed behavior.[1,3] It is known that polymer/polymer diffusion or interdiffusion is related to miscibility of the diffusing species[4,5] and to the

interface that is formed as soon as contact between them is established.[6,7] The first molecular interpretation of this phenomenon was done by Voyutski,[8] followed by de Gennes[9-11] who indicated the importance of Flory-Huggins thermodynamic interaction parameter χ between the components involved in the process. Different studies reported an enhanced diffusion in polymer blends characterized by a negative Flory interaction parameter.[12,13] Even if compatibility between polymers plays a crucial role in the diffusion mechanism, other factors are also important, such as chemical composition,[13] chain orientation,[7] microstructure,[7] chain ends,[14,15] morphology and topology,[16,17] molecular weight,[13] polydispersity index[18] and temperature.[13,19] For example, diffusion becomes faster at high temperatures through an Arrhenius temperature dependency, while an increase in molecular weight of penetrant and matrix could slow the diffusion process. The topology of polymers which relates to chain connectivity is one of the least understood factors of the diffusion process. A lot of research has been undertaken on star or branched polymers versus linear chains[17] and showed that their motion decreases with increasing the number of arms,[20] but very little research has been done on cyclic polymers diffusion due to limited availability of these polymers.

To understand polymer interdiffusion behavior, a critical parameter that must be considered is entanglement molecular weight M_e of the species involved in this process, which represents the molecular weight between temporary entanglements, as schematically represented in Figure 2.1. The critical molecular weight, $M_c \sim 2\ M_e$, must be considered in the description of a diffusion mechanism of polymers. It is well known that below M_c, the steady-state viscosity of polymers (at zero shear rate) is proportional with $M^{1.0}$, while the exponential dependence changes to $M^{3.4}$ above M_c.[21] As a result,

polymers might diffuse by following different mechanisms depending on their molecular weight.

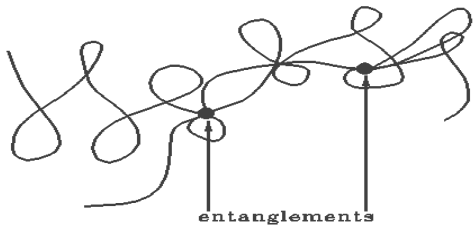

Figure 2.1 – Schematic representation of polymer entanglements. Entanglement molecular weight (M_e) represents molecular weight between temporary entanglements.

Therefore, a classification of interdiffusion processes can be done, as a function of molecular weights of diffusing species with respect to their specific M_e, into the following categories:

(i) Diffusion of small chains into a medium formed by small polymer chains, such as oligomer/oligomer diffusion or diffusion of oligomers into diluted polymer solution. This case is met when both species have the molecular weight below M_e.

(ii) Diffusion of short chains in a polymer network of entangled chains, such as oligomer diffusion in concentrated polymeric solutions or in polymer melts, if the diffusant has a molecular weight below M_e and the matrix is above its M_e. The research presented in this dissertation belongs to this case, because the poly(methyl methacrylate) PMMA matrix has a molecular weight above M_e and

the molecular weight of poly(oxyethylene) POE diffusant was kept in all the experiments presented here below M_e.

(iii) Diffusion of long chain polymers into an entangled chains network, such as polymer diffusion in concentrated solutions or in polymer melts, if both species have the molecular weight well above their M_e.

Another important characteristic of an amorphous or semi-crystalline polymer that must be considered in polymer diffusion characterization is the glass transition temperature T_g, which is called pseudo-second order transition because it results from polymer chain rearrangement (without involving latent heat) and not from a thermodynamic phase change as in the case of a first order transition, such as melting or crystallization. At a temperature below T_g, the polymer chains are in a glassy state, where the mobility of the segments is restricted. Above its T_g, the polymer is in a rubbery phase, where the mobility of polymer segments is higher and creates more paths for a penetrant to move through it. In addition, diffusion coefficients of polymers in the glassy state have a stronger reliance on molecular size than in the rubbery phase.[22] However, all polymer molecular rearrangements are available in both states, with the exception that the activation energy required to make these movements must be higher in the case of glassy versus rubbery polymers. It must be mentioned that changes in T_g during interdiffusion might have a huge impact on the transport behavior of polymers. Hence, during diffusion experiments where there are large differences in the thermal properties of the diffusant species, some systems would change from glassy to the rubbery state when one component acts as a plasticizer for the other. The mechanism might be changing at the interface between glassy and plasticized regions.

Free volume, which is an intrinsic property of the polymer, is another factor that must be taken in account when diffusion is evaluated. Initially, free volume was described as "microvoids",[23] but it could be better understood as the ability of the polymer to form temporary "holes" or "pores" in the matrix. The concept of free volume is well known in polymer science and it is defined as the volume not occupied by matter. These extremely small molecular-scale pores are dynamic and transient and each free volume "pore" depends on vibrations and translations of neighboring polymeric chains. The movement of polymer chains might open or close these "pores" or micro-channels between them, providing "pathways" for diffusion. However, the transport properties in a polymer are very dependent on the amount of the free volume present in the system. If the polymer has a low molecular weight, the free volume will be bigger due to the higher number of chain ends and lower entanglement density, and penetrant will diffuse faster than in the case of high molecular weight matrix. Crystallinity, temperature, thermal history of polymer matrix or mobility given by the chain side groups and end groups are some of the factors influencing the amount of free volume, and implicit diffusion. For example, the importance of polymeric film processing has been reflected in non-identical diffusion behavior obtained for the same penetrant/matrix system if the film has been prepared by solvent casting followed by drying at different temperatures, such as a higher temperature treatment might result in smaller diffusion coefficients due to total removal of possible residual solvent.[24] Crystalline regions in polymers are more ordered than amorphous regions and at a very basic level it could be assumed that diffusion will be slower with increasing degree of crystallinity, and consequently decreasing free volume

present in these regions. However, diffusion processes in semicrystalline polymers are different from those in amorphous macromolecules.

Independent of polymer chain motion, voids or pores could be present in the polymer matrix as "permanent defects" that might arise from film preparation, such as air trapping, fast solvent evaporation or during penetrant diffusion into matrix, as a result of swelling. The volume fraction of these voids will be dependent on the molecular weight of the polymer. For low molecular weight matrices, the probability of voids present will be higher than for high molecular weight matrices. Pores may also provide sites into which penetrant molecules, especially liquids can move quickly at the beginning of diffusion process. A slower diffusion process could be seen as the penetrant molecules are absorbed and condensed into these pores, but later the transport behavior might change again resulting in a faster diffusion until the equilibrium is reached.[24]

As previously mentioned in this section, there are many other factors that influence and control diffusion processes, but here the discussion has been focused around those that are most significant to my research.

2.2 DIFFUSION EVALUATION IN POLYMERS

Interdiffusion is a description of a process by which different species become mixed at molecular level. In the case of a miscible or partially miscible binary polymeric system, the spontaneous interdiffusion of the phases that are in contact with each other can be described by an interdiffusion coefficient and two self-diffusion

coefficients. For a correct evaluation of polymer diffusion, it is critical to clarify the differences between these coefficients. While the interdiffusion coefficient is related to change in concentration of both species in time, self-diffusion coefficient is connected to the motion of molecules without invoking the presence of a concentration gradient. Therefore, interdiffusion coefficients are determined by using mathematical models, while physical mechanisms of diffusion are interpreted by self-diffusion coefficients. Nevertheless, those constants are connected with each other because the change in concentration is related to the diffusion mechanism of penetrant and relaxation mechanism of the matrix.

2.3 MATHEMATHICAL MODELS OF DIFFUSION

Therefore, understanding, predicting and controlling diffusion of small or large molecules in polymers still remains a challenging topic for research. In order to achieve these goals it is very important to apply the most suitable mathematical model characteristic to a specific diffusion process. This is the first step in approaching a physical interpretation of diffusion.

Fick established the first mathematical model of diffusion[1] which was the starting point for numerous diffusion models in polymer system. Eq.1 is known as Fick's first law and describes the diffusion process that occurs in one dimension:

$$J = -D\frac{\partial c}{\partial z} \qquad \text{Eq.1}$$

where J is the flux (rate of transfer) per unit area of section, D the diffusion coefficient, c the concentration of diffusing species and z is axis measured normal to the section where diffusion occurs. According to Fick's law, D is defined as the rate of transfer of diffusant across the diffusion section divided by concentration gradient at this specific section. The negative sign is present in Eq.1 because diffusion occurs in the direction opposite to that of increasing concentration.

The fundamental differential equation of diffusion in an isotropic medium, known as Fick' second law, may be written as:[1]

$$\frac{\partial c}{\partial t} = D\frac{\partial^2 c}{\partial z^2} \qquad \text{Eq.2}$$

The above equation has been derived from Eq.1 by considering a parallelepiped having the sides parallel to coordinate axes (x, y, z) and assuming a constant penetrant diffusion coefficient with one-dimensional movement, for example a gradient of concentration only along the z-axis.

Interdiffusion processes that occur by mixing two species can be characterized by one diffusion coefficient if the process does not involve a volume variation. Then an equal quantity of each component is moving in opposite directions, and a single diffusion parameter is related to both species. This is called the interdiffusion coefficient D_m, but is also referred to as the mutual, collective or cooperative diffusion coefficient. Not only Fickian models can be used to calculate a diffusion constant that would be specific to a certain type of diffusion, but other mathematical models have also been

applied. However, depending on the rates of penetrant diffusion and polymer relaxation, interdiffusion processes specific to polymeric systems can be classified into the following classes:[3]

(i) *Fickian diffusion* or *Case I*: characteristic of rubbery polymers, when matrix polymer relaxation is much faster compared to the penetrant diffusive motion. This process is often observed for polymer networks when the temperature of study is well above T_g of the system. In cases when the penetrant produces changes in the polymer matrix, such as swelling or plasticization, the interdiffusion mechanism could possibly deviate from the Fickian behavior.

(ii) *Case II*: occurs typically in a glassy polymer, when the matrix relaxation is much slower than penetrant diffusion and temperature of study is below T_g. In this case, as the penetrant molecules are moving into the glassy polymer, the matrix starts to swell and finally becomes rubbery.

(iii) *Non-Fickian* or *anomalous diffusion*: referred as an intermediate case when rates of diffusion and relaxation are comparable. One of the characteristics usually seen here is a sharp penetrant front advancing through a matrix, rather than an exponential type diffusion profile. It should be noted that in literature is not a clear distinction between *Case II* and *anomalous diffusion*.

(iv) *Super-anomalous diffusion* or *Super Case II*: related to those cases that do not follow any of the diffusion models described above. The very little information found in literature about this behavior is associated with a difference between initial and final diffusion. Therefore, at the end of process an acceleration period

might be observed which can be different than the induction period seen at the starting point.[24]

Sometimes during diffusion, penetrant/matrix systems might be characterized by a combination of *Fickian* and *Case II* diffusion, due to different changes that could occur in the system, such as a decrease in glass transition temperature followed by plasticization process.

Experimentally, the type of diffusion or transport mechanism can be determined from diffusional exponent n, and the diffusion constants can be estimated from k, by using the equation described below:[25]

$$\frac{M(t)}{M_\infty} = kt^n \qquad \text{Eq.3}$$

where $M(t)$ represents the amount of diffusant per unit area of polymer that is changing in time t according to Eq.3, M_∞ is the mass of diffusant uptake as time approaches infinity (at equilibrium) and k is a constant which incorporates the characteristics of matrix and penetrant. In fact, this equation is a generalized solution of Fick' second law described above by Eq.2 and it has been demonstrated to be a valid approximation for the first 60% of normalized penetrant uptake. The values of n presented below have been determined for the case of diffusion through a polymer film.

(i) *Fickian diffusion* or *Case I* is characterized by n = 0.5. This process is described by an interdiffusion coefficient, D_m which can be determined from k, with the appropriate set-up of initial and boundary conditions. Also, it must be emphasized that n, as well as k are strongly dependent of sample geometry.

Therefore, $n = 0.5$ only for a slab geometry, while in case of another geometry type, n might have a different value, such as $n = 0.45$ for a cylinder or $n = 0.43$ for a sphere.[25]

(ii) *Case II* is characterized by $n = 1$. As discussed above, a glassy polymer matrix swells as penetrant is diffusing into polymeric matrix and an interface is developed between the swollen region and the glassy region. In this case, the interface advances with a constant velocity that follows the equation described below:

$$z = kt \qquad \text{Eq.4}$$

where z is interface penetration distance, k is a constant and t is the time. Now, the physical significance of k is related to penetrant velocity or matrix relaxation, K_{II}. Figure 2.2 gives a better understanding of *Case II* diffusion.

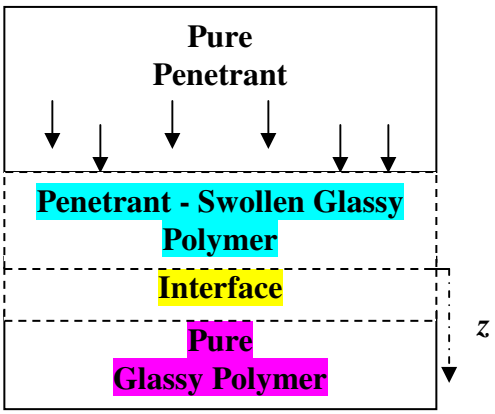

Figure 2.2 – Schematic representation of *Case II* diffusion. The penetrant starts to diffuse into a polymer matrix. A rapid increase in penetrant concentration in the swollen region leads to a sharp penetration front (interface) which starts to advance at a constant rate.

(iii) *Case III* or *anomalous diffusion* is characterized by $0.5 < n < 1$. This is an intermediate non-Fickian diffusion case, which cannot be characterized by a single diffusion equation, but a combination between *Case I* and *Case II* might be the best approximation for this process. Then, an interdiffusion coefficient, D_m, and a matrix relaxation constant (penetrant velocity), K_{II}, can be used to describe the anomalous diffusion and a "simple algorithm" can be written by coupling both transport models:[25]

$$\frac{M(t)}{M_\infty} = k_1 t^{0.5} + k_2 t \qquad \text{Eq.5}$$

The physical meaning of k_1 and k_2 is related to D_m and, respectively K_{II}.

(iv) *Super–anomalous diffusion* occurs when $n > 1$. As for *Case III* diffusion, this model cannot be described by a specific equation. It is expected that in this instance, the percentage of the non-Fickian component should be higher than in *Case III*, because the diffusion is closer to *Case II* than *Case I*, as the diffusional exponent indicates.

Some articles published in literature classified diffusion as Fickian and non-Fickian or anomalous processes. Therefore, only three classes are described: *Fickian* if $n = 0.5$, *Case II* if $0.5 < n < 1$ and *Super Case II* if $n > 1$.[26]

Another way that could be used to describe diffusion behavior is related to diffusional Deborah number (D_e) introduced by Ventras[27] and defined as the ratio between characteristic relaxation time of matrix and characteristic diffusion time of penetrant.[28] If $D_e << 1$ characteristic to Fickian mechanism, then the relaxation time is

much smaller than diffusion time and the changes in polymer structure take place very quickly. Case II diffusion is described by D_e>>1 (a long relaxation time compared with a small diffusion time), when a penetrant is moving through a matrix surface that behaves as an elastic medium until the concentration reaches the equilibrium value and the interface begins to move into the polymeric matrix. Anomalous diffusion is defined by D_e = 1, when relaxation and diffusion times are of the same order of magnitude and the instantaneous molecular configuration differs from its equilibrium state, because changes in segmental motion occur as the diffusant moves into the matrix (plasticization effect).

Thus, the Deborah number and diffusion exponent have the same meaning and both can be used to elucidate the mathematical model involved in the diffusion processes.

2.4 DIFFUSION MECHANISMS

The diffusion in a binary system is characterized not only by a mutual diffusion coefficient, but also by two self-diffusion coefficients specific to each component of the system in study. The center-of-mass or self-diffusion coefficient, D_s, of a polymer chain is related to the mean square distance traveled by its center of mass in time. In order to describe the self diffusion of polymers, various theories have been proposed depending on the polymer molecular weight and geometry.

The reptation theory proposed by de Gennes[11] and Doi & Edwards[3] is the most popular diffusion mechanism applied to all polymers above their M_e that describes the

snake-like motion of a polymer chain along a tube with a given contour length formed by physical entanglements (see Figure 2.3).

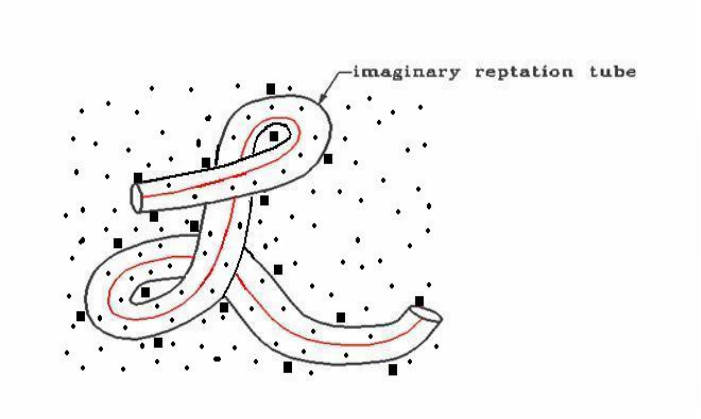

Figure 2.3 – Schematic representation of reptation model. A single chain is represented as a snake enclosed into a tube developed by topological constraints (filled squares). The small dots are sections through the neighboring polymeric chains.

In this case, the self-diffusion coefficient is related to the molecular weight by the following equation:

$$D_{rep} = \frac{k_B T a^2}{3N^2 \zeta b^2} \qquad \text{Eq.6}$$

where: D_{rep}= self-diffusion coefficient following reptation mechanism; k_B = Boltzmann constant; T = temperature; a = distance between entanglements ("topological constraints") or tube diameter; N = number of monomeric segments; b = length of a monomer; ζ = monomeric friction coefficient.

This theory predicts that a linear chain moves following its chain ends. In the case of cyclic polymers, the lack of chain ends might exclude the possibility of these species to move in the "original sense of the reptation theory".[29]

Rouse theory[3] is another popular theory that predicts the self-diffusion coefficient to be proportional to the inverse molecular weight for all polymers that are below their entanglement molecular weight. In this case the polymer coils are described as a chain of beads connecting through entropic springs.

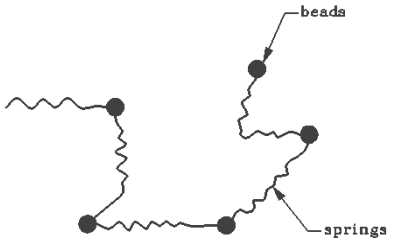

Figure 2.4 – Schematic representation of Rouse model. Polymer coil is described as a chain of beads connected by entropic springs.

A polymer chain that follows a Rouse mechanism moves according to the following equation:

$$D_R = \frac{k_B T}{N\zeta} \qquad \text{Eq.7}$$

where D_R is self-diffusion coefficient following Rouse mechanism.

Although the molecular weight of the diffusing chain has a critical role in the diffusion mechanism, the matrix molecular weight also has a very big influence.

Therefore, if a polymer chain is moving into a matrix of different molecular weight, its diffusion behavior is expected to be dependent on the molecular weight of the matrix.[30]

Cleary linear polymers may have different diffusion mechanisms from equivalent molecular weight branched or cyclic polymers due to differences in topology and morphology. Although, a lot of research has been done on linear or branched polymers and only few studies were reported on dynamics of entangled rings.[29, 31, 32] The diffusion of highly entangled rings into cyclic matrices has been described as an "exponentially suppressed reptation"[5] and the self-diffusion coefficient (D_{ring}) has an exponential molecular weight dependence:[5]

$$D_{ring} \propto e^{-\beta M} \qquad \text{Eq.8}$$

In case of dynamics of entangled rings into linear melts, Klein[5] proposed mechanism which is dependent on the ring size. If the rings are small enough to not enclose any entanglements, then the diffusion behavior is expected to be similar to that of an entangled linear polymer, where the second half of a ring has to retrace its first half. [31] The probability of cyclic molecules adopting this configuration diminishes with increasing size. In the case of intermediate cyclic molecular size, the motion is expected to follow a mechanism that could be a combination between pure reptation, exponentially suppressed reptation and constraint release or tube renewal.

A very good representation of possible configurations that ring polymers could take it in an entangled matrix was given by Klein,[5] as shown in Figure 2.5.

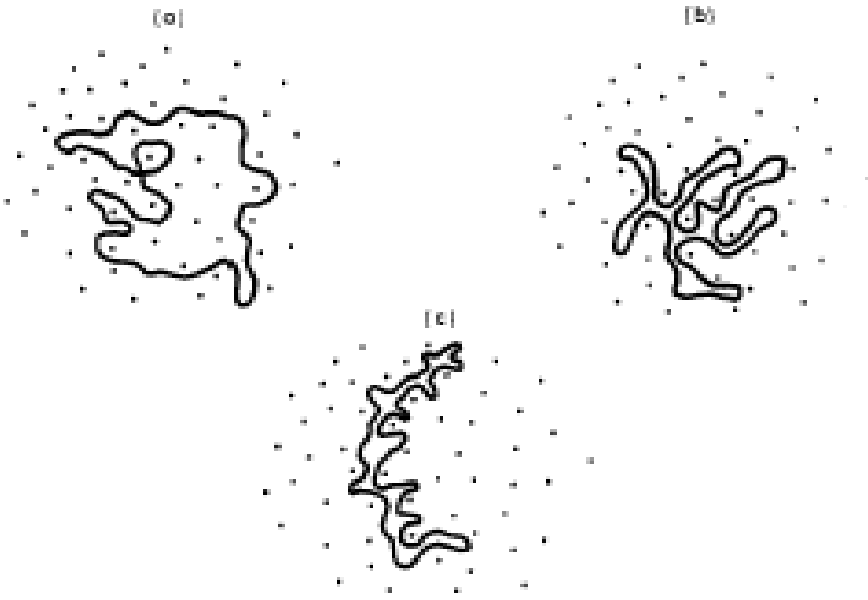

Figure 2.5 – Possible configurations for cyclic polymers in an entangled matrix.[5] The dots represent physical entanglements. (a) "Pinned" configuration; (b) "Unpinned ramified" configuration; (c) "Unpinned non-ramified" configuration.

Cyclic polymer movement in an entangled matrix could adopt one of the three configurations presented in Figure 2.5.[5] In general, if a ring encloses neighboring entanglements as shown in Figure 2.5 (a.), the configuration is named "pinned" so that translational diffusion cannot occur and the ring is expected only to rotate around its center of mass. It is possible but with low probability that a ring polymer will adopt an "unpinned ramified" configuration as shown in Figure 2.5 (b.), where the ring does not enclose any constraints. In this case, the ring will diffuse in the same manner as a star polymer, by adopting a reptation mechanism for each arm (arm retraction). The probability of an entangled cyclic polymer adopting an "unpinned non-ramified" configuration as shown in Figure 2.5 (c.) is very low, but if this occurs, the ring will follow a normal reptation mechanism typified by a linear polymeric chain. In this case,

the diffusion coefficient of an entangled ring polymer D_{ring} is approximately two times bigger than the diffusion coefficient of linear analogous polymer D_{linear}, because the cyclic will follow the same path as a linear one which has half of its chain size:[5]

$$D_{ring} \cong 2D_{linear} \qquad \text{Eq.9}$$

It is important to note that Eq.9 might be valid only for small ring sizes lower or comparable with 10 entanglements.

The results achieved by Matsushita et al.[29] from comparing the diffusion of cyclic polystyrene PS versus corresponding linear one at high molecular weight (3-4 times higher than M_c of PS) based on dynamic secondary ion mass spectroscopy in conjunction with neutron reflectivity measurements indicate that cyclic polymers moves 2.2 times faster than linear chains.

Even if here we evaluated an interdiffusion process, a discussion around self-diffusion of cyclic versus linear polymers which are related to this research follows next. Simulation studies by Muller & Cates[16] and also Szamel & Brown[33] have both shown that self-diffusion of rings is faster than that of equivalent molecular weight linear chains. The faster ring diffusion in the melt compared to linear chains is explained by smaller size, more compact structure and less interpenetration. An open question is related to the correlation between these studies to experimental results.

The influence of topology and chain ends of unentangled polymers has been studied by Nam et al.[34] by looking at cyclic and linear poly (oxyethylene) (POE) melts. The values of self-diffusion coefficients determined at 56 ^{o}C shown that cyclic POE

diffuses faster than linear specie having same molecular weight and hydroxyl chain ends, but slower that linear ones with methoxy-terminated groups. The retard motion of hydroxyl-terminated linear POE versus methoxy-terminated homologous has been explained by the presence of hydrogen bonding. If the influence of chain ends is eliminated from discussion and only topology is considered, the slower diffusion of cyclic POE compared to linear methoxy-terminated POE is explained by the high local densities of rings as a result of smaller size (absence of free chain ends) versus linear ones. It is very important to specify that by increasing molecular weight, the contribution of chain ends to diffusion becomes negligible.

Some studies on cyclic/linear blends miscibility have been followed by many groups. Cates[16] predicted that blends of chemically identical cyclic/linear polymers should have a negative value of Flory-Huggins interaction parameter χ which is an indication of good miscibility. They suggested a possible miscibility of non-identical ring/linear combinations, even in cases where similar linear/linear combinations are immiscible. Further, MacKnight et al.[35] evaluated the topological effects on blend miscibility by looking at linear or cyclic polycarbonate (PC) blended with linear polystyrene (PS) and the results indicated that χ is smaller for cyclic PC/linear PS blends than for linear/linear combinations. These results were explained in terms of topological repulsion between rings validating Cates & Deutsch theory. Later, Singla and Beckham[36] compared cyclic poly(oxyethylene) oligomers into linear polystyrene versus linear poly(oxyethelene)s blends by using differential scanning calorimetry and a significantly enhanced miscibility of cyclic POE/ linear PS blends has been reported.

All the studies done until now on the influence of polymer topology to diffusion processes are still in premature stage. Topology remains an open field for researchers. Majority of these few studies found in literature have been done on self diffusion rather than interdiffusion.

2.5 CONNECTION BETWEEN SELF-DIFFUSION AND INTERDIFFUSION COEFFICIENTS

It is well known that the chemical potential gradient, which is proportional with Flory-Huggins interaction parameter, χ, is considered to be the driving force for diffusion. The interdiffusion between two species is dependent on χ, which describes the molecular interactions between them. For example, in cases where physical interactions are present, such as hydrogen bonds, the value of χ is negative, which indicates a low enthalpy of interaction and favors the interdiffusion between the two species. In miscible blends of polymers with identical chain lengths and mobility, the mutual diffusion coefficient D_m may be expressed as:[37]

$$D_m = D_s\left[1 - 2\chi N c(1-c)\right] \qquad \text{Eq.10}$$

where c is the volume fraction of one polymer, D_s is self-diffusion coefficient and N is the degree of polymerization. Eq.10 cannot be applied if the polymers have different

mobility, because glass transition temperature changes with composition, and hence free volume of the system.

In the case of compatible polymers, two theories that connect D_m and D_s have been proposed. These theories invoke the symmetry of the concentration profiles for interfaces with similar molecular weights and symmetric boundary conditions and predict that interdiffusion is dominated by one of the diffusing components:

(i) The *slow theory*, defined by de Gennes[10] and Brochard,[38] considers the diffusion process being controlled by the slow component which is characterized by a lower mobility. One of the limitations of this model is that it does not take into consideration the physical interactions between the two components. The equation specific to slow mode theory can be expressed as:[39, 40]

$$\frac{1}{D_m^{slow}} = (N_A + N_B)\phi_A\phi_B\left(\frac{\phi_A}{D_s^B} + \frac{\phi_B}{D_s^A}\right) \qquad \text{Eq.11}$$

where: D_m^{slow} = mutual diffusion coefficient (cm^2/s); ϕ_A = volume fraction of interdiffusing specie A; ϕ_B = volume fraction of interdiffusing specie B; N_A = degree of polymerization of component A; N_B = degree of polymerization of component B; D_s^A = self-diffusion coefficient of specie A; D_s^B = self-diffusion coefficient of specie B.

ii) The *fast theory*, proposed by Crank[1] and Kramer,[41] considers the diffusion process being controlled by the fast component which swells the slow component. In this case, the chemical potential gradient of vacancies across

the interface is assumed zero indicating that the two polymeric species are in thermodynamic equilibrium during interdiffusion process. The equation describing the fast mode theory is known as Hartley-Crank equation:[39]

$$D_m^{fast} = \frac{1}{(N_A + N_B)\phi_A\phi_B}\left(\phi_B D_s^A + \phi_A D_s^B\right) \qquad \text{Eq.12}$$

where: D_m^{fast} = mutual diffusion coefficient (cm^2/s); ϕ_A = volume fraction of interdiffusing specie A; ϕ_B = volume fraction of interdiffusing specie B; N_A = degree of polymerization of component A; N_B = degree of polymerization of component B; D_s^A = self-diffusion coefficient of specie A; D_s^B = self-diffusion coefficient of specie B.

Clearly, these theories do not agree with each other, but both are based on mathematical models that were developed without including important factors, such as the dependence of the friction coefficients on the system composition. This assumption might be valid in the case polymer of pairs with similar properties, but it will not be true for polymer interfaces with dissimilar properties.[42] Experimental results compared with predictions made by using both theories could be in agreement with one of those theories or in totally disagreement with both. While the fast mode model is more consistent with lower molecular weight data, the slow model is more consistent with higher molecular weights having some deviations at lower molecular weights. Therefore a more accurate theory than either of these two was needed to represent the interdiffusion in the whole molecular weight range.

Recent work[40] has shown that fast and slow theories are in fact opposite ends of the same theory. Hence, the introduction of "ANK"[40] theory validated by scattering experimental data shows that the interdiffusion coefficient in a binary mixture at finite vacancy concentration cannot be in general expressed only in terms of self-diffusion coefficients of the components, but it must involve in addition a cooperative diffusion coefficient which defines the relaxation of total density fluctuations. The mobility of system can be expressed in terms of Onsager coefficients:[39]

$$\Lambda_{ANK} \propto \left[\frac{1}{(N_A + N_B)\phi_A\phi_B}\right]^2 \left(\Lambda_A\phi_B^2 - 2\phi_A\phi_B\Lambda_{AB} + \Lambda_B\phi_A^2\right) \qquad \text{Eq.13}$$

where Λ_{ANK} is the Onsager coefficient related to the mobility of the system, Λ_A and Λ_B are the Onsager coefficients related to the mobility of species A and B and Λ_{AB} is the Onsager coefficient defining the mobility of one specie in relation with the other. Then, the disagreement between the fast and slow mode theories can be possibly settled by "ANK" theory which refers to them as the limits of the vacancy concentration. So, in case of zero vacancy, D_m can be expressed by using the slow mode theory, while the fast mode theory will be the best fit for the case of large vacancy.

2.6 METHODS TO EVALUATE INTERDIFFUSION

Numerous techniques have been exploited to study the diffusion of a binary polymeric system. Some of them were developed to measure the mutual diffusion coefficient and others to evaluate the self-diffusion coefficients of the species that are in contact with each other. The experimental techniques, as well as the range of the diffusion coefficients obtained from using them in evaluation are summarized in literature.[42]

Diffusion in similar polymers has been extensively assessed by using numerous techniques, such as neutron reflectivity,[43] optical wedge microinterferometry,[44] transmission electron microscopy,[19] or dynamic light scattering.[45] Many of these techniques have good spatial resolution, but labeling requirement could be considered a big disadvantage that can affect the miscibility and phase behavior of polymer blends[20] and therefore slowing down the interdiffusion process.[21]

Since ATR-FTIR spectroscopy does not require labeling, it can be considered one of the most accurate techniques used for interdifussion studies. Many research groups utilized this method to evaluate interdiffusion between polymers with dissimilar properties,[30,42] as well as to track diffusion of small molecules into polymers.[6,46] A comprehensive part of this thesis dedicated to ATR-FTIR spectroscopy follows in next chapter. Even if gravimetry is one of the most conventional methods employed for diffusion evaluation of small penetrants into polymers, still ATR-FTIR spectroscopy can be considered a more robust one because the information at molecular level can be obtained from here.[6,46]

Studies on diffusion of poly(ethylene glycol) oligomers into high molecular weight deuterated PMMA have been done by Bucknall et al.[43] by using neutron reflectivity technique, but not one study on cyclic POE oligomers diffusion into PMMA matrix has been found in literature.

2.7 CONCLUSIONS

In this chapter, diffusion theory was reviewed. The factors influencing the diffusion in polymers, as well as a summary of theoretical models and their uses in explaining the diffusion process were presented here. The limited data present in literature on diffusion of cyclic polymers was discussed in this chapter.

Nevertheless, a critical evaluation of this transport phenomenon can be done only by having a clear understanding of diffusion and a good distinction between different mathematical models and diffusion theories involved in this process.

2.8 REFERENCES

1. Crank, J., *The Mathematics of Diffusion, 2nd Ed.* In Oxford University Press: Oxford, U., Ed. **1975**.

2. Cussler, E. L., *Diffusion, mass transfer in fluid systems*. In Press, C. U., Ed. **1997**.

3. Doi, M.; Edwards, S. F., *The Theory of Polymer Dynamics*. In Clarendon Press: Oxford, U., Ed. **1986**.

4. Brochard, F.; Jouffroy, J.; Levinson, P., Polymer polymer diffusion in melts. *Macromolecules* **1983,** *16*, (10), 1638-1641.

5. Klein, J., The interdiffusion of polymers. *Science* **1990,** *250*, (4981), 640-646.

6. Laot, C.; Marand, E.; Oyama, H. T., Spectroscopic characterization of molecular interdiffusion at a poly(vinyl pyrrolidone) vinyl ester interface. *Polymer* **1999,** *40*, (5), 1095-1108.

7. Lorec, G.; Baley, C.; Sire, O.; Grohens, Y., Characterization of interdiffusion between PVDF and stereoregular PMMA by using ATR-FTIR spectroscopy. *Macromolecular Symposia* **2005,** *222*, 265-271.

8. Voyutski, S. S., Some comments on interfacial contact and bonding in autohesion. *Journal of Adhesion* **1971,** *3*, (1), 69.

9. deGennes, P. G., Reptation of a polymer chain in presence of fixed obstacles. *Journal of Chemical Physics* **1971,** *55*, (2), 572.

10. deGennes, P. G., Dynamics of fluctuations and spinodal decomposition in polymer blends. *Journal of Chemical Physics* **1980,** *72*, (9), 4756-4763.

11. deGennes, P. G., Compatible polymer systems - special properties for mutual diffusion and for adhesion. *C.R. Acad. Sci., Serie II* **1981,** *292*, (23), 1505-1507.

12. Composto, R. J.; Mayer, J. W.; Kramer, E. J., Fast mutual diffusion in polymer blends. *Physical Review Letters* **1986,** *57*, (11), 1312-1315.

13. Kanetakis, J.; Fytas, G., Mutual diffusion in compatible polymer blends. *Macromolecules* **1989,** *22*, (8), 3452-3458.

14. Bairamov, D. F.; Chalykh, A. E.; Feldstein, M.; Siegel, R. A., Impact of molecular weight on miscibility and interdiffusion between poly(N-vinyl pyrrolidone) and poly(ethylene glycol). *Macromolecular Chemistry and Physics* **2002,** *203*, (18), 2674-2685.

15. Dormidontova, E. E., Influence of end groups on phase behavior and properties of PEO in aqueous solutions. *Macromolecules* **2004,** *37*, (20), 7747-7761.

16. Mueller, M.; Wittmer, J. P.; Cattes, M. E., Topological effects in ring polymers. *Physical Review E* **2000,** *61*, (4), 4078-4089.

17. Sikorski, A.; Romiszowski, P., Motion of star-branched vs. linear polymer: A Monte Carlo study. *Journal of Chemical Physics* **1996,** *104*, (21), 8703-8712.

18. Burchard, W.; Schmidt, M.; Stockmayer, W. H., Information on polydispersity and branching from combined quasi-elastic and integrated scattering. *Macromolecules* **1980,** *13*, (5), 1265-1272.

19. Gilmore, P. T.; Falabella, R.; Laurence, R. L., Polymer-polymer diffusion - Effect of temperature and molecular weight on macromolecular diffusion in blends of poly(vinyl chloride) and poly(epsilon caprolactone). *Macromolecules* **1980,** *13*, (4), 880-883.

20. Roovers, J.; Toporowski, P. M., Hydrodynamic studies on model branched polystyrenes. *Journal of Polymer Science - Part B: Polymer Physics* **1980,** *18*, (9), 1907-1917.

21. Fetters, L. J.; Lohse, D. J.; Richter, D., Connection between polymer molecular weight, density, chain dimensions, and melt viscoelastic properties. *Macromolecules* **1994,** *27*, (17), 4639-4647.

22. Guo, J.; Barbari, T. A., A dual mode, local equilibrium relaxation model for small molecule diffusion in glassy polymer. *Macromolecules* **2008,** *41*, (20), 7762-7764.

23. Turnbull, D.; Cohen, M. H., Free volume model of amorphous phase - glass transition. *Journal of Chemical Physics* **1961,** *34*, (1), 120.

24. Duncan, B.; Urquhart, J.; Roberts, S., Review of measurement and modelling of permeation and diffusion in polymers. *UK, National Physical Lab* **2005**, 11.

25. Peppas, N. A.; Brannon-Peppas, L., Water diffusion and sorption in amorphous macromolecular systems. *Journal of Food Engineering* **1994,** *22*, (1-4), 189-210.

26. Thomas, N. L.; Windle, A. H., A theory of Case II diffusion. *Polymer* **1982,** *23*, (4), 529-542.

27. Ventras, J. S.; Jarzebski, C. M.; Duda, J. L., Deborah number for diffusion in polymer-solvent systems. *AlCHE. Journal* **1975,** *21*, (5), 894-901.

28. Tomba, J. P.; Carella, J. M.; Pastor, J. M., Liquid-glassy polymer diffusion. *Macromolecules* **2005,** *38*, (10), 4355-4362.

29. Kawaguchi, D.; Masuoka, K.; Takano, A.; Tanaka, K.; Nagamura, T.; Torikai, N.; Dalgliesh, R.; Langridge, S.; Matsushita, Y., Comparison of interdiffusion behavior between cyclic and linear polystyrenes with high molecular weights. *Macromolecules* **2006,** *39*, (16), 5180-5182.

30. Jabbari, E.; Peppas, N. A., Matrix effects on interdiffusion at the polystyrene and poly(vinyl methyl ether) interface. *Macromolecules* **1995,** *28*, (18), 6229-6237.

31. Klein, J., Dynamics of entangled linear, branched, and cyclic polymers. *Macromolecules* **1986,** *19*, (1), 105-118.

32. Tead, S. F.; Kramer, E. J.; Hadziioannou, G., Polymer topology and diffusion - A comparison of diffusion in linear and cyclic macromolecules. *Macromolecules* **1992,** *25*, (15), 3942-3947.

33. Brown, S.; Szamel, G., Computer simulation study on structure and dynamics of ring polymers. *Journal of Chemical Physics* **1998,** *109*, (14), 6184-6192.

34. Nam, S.; Leisen, J.; Breedveld, V., Dynamics of unentangled cyclic and linear poly(oxyethylene) melts. *Polymer* **2008,** *49*, (25), 5467-5473.

35. Nachlis, W. L.; Bendler, J. T.; Kambour, R. P.; MacKnight, W. J., Topological effects on blend miscibility. *Macromolecules* **1995,** 28, (*23*), 7869-7878.

36. Singla, S.; Beckham, H. W., Miscible blends of cyclic poly(oxyethylene) in linear polystyrene. *Macromolecules* **2008,** *41*, (24), 9784-9792.

37. Jones, R. A. L.; Klein, J.; Donald, A. M., Mutual diffusion in a miscible polymer blend. *Nature* **1986,** 321, (*6066*), 161-162.

38. Brochard, F.; deGennes, P. G., Polymer-polymer interdiffusion. *Europhysics Letters* **1986,** *1*, (5), 221-224.

39. Akcasu, A. Z., The "fast" and "slow" mode theories of interdiffusion in polymer mixtures: Resolution of contraversy. *Macromolecular Theory and Simulation* **1997,** 6, (*4*), 679-702.

40. Akcasu, A. Z.; Nagele, G.; Klein, R., Remarks on fast and slow mode theories of interdiffusion. *Macromolecules* **1997,** *28*, (19), 6680-6683.

41. Green, P. F.; Palstrom, C. G.; Mayer, J. W.; Kramer, E. J., Marker displacement measurements of polymer polymer interdiffusion. *Macromolecules* **1985,** *18*, (3), 501-507.

42. Jabbari, E.; Peppas, N. A., Use of FTIR-ATR to study interdiffusion in poly(styrene) and poly(vinyl methyl ether). *Macromolecules* **1993,** *26*, (9), 2175-2186.

43. Bucknall, D. G.; Higgins, J. S.; Butler, S. A., Early stages of oligomer-polymer diffusion. *Chemical Engineering Science* **2001,** *56*, (19), 5473-5483.

44. Bairamov, D. F.; Chalykh, A. E.; Feldstein, M.; Siegel, R. A., Dissolution and mutual diffusion of poly(N-vinyl pyrrolidone) in short chain poly(ethylene glycol) as observed by optical wedge microinterferometry. *Journal of Applied Polymer Science* **2002,** *85*, (5), 1128-1136.

45. Murschall, U.; Fischer, E. W.; Herktmaetzky, C.; Fytas, G., Investigation of the mutual diffusion in compatible mixture of 2 homopolymers by photon-correlation spectroscopy. *Journal of Polymer Science, Part C - Polym Letters* **1986,** *24*, (4), 191-197.

46. Fieldson, G. T.; Barbari, T. A., The use of FTIR-ATR spectroscopy to characterize penetrant diffusion in polymers. *Polymer* **1993,** *34*, (6), 1146-1153.

CHAPTER 3

EXPERIMENTAL DETAILS

This chapter provides information related to all experimental details of the research study presented in this dissertation. Detailed descriptions of materials and techniques, as well as main characteristics of diffusant and matrix, experimental set-up, data collection and data analysis protocols are provided here. Gravimetric studies were used to compare the results obtained from ATR-FTIR spectroscopy. Differential scanning calorimetry was used for glass transition temperature measurements and it is discussed at the end of this chapter.

In the first section, the discussion focuses around materials and equipment used for analysis. All the samples were prepared by following the same experimental procedure which is presented in the second section. Infrared spectra generation and analysis are discussed in the third section.

3.1 MATERIALS

The interdiffusion systems studied here are made by two components:

a. Matrix - poly(methyl methacrylate) PMMA;

b. Diffusant - linear poly(oxyethylene) lPOE and cyclic poly(oxyethylene) cPOE.

All materials were purchased from Aldrich Chemicals, except for the cyclic oligomers which have been prepared through a ring closure of end-functionalized linear precursors[1] followed by separation of cyclic components. Atactic poly(methyl

methacrylate) (PMMA) with weight-average molecular weight M_w of 120,000 g/mol and number-average molecular weight M_n of 99,000 g/mol was used as the matrix polymer for these studies and toluene (HPLC grade, 99.8%) as the solvent for preparing the films by solution casting. Linear poly(oxyethylene) (lPOE) oligomer with a narrow molecular weight distribution (PDI ~ 1.05) and number-average molecular weight M_n of 500 g/mol, has been used as diffusant specie. The chain end-groups of the linear POE oligomers [commonly known as poly(ethylene glycol) dimethyl ether] are methoxy $-OCH_3$. The cyclic POE oligomers with M_n of 400 g/mol and 1000 g/mol (PDI ~1.02) have been synthesized by cyclization reaction of analogous hydroxyl-terminated linear POE with toluene-sulfonylchloride (TsCl) under alkaline conditions (KOH) followed by purification from linear byproducts by inclusion complexation of the linear byproducts with cyclodextrin.[2]

3.1.1 Poly(methyl methacrylate) PMMA matrix

Poly(methyl methacrylate) or poly(methyl 2-methylpropionate) is an amorphous thermoplastic and a transparent material. The repeat unit of PMMA has a molecular weight of 100 g/mol; its chemical structure is shown in Figure 3.1.

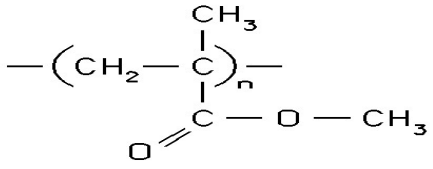

Figure 3.1 – Repeat unit of poly(methyl methacrylate).

PMMA is a hydrophobic polymer with a density of 1.19 g/cm^3 (ρ_{PMMA} = 1.19 g/cm^3). It has a refractive index of 1.492 determined at λ = 589.3 nm and 20 ^{o}C, $n_D^{20} = 1.492$ and it is soluble in different organic solvents, such as toluene or cyclohexanone.[3]

Poly(methyl methacrylate) could be obtained at different molecular weights, but the grade of PMMA used in this research (M_w = 120,000 g/mol), labeled as PMMA120K belongs to an entangled polymer, because its molecular weight is above M_{ePMMA} = 10,000 g/mol.[4] The entanglement density of PMMA120K, which can be calculated as the ratio between polymer number-average molecular weight and its entanglement molecular weight is 10. An entangled polymer characterized by a high entanglement density will relax slower than one with a lower number of entanglements. Therefore, matrix molecular weight and relaxation behavior might have an influence on penetrant diffusion. The steady-state viscosity of PMMA120K is expected to vary with $M_{PMMA}^{3.4}$, because its molecular weight is greater than the critical molecular weight, $M_{PMMA} > 2M_{ePMMA}$.[5]

3.1.2 Poly(oxyethylene) POE diffusant

Poly(ethylene glycol) PEG and poly(ethylene oxide) PEO are polymers having identical repeat units, as shown in Figure 3.2, but they can have different end groups.[6] The repeat unit of PMMA has a molecular weight of 44 g/mol. PEG refers to an oligomer or polymer of ethylene oxide having low molecular weight and hydroxyl chain ends, while poly(ethylene oxide) is used for higher molecular weights. Both are prepared by polymerization of ethylene oxide and are the most commercially available important

polyethers. Because of different physical properties as a result of chain length effect (e.g. viscosity), they can be used in different applications.

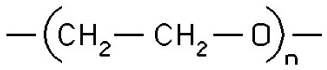

Figure 3.2 – Repeat unit of poly(oxyethylene).

PEG is used in a variety of products, such as dispersant in toothpaste, plasticizer for glassy polymers or antistat additive in polyolefins packages.[7]

All the oligomers used here have their molecular weight below the entanglement molecular weight (M_{ePOE} = 1.6 kg/mol),[4] so in this case the chains are unentangled. Due to the fact that the linear chains have ends and the cyclic ones do not, I named all of them as poly(oxyethylene). As I mentioned above, the linear oligomer of 500 g/mol, molecular weight used in these studies, labeled as lPOE500 is a clear liquid at room temperature. The 400 g/mol cyclic poly(oxyethylene), labeled as cPOE400, is a viscous liquid at room temperature, while the 1000 g/mol cyclic poly(oxyethylene), cPOE1000, is in a waxy solid state at room temperature. POEs are hydrophilic polymers and soluble in water.

3.2 ATR–FTIR SPECTROSCOPY

The diffusion between PMMA and POE oligomers was studied by using attenuated total reflectance Fourier transform infrared (ATR-FTIR) spectroscopy. A detailed description of this technique is given here since it was the primary method used to study diffusion.

3.2.1 Principles of ATR – FTIR spectroscopy

IR spectroscopy has been an important tool for investigating different aspects of molecular structure. By using this method, the interaction of electromagnetic radiation with a substance that produces a response which is dependent on the properties of the system is studied. When a sample absorbs IR radiation at a specific wavenumber (cm^{-1}) or wavelength (μm), the intensity of the radiation will decrease. The mathematical transformation of this change results in an absorption peak that is characterized by two parameters: the wavelength or wavenumber at which the maximum absorption occurs and the intensity of the absorption at this wavelength. The correlation between the functional groups of a molecule and the wavenumbers at which they absorb IR radiation can be found in the literature.

FTIR is one of the most common spectroscopic methods used for surface or bulk characterization. The main component in a FTIR spectrometer is an interferometer, which is a device that splits and recombines a beam of light to disperse the incident radiation into its component frequencies thereby producing an interferogram.[8] The most

commonly used system is a Michelson interferometer, which has two arms oriented perpendicular to each other and a beam splitter that separates the beam coming from an IR source.[9] The incident beam strikes the beam splitter and half of the light is transmitted through the beam splitter and the rest is reflected by two mirrors, one stationary and the other movable. Then, the two components are reflected back and recombined at the beam splitter with half of the light traveling toward the sampling area and half back toward the source. If the mirrors are at equal distances from the beam splitter, the pathways followed by light beams are identical and a maximum flux is obtained at the detector after reflection, generating a "center burst".[9] When the moving mirror is displaced from this equidistant point, the optical path length changes and the radiation destructively interferes with itself at the beam splitter. As a result, the flux reaching the detector decreases rapidly as a function of mirror displacement. The signal is a cosine wave, giving an interferogram (Fourier transform of the spectrum), which is function of time and contains the basic information on the intensities characteristic to the spectrum, but in a form that is not directly interpretable. Digitization of the interferogram at precisely spaced intervals is accomplished by using an auxiliary interferometer, which is generally equipped with a He-Ne laser. The interferogram is sampled at a zero crossing of the laser cosine function and the path difference between two successive data points in the digitized interferogram is a multiple of half the wavelength of the laser (633 nm/2 = 316 nm). The laser works as an internal wavelength calibration standard.[9] By computing the cosine Fourier transform of the interferogram, the spectroscopic information is converted to a more familiar form, as a spectrum which is a function of frequency.

The spectra obtained from FTIR are dependent on optical spectroscopic techniques, which can be classified by reflection and non-reflection techniques. Transmission or emission spectroscopy represents different examples of non-reflection techniques that are commonly used in polymer spectroscopy. Depending on the angle of incidence or the magnitude of change in the refractive index, the reflection techniques can be divided into external and internal reflective methods.[9]

Attenuated total reflection (ATR) or internal reflection spectroscopy (IRS) is one of the techniques widely used to study the surface of different polymeric materials, such as opaque solids or thin films that are characterized by low transmission. As the name implies, ATR measures what happens to a totally reflected IR beam when it impinges with a sample. This technique requires an ATR crystal which is an optically dense medium representing the propagating medium called "the internal reflection element" (IRE). The sample that is in contact with the crystal is called a "rare medium" due to its lower refractive index; it represents the absorbing medium.

As shown in Figure 3.3, if an IR beam impinges on an ATR crystal at a certain angle, the beam will be refracted, transmitted and then totally reflected at the crystal sampling interface. When a sample is placed in contact with the crystal, IR radiation interacts with the sample at the interface through an evanescent wave. The nature of this interaction is dependent on both refractive indices of the ATR crystal (n_1) and the sample (n_2).

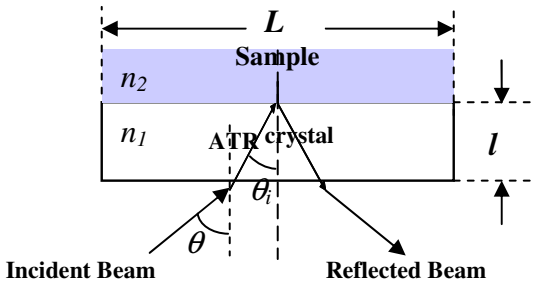

Figure 3.3 – Schematic representation of a single beam ATR system.

In case of a flat crystal, the total number of reflections (N_R) that the light will undergo as it propagates before it emerges from the crystal is defined below:[10]

$$N_R = \frac{L}{l} \times \tan^{-1}(\theta_i) \qquad \text{Eq.14}$$

where L is the crystal length; l is the crystal thickness and θ_i is the incident angle.

In order to obtain a total internal reflection, the incident angle (defined as the angle with respect to normal to the face of ATR crystal) must be bigger than the critical or limiting angle (θ_c), which is given by the following equation:

$$\theta_c = \sin^{-1}\left(\frac{n_2}{n_1}\right) \qquad \text{Eq.15}$$

where n_1 is the ATR crystal refractive index; n_2 is the sample refractive index and $n_1 > n_2$. Eq.15 derives from Snell's law, where the value of refracted angle of the transmitted beam is equal to 90^o. At each reflection, an evanescent field is generated in the rare

medium and its intensity (I) undergoes an exponential decay with distance (z), defined by:

$$I = I_0 e^{-z/d_p} \qquad \text{Eq.16}$$

where I_0 is the intensity of the incident radiation at the interface and d_p is the depth of penetration defined as the distance where the evanescent wave is reduced by a factor of 1/e or 37% of the initial intensity at the surface.[11] However, this value was obtained by assuming $z = d_p$. Therefore, by substituting this into Equation (16), the amplitude of the electrical field in the penetration depth is obtained: $E = E_0 e^{-1} = 0.37 E_0 = 37\% E_0$. The name "evanescent" is derived from the latin word "evanescere", meaning "tendency to vanish".

In order to understand how d_p was obtained, a detailed representation of a single evanescent beam path is shown in Figure 3.4, where E_o represents the initial intensity of the of the electric field at the boundary between the ATR crystal and the sample and E is its intensity in the penetration depth.

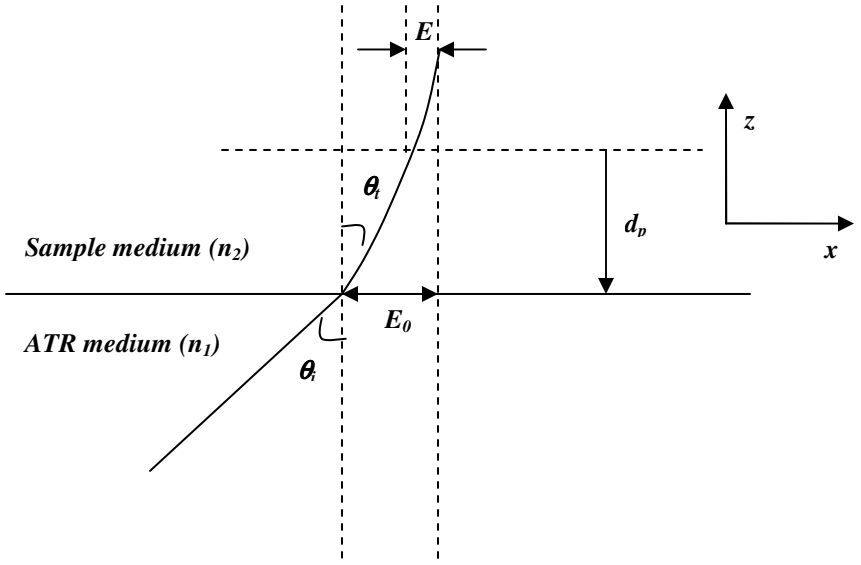

Figure 3.4 – Detailed representation of evanescent wave path.

By knowing the magnitude of the penetration depth, we are able to determine the depth to which the sample can be analyzed. Therefore, this is very important when the chemical structure of the sample could be varying with depth. The penetration depth can be calculated by using the following formula:[12]

$$d_p = \frac{\lambda}{2\pi n_1 \sqrt{\left(\sin^2 \theta_i - n_{21}^2\right)}} \qquad \text{Eq.17}$$

where λ is the IR wavelength of the light, θ_i is the incident angle and $n_{21} = n_2/n_1$ (ratio between refractive index of sample and refractive index of ATR crystal). So, if θ_i is equal to θ_c, the light emerges in a direction parallel to the boundary between crystal and sample, but if θ_i exceeds θ_c, the light enters the rare medium but decays exponentially with a distance away from the crystal. Starting from Snell's law:

$$n_1 \sin\theta_i = n_2 \sin\theta_t \qquad \text{Eq.18}$$

Rearranging gives:

$$\sin\theta_t = n_{12} \sin\theta_i = \frac{\sin\theta_i}{n_{21}} \qquad \text{Eq.19}$$

where θ_t is the refracted angle of the transmitted beam in the second medium. For angles bigger than θ_c, θ_t becomes imaginary and the cosine function can be obtained from:

$$\sin^2\theta_t + \cos^2\theta_t = 1 \qquad \text{Eq.20}$$

By combining Eq.19 and Eq.20, we can express the cosine function of angle θ_t, as:

$$\cos\theta_t = -i\sqrt{\left(1 - \frac{\sin^2\theta_i}{n_{21}^2}\right)} \text{ or } \cos\theta_t = i\frac{\sqrt{\sin^2\theta_i - n_{21}^2}}{n_{21}} \qquad \text{Eq.21}$$

Also, the phase factor of the transmitted wave (τ) is described by the following equation:[13]

$$\tau = \omega\left(\theta_t - \frac{x\sin\theta_t + z\cos\theta_t}{v_2}\right) \qquad \text{Eq.22}$$

where ω is angular frequency ($\omega = 2\pi\upsilon$), x and z are the directions of propagation of the wave and v_2 is the velocity of the propagated wave in the sample at a specific time.

The electrical field amplitude (E) is proportional with:

$$E \approx e^{-i\tau} \qquad \text{Eq.23}$$

Then, we can write the following equation, which characterizes a non-homogenous wave which propagates along the boundary in the plane of incidence (x direction), and it varies exponentially with the distance z:[13]

$$e^{-i\tau} = e^{-i\omega\left(\theta_t - \frac{x \sin \theta_i}{n_{21} v_2}\right)} e^{-\frac{\omega z}{v_2}\left(\frac{\sqrt{\sin^2 \theta_i - n_{21}^2}}{n_{21}}\right)} \qquad \text{Eq.24}$$

Only a negative sign in front of the square root corresponds to the real situation, since the amplitude decreases very rapidly from the interface, otherwise this would tend to infinity with increasing distance.

Further, the second term of Eq.24 could be equated with the exponential decay of the evanescent wave from Eq.16 giving:

$$-\frac{\omega z}{v_2}\frac{\sqrt{\sin^2 \theta_i - n_{21}^2}}{n_{21}} = -\frac{z}{d_p} \qquad \text{Eq.25}$$

Starting from the definition of refractive index of the rare medium, where v_c is the speed of light in vacuum:

$$n_2 = \frac{v_c}{v_2} = \frac{\lambda\omega}{2\pi v_2} \qquad \text{Eq.26}$$

By rearrangement and substitution of v_2 into Eq.26, the expression of d_p is obtained:

$$\frac{\omega 2\pi n_2}{\lambda \omega}\frac{\sqrt{\sin^2\theta_i - n_{21}^2}}{n_{21}} = \frac{1}{d_p} \qquad \text{or} \qquad d_p = \frac{\lambda n_2}{2\pi n_2 n_1 \sqrt{\sin^2\theta_i - n_{21}^2}} \qquad \text{Eq.27}$$

Since the majority of the information is obtained within the depth of penetration, it is critical to understand this concept.

Experimentally, the depth of penetration has been understood by preparing samples made from identical material and under the same conditions, but having different thicknesses and collecting ATR spectra using identical settings (same ATR crystal, angle of incidence). Within the depth of penetration, it was obtained the same absorbance intensity specific to a certain wavelength no matter if film thicknesses were different.

Also, Mirabella[14] introduced the concept of "sampling depth", defined as the sampled depth normal to the surface and observed that its value is approximately three times greater than the corresponding d_p calculated under the same conditions. However, only 5% of the initial value remains at the "sampling depth", leading to the conclusion that d_p is the effective thickness that should be used for internal reflection evaluation. Thus, the absorber will be detected at depths smaller than the "sampling depth" because the strength of interaction between electrical field component and sample will decrease as this depth is approached. In order to have a better clarification between "depth of penetration" and "sampling depth", Figure 3.5 is an illustration of exponential decay of relative intensity of IR light as a function of distance away from an ATR crystal.

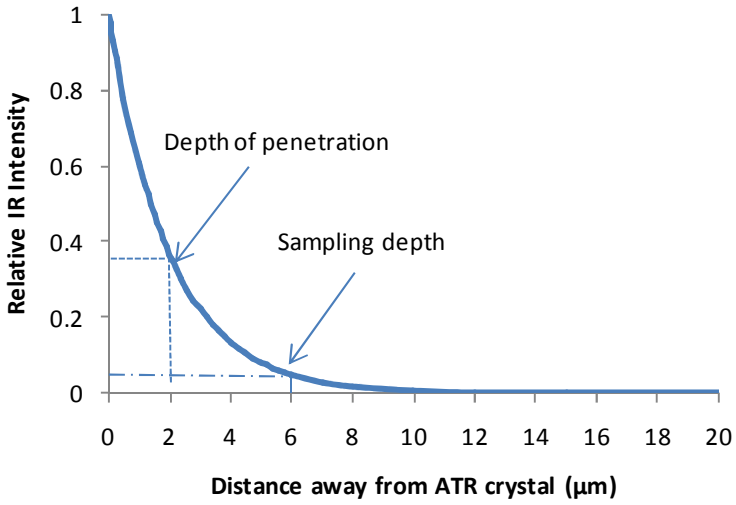

Figure 3.5 – Relative IR intensity as a function of distance away from ATR crystal.

As we can see from the depth of penetration formula (see Eq.17), it is possible to evaluate the sample surface at various depths by changing the type of the crystal (and hence n_2) or the angle of incidence. Figure 3.6 is an example of penetration depth variance with the refractive index of the ATR crystal, d_p decreases proportionally with increasing n_1 for a specific λ and constant θ_i and n_2. By maintaining constant θ_i, n_1 and n_2, d_p increases with λ. Also, d_p decreases proportionally with increasing θ_i for a specific λ and constant n_1 and n_2. An illustration of penetration depth dependence on these parameters, using a zinc selenide crystal into a sample characterized by a refractive index of 1.5 is shown in Figures 3.6 - 3.8. The type of crystal and the range of wavenumbers chosen into these analyses are relevant for this research.

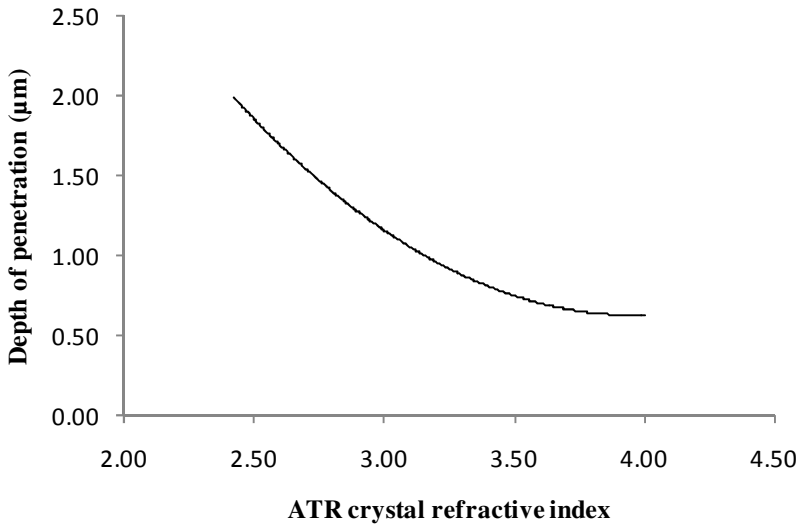

Figure 3.6 – Variation of penetration depth with type of crystal (different n_1). [$\theta_i = 45^o$; λ =9.02 µm (wavenumber = 1109 cm^{-1}) and $n_2 = 1.5$]. The value of the incident angle and wavenumber are specific to this research.

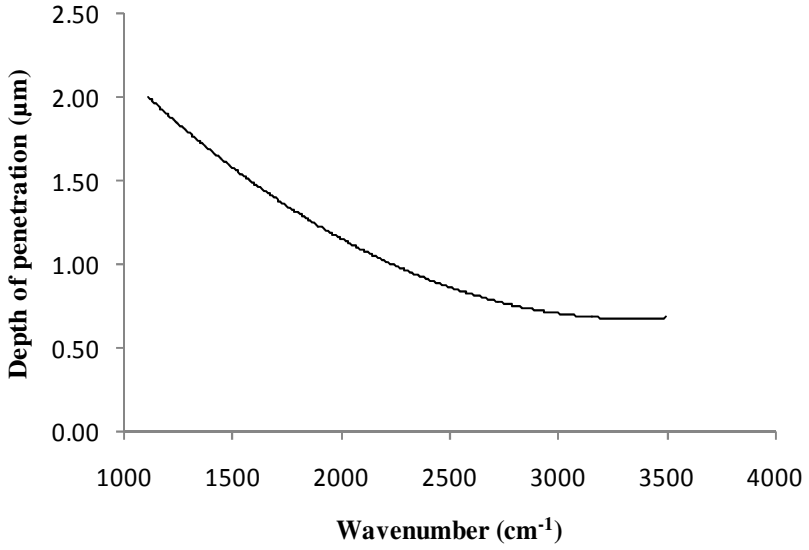

Figure 3.7 – Variation of penetration depth with wavenumber. [$\theta_i = 45^o$; $n_1 = 2.42$ (ZnSe) and $n_2 = 1.492$]. The value of the incident angle and type of crystal are specific to this research.

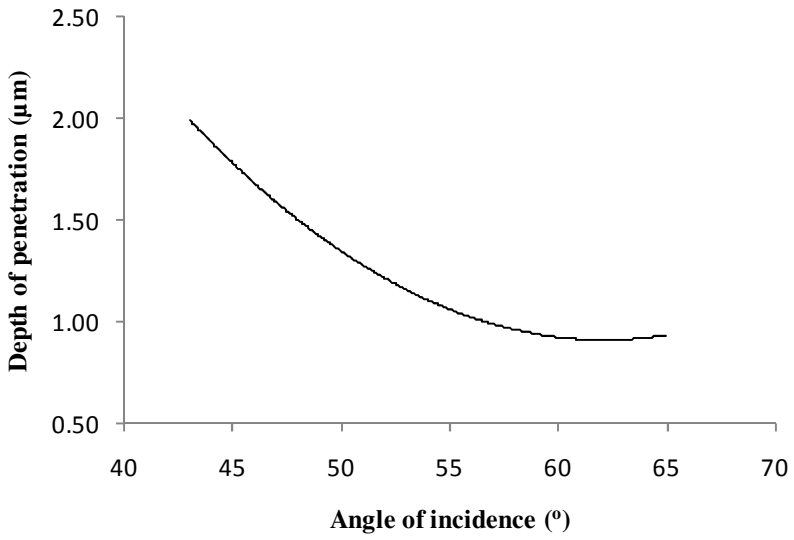

Figure 3.8 – Variation of penetration depth with angle of incidence. [λ =9.02 µm (wavenumber = 1109 cm^{-1}); n_1 = 2.42 (ZnSe) and n_2 = 1.492]. The value of the wavelength and type of crystal are specific to this research.

3.2.2 Advantages and disadvantages of ATR–FTIR spectroscopy

Several advantages make the ATR technique a very useful experimental method for surface characterization. A lot of research groups have used this method for interdiffusion studies for the following reasons:[15,16]

a. Data are collected *in situ* and in real time;

b. It is possible to evaluate various penetration depths for the same analyzed material and conditions; the depth can be vary by changing the ATR crystal;

c. It has minimal sampling errors compared with other techniques that require labeling or deuteration;

d. It could be considered a “non-destructive” technique because not all samples are damaged. Then, if the samples are not coated directly onto the ATR crystal they can be reused for other analyses;
e. It can be used to study liquid and solid single or multicomponent samples (such as mixtures, blends or thin coatings), if each component shows distinguishable IR absorption bands;
f. Being a surface technique, it is possible to be apply to very thin film evaluation with the condition that its thickness is at least equal with the characteristic penetration depth;
g. Any surface modifications such as, chemical or physical interaction could be seen by changes in the IR absorption spectrum;
h. Interdiffusion coefficients could be measured over a wide range of values 10^{-5} – 10^{-16} cm^2/s.

In order to have a good understanding of this technique in diffusion evaluation, its limitations should be discussed here:[15,16]

a. It is necessary to have very good contact between sample and crystal, in order to obtain an accurate penetration of evanescent wave into the sample;
b. It is difficult to reproduce the sample/ATR crystal contact, unless the studied film is coated onto the crystal;
c. The concentration of penetrant into a matrix during interdiffusion is calculated and not measured directly; a concentration – absorbance calibration curve obtained by collecting spectra of blends made from the two components of known concentration can be used in order to minimize the errors.

3.2.3 Selection of ATR crystal

Several requirements should be considered in choosing an ATR crystal, such as refractive index, spectral range, chemical properties, temperature resistance or surface quality. A basic review of the most common ATR crystal materials[17] is summarized in the following table:

Table 3.1 – Characteristics of ATR crystals.

ATR Material	ATR refractive index (n_1)	Spectral range (cm^{-1})	Chemical properties
Zinc Selenide (ZnSe)	2.42	15,000 - 525	Attacked by NH_3 and EDTA.
Silicon (Si)	3.42	9,500 – 1,500	Affected by strong acids - HF, HNO_3. Soluble in alkalis.
Germanium (Ge)	4.00	4,500 – 400	Affected by strong acids.
Amtir (Se, As and Ge)	2.50	20,000 - 700	Resistant to strong acids.
Diamond/ZnSe	2.42	30,000 - 525	Resistant to strong acids and alkalis.

In the experiments presented here, a crystal made from zinc selenide with a 1.8 mm diameter (2.54 mm^2 area), called MIRacle™ ATR crystal, has been purchased from PikeTechnologies. It has a refractive index of 2.42 and it is a hemispherical single bounce crystal.[18] A big advantage of ZnSe versus the other crystal types is its price. For example, ZnSe is three times less expensive compared to diamond and the crystal can be refurbished if it is scratched. Even if the hardness of ZnSe is smaller than other ATR crystals, ZnSe remains a good choice for our experiments, because the film was coated straight on the crystal and, therefore the contact between the crystal and the sample was made without a need for pressure. Another important factor in choosing the crystal is

related with the number of internal reflections. Theoretically, it is known that a multiple reflection ATR crystal should provide a high optical throughput. However, a multiple reflection crystal provides benefits for measurements of low concentration components of a sample. Since this is not the case here, we concluded that a single internal reflection would be adequate for these studies.[19] A picture of the ZnSe ATR crystal plate used in these studies is shown in Figure 3.9.

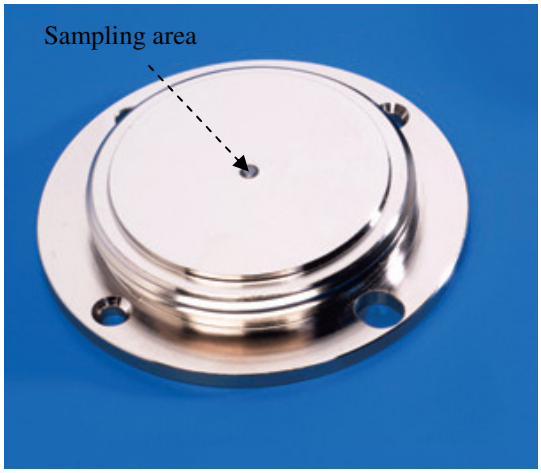

Figure 3.9 – Picture of ZnSe crystal plate for MIRacle™ ATR.[18]

A detailed representation of the IR light pathway within a MIRacle™ single reflection ZnSe ATR crystal can be seen in Figure 3.10.[18]

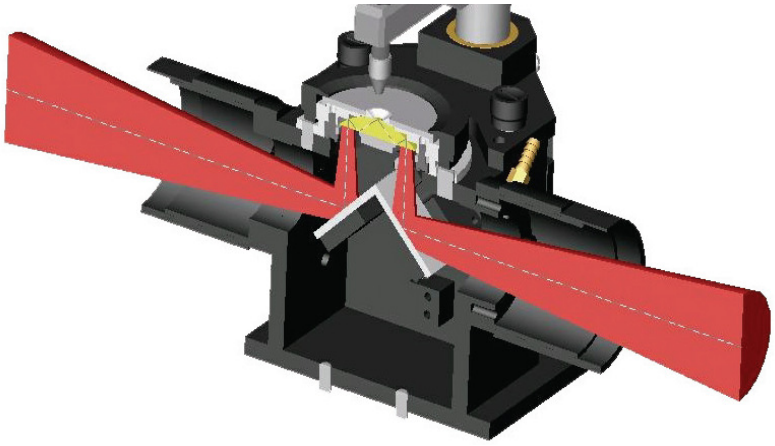

Figure 3.10 – Optical design of a single bounce ZnSe ATR crystal attachment.[18]

In general, the diameter of a PMMA film coated on the crystal was at least three times larger than the sampling area. As it is represented in Figure 3.10, the IR beam undergoes a single internal reflection as it propagates through the crystal before emerging at the other end. The IR beam is sent to the middle of the crystal at an incident angle of 43^{o}.

Spectral distortions might appear, if the incident angle is too close to the critical angle (within 1^{o}-2^{o}). In our case, the spectral distortions were avoided because the incident angle was 43^{o}, which is well above the critical angle that was calculated to be θ_c ~ 38^{o} by using Eq.15.

3.2.4 Preparation of PMMA/POE samples

In order to have good contact between the crystal and the polymer, PMMA films (between 18 – 106 μm) were cast directly from ~ 15 wt % PMMA (M_w = 120,000 g/mol) in toluene solutions on the ZnSe ATR crystal. We considered spin coating in the beginning of my studies, but this method was eliminated because the film obtained was too thin for the studies performed here. Many things were tried, such as increasing the concentration of the polymeric solution or slowing down the speed of the spin coater or even preparing the film on a glass slide and after transferring to the crystal, but none of those worked well. So, casting from solution has been identified as the right method for this case, because of the following reasons:

a. Construction of ATR crystal - As can be visualized in Figure 3.9, the crystal is mounted into a metal plate and between the crystal and the plate is a gap. Also,

the shape of the crystal is hemispherical and more of the polymeric solution has the tendency to go into this gap and only a very thin film will be cast on the top of the crystal which might not be enough for our diffusion studies, because the thickness must be at least 2 μm (thickness of the entire film must be ≥ than depth of penetration).

b. Temperature of studies – As will be discussed later, some of the diffusion studies were conducted at 110 ^{o}C above glass transition temperature of PMMA and at this temperature the diffusion of POE into PMMA has been determined to be very fast and as a result the necessity of having a thick PMMA film was mandatory for ATR – FTIR spectroscopy measurements done here.

The solution was obtained by dissolving poly(methylmethacrylate) (~ 0.75 g, M_w = 120,000 g/mol) in toluene (5 ml), and the mixture was sonicated for at least five hours or until the solution became clear to ensure complete mixing. The drops of PMMA solution were placed on ZnSe crystal by using glass pipettes. About 300 μl of solution were used to prepare each film. The smooth films were obtained by slowly evaporation of solvent under saturated atmosphere with toluene (ATR crystal attachment coated with the PMMA film was placed into a glass Petri dish and covered with a glass top) at room temperature for 24 hours, followed by drying under vacuum for 5 hours at 20 ^{o}C, and further drying under vacuum for another 4 hours at 60 ^{o}C to remove any residual solvent. The films were examined for cracks by using an optical microscope Bausch & Lomb with a magnification of 50X and they showed surface free of cracks. It must be emphasized that all the films used in my studies were evaluated for cracks by using an optical microscope and only those without cracks were used for further diffusion evaluation.

The thickness of all poly(methyl methacrylate) films was determined by using a profilometer, Surfcom 480A distributed by TKS (see Figure 3.11), which gives the contour of the surface.

Figure 3.11 – Picture of profilometer used in thickness measurements.

The steps described below were followed in all the profilometry measurements:

a. Before starting measurements, the calibration of the instrument was done. The profile of a metal plate with a known roughness (3.18 µm) was determined. The profilometer passed the calibration, if the roughness was determined to be 3.18 µm ± 0.1 µm.

b. The profile of the crystal without the PMMA film was collected and the value of the thickness was determined. A picture of ZnSe ATR crystal profile is shown in Figure 3.12., where H_{max} represent the profile of the crystal by itself.

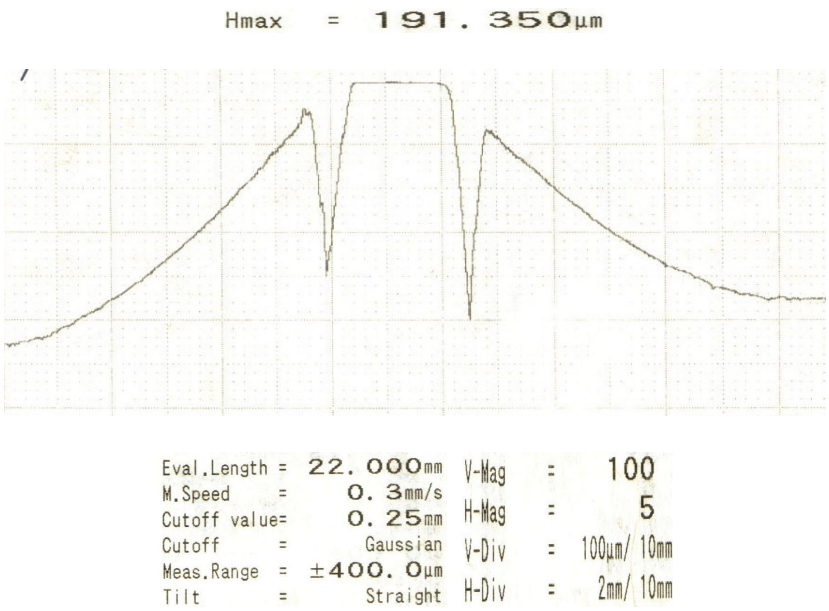

Figure 3.12 – Profile of ZnSe crystal without PMMA film coating.

c. After the PMMA film was coated on the crystal and dried by following the method described earlier, another profile was taken and a new height was determined. It must be mentioned that the calibration of instrument was checked again before taking the new profile. Also, the starting point used in taking the profile of ATR crystal coated with polymeric film must be identical with that taken on the crystal by itself. Figure 3.13 is an example of the ZnSe ATR crystal profile coated with PMMA film. In this case H_{max} represents the profile of the crystal coated with the polymeric film.

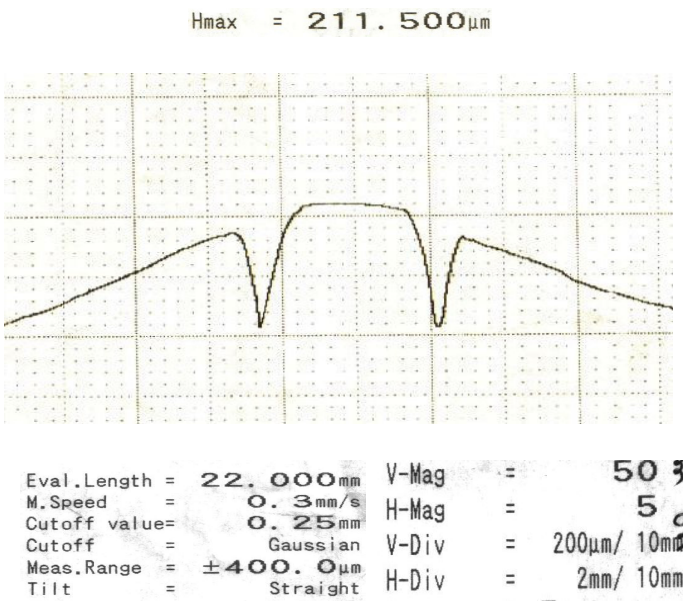

Figure 3.13 – Profile of ZnSe crystal coated with PMMA film.

d. The thickness of the film was determined as the difference between the H_{max} of the crystal cast with PMMA film and H_{max} of the crystal by itself. In the example shown above, the thickness of the film is determined as: 211.50 µm – 191.35 µm = 20.15 µm.

Another method that can be used to measure the thickness of a film is ellipsometry. This method was considered, but it was not used since the PMMA film thicknesses prepared for these studies were above its maximum value (~ 10 µm).

The interdiffusion studies between PMMA120K and linear or cyclic POE oligomers (diffusant) were carried out at 60 ^{o}C, 85 ^{o}C and 110 ^{o}C. A heated cell (plate) connected to a temperature controller (Watlow988, Pike Technologies) was attached to the system. The ATR crystal plate was placed onto the ATR attachment as shown in Figure 3.14 and the heating element was attached to the crystal (See Figure 3.15).

Figure 3.14 – Picture of ATR crystal coated with PMMA matrix film.

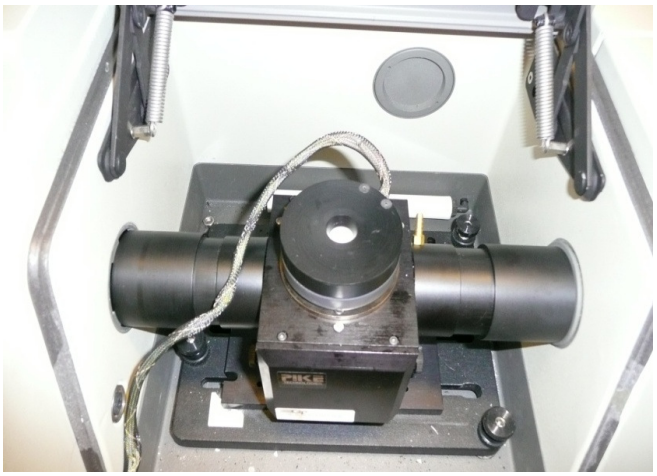

Figure 3.15 – Picture of ATR attachment with variable temperature accessory mounted on the top.

The ATR accessory (including the heating cell on the top) was attached to the spectrometer and heated up to the desired temperature of measurement, respectively 60 ^{o}C, 85 ^{o}C or 110 ^{o}C. To maintain a constant temperature environment, aluminum foil was placed on the top of the heating cell. Figure 3.16 represents a picture of the final set-up.

Figure 3.16 – Picture of Bruker Vector 22 FTIR spectrometer with ATR accessory.

The PMMA film cast on the crystal was heated up to the desired temperature of study for 30 minutes to ensure a constant and uniform temperature of the film.

About 20 µl of the poly(oxyethylene) penetrant, linear (lPOE500) or cyclic oligomer (cPOE400 or cPOE1000) were placed on the top of the heated polymeric film by using a micropipette. Before the placement, the penetrant was heated up separately in a vial to minimize errors that might appear if the components had different temperatures at the beginning of the interdiffusion process. To maintain a controlled and uniform diffusion process, we wanted to have an infinite reservoir of POE on the top of PMMA. The maximum size of PMMA films was about 106 µm. From DSC studies (described in Chapter 4) we know the equilibrium concentration of POE into PMMA is about 40 wt % for linear and about 50 wt % for cyclic. Thus 20 µl should be more than enough to provide an infinite reservoir of diffusant. Furthermore, we conducted studies using less

than 10 µl of penetrant and observed a slowing down of the diffusion. Also, at the end of the experiments the residual POE was left on the top of POE films.

The main characteristics of these materials, including the abbreviation of each component of the interdiffusion system, as well as temperature of study are shown in Table 3.2.

Table 3.2 - Main characteristics of polymers and temperature of interdiffusion studies.

Main Characteristics of polymers		POE end groups	MW (g/mol)	Abbreviation	T_g (°C)	Physical State at room temperature	Temperature of study
PMMA Polymer matrix		-	120,000	PMMA120K	105	solid	
POE Oligomer diffusants	Linear	$-OCH_3$	500	lPOE500	-70	liquid	60 °C, 85 °C, 110 °C
	Cyclic	-	400	cPOE400	-70	liquid	110 °C
		-	1000	cPOE1000	-55	waxy	

3.2.5 Equipment set-up

A Bruker Vector 22 FTIR spectrometer with ATR accessory was used to obtain infrared spectra which were collected at a resolution of 4 cm^{-1} (a spectrum contains a data point every 4 cm^{-1}) with 32 averaged scans. A single scan corresponds to one translation of the moving mirror back and forth that has a characteristic mirror velocity. The spectrometer is equipped with a DTGS detector (deuterated triglycine sulfate) which acts as a transducer, by transforming the infrared intensity into an electrical signal that is converted by using a Fourier transform function into a spectrum. The detector produces an electrical signal proportional with the amount of IR radiation striking it and sends the signal for processing to a computer. There are a variety of detectors that could be used for collecting FTIR data, each type being sensitive to a unique frequency range and

allows analysis of a wide range of sample types. The most common types of detectors that respond to frequencies from the mid-IR range are triglycine sulfate (TGS) or deuterated triglycine sulfate (DTGS) and mercury cadmium telluride (MCT).[17] The descriptions of the spectrometer used in these studies, as well as the sampling parameters are given in Table 3.3. The instrument is connected to a data station running "Opus" software.

Table 3.3 – FTIR spectrometer and data collection description.

Spectrometer	Bruker Vector 22
Source	IR (MIR - Globar)
Detector	DTGS
X - axis	Wavenumber (cm^{-1})
Y - axis	Absorbance
First X value	600 cm^{-1}
Last X value	4000 cm^{-1}
Number of sample scans	32
Resolution	4 cm^{-1}

The sample set-up procedure consists of the following steps:

a. After drying the film, but before starting to prepare the system for interdiffusion studies at high temperatures, the spectrum of PMMA was collected and room temperature. The quality of the PMMA spectrum gives us a good indication of film quality.

b. The cell (plate) of the heating unit was mounted on top of the PMMA film and this system was preheated to 60 ^{o}C, 85 ^{o}C or 110 ^{o}C for 30 minutes, as explained above. To obtain a constant temperature of the film, preheating was a necessary step.

c. The spectrum of PMMA (heated up to the desired temperature of study) was collected again (at least 2 times) before the POE was added onto the top of the film. No changes between the spectrum taken at room temperature and the spectrum collected at high temperature were seen. This time was considered time zero.

d. The POE liquid (which was heated up) was transferred instantaneously to the PMMA film and within 5 seconds the first POE/PMMA interdiffusion spectrum has been collected. This initial spectrum is also a valuable quality check of the set-up, because the presence of cracks in the film or wicking of POE around the film can be identified only by looking at this spectrum. If any of these problems were observed, the experiment was stopped. All of these details are described in the following section of this chapter.

e. Spectra were collected every minute until the interdiffusion process was completed and equilibrium was reached. It must be emphasized that during the entire interdiffusion process, the changes in film quality that might appear due to possible film fractures or delamination of the film from the ATR crystal are visualized instantaneously in the spectra. If any of these problems were observed, the experiment was stopped immediately.

3.2.6 Spectra collection

A background spectrum was collected and stored for each system before coating the PMMA film onto the ATR crystal. An example of a background spectrum is shown in Figure 3.17.

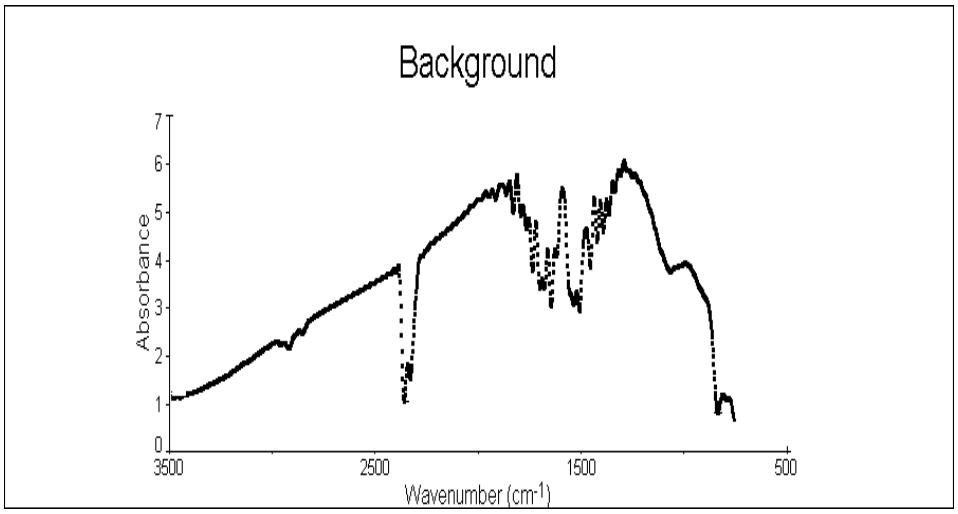

Figure 3.17 – A single beam background spectrum.

The strong peak seen at 2350 cm^{-1} and the fingerprint region shown between 1850 cm^{-1} and 1350 cm^{-1} are due to carbon dioxide and water vapors, respectively.

A spectrum of the uncoated ATR crystal was collected to check for any contamination. If peaks were observed in this spectrum, the crystal was cleaned further with solvent and another spectrum collected again until no peaks were observed.

If a spectrum is collected 5 minutes after coating the PMMA film on the ATR crystal, as expected, the solvent is still present in the PMMA film because the time was insufficient to permit the entire solvent removal. A literature spectrum of toluene[20] is provided in Figure 3.18. Usually, the bands in the 1610 – 1500 cm^{-1} region are shown by most six-membered aromatic ring systems and constitute a valuable identification of such

systems.[21] Further bands are shown by aromatic rings in the fingerprint region between 1225 and 650 cm^{-1}.

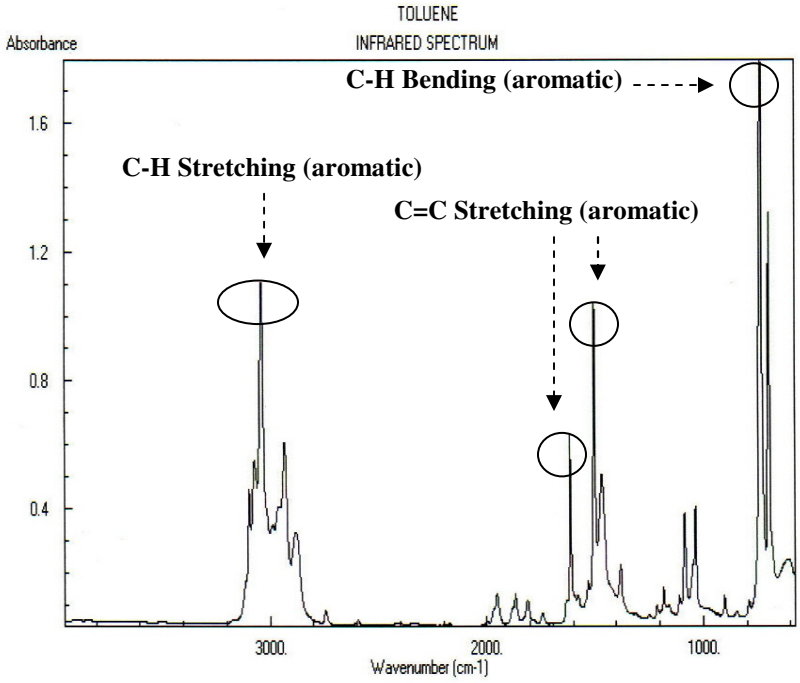

Figure 3.18 – IR spectrum of toluene.[20]

Figure 3.19 (a) shows the spectrum of a PMMA120K film taken 5 minutes after coating on the ZnSe ATR crystal, while for a better visualization Figure 3.19 (b) shows only the area between 3500 cm^{-1} and 1000 cm^{-} because the intensities of peaks specific to toluene at ~ 670 cm^{-1} are very high. Thus, the peaks at 1602 cm^{-1} and 1500 cm^{-1} specific to toluene are powerful tools for a quality check of the PMMA film. If these peaks are present in a spectrum of a PMMA film obtained by toluene casting, then the residual solvent was not entirely removed.

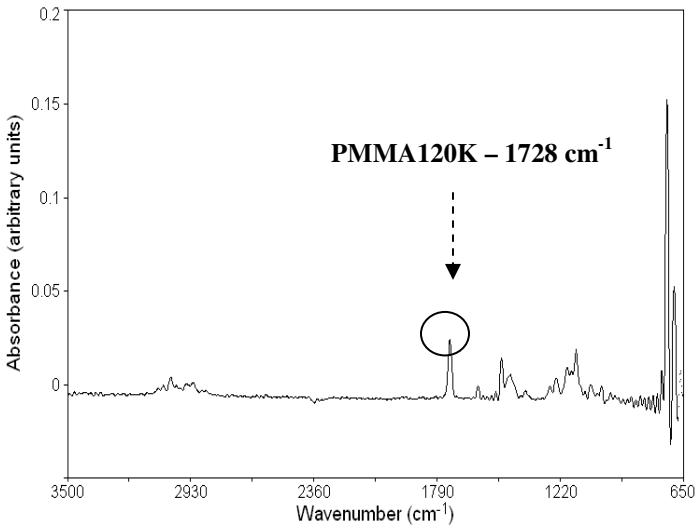

(a)

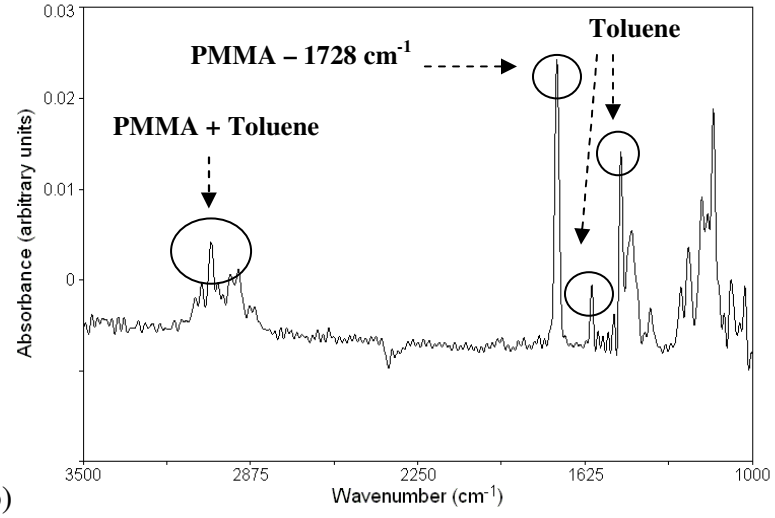

(b)

Figure 3.19 – (a) Initial spectrum of PMMA120K coated on ZnSe crystal by solvent removal from 15% PMMA solution in toluene – 5 minutes after coating. (b) Initial spectrum (wavenumber region of 3500 cm^{-1} and 1000 cm^{-1}) of PMMA120K coated on ZnSe crystal by solvent removal from 15% PMMA solution in toluene – 5 minutes after coating.

To ensure that the solvent was completely removed, the spectrum of the PMMA120K matrix film was taken just before starting each interdiffusion experiment. Figure 3.20 corresponds to a PMMA120K spectrum collected after drying under the conditions described above.

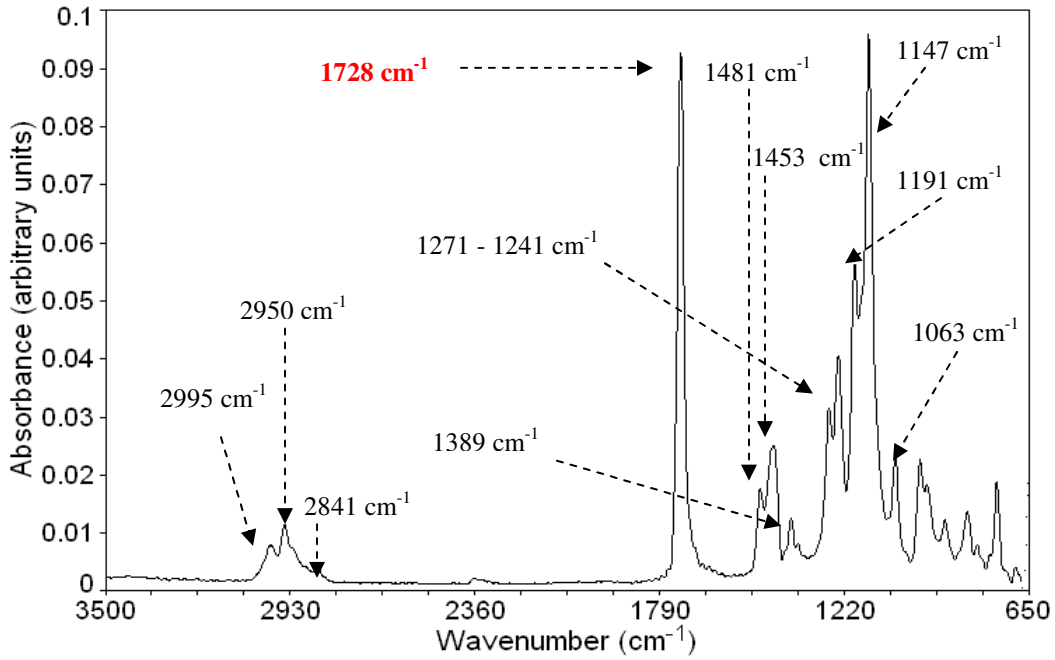

Figure 3.20 – Spectrum of PMMA120K film taken after drying and before initializing diffusion of POE into PMMA.

No residual toluene solvent can be seen in this spectrum. A transmission spectrum of PMMA taken from the literature[22] is shown in Figure 3.21.

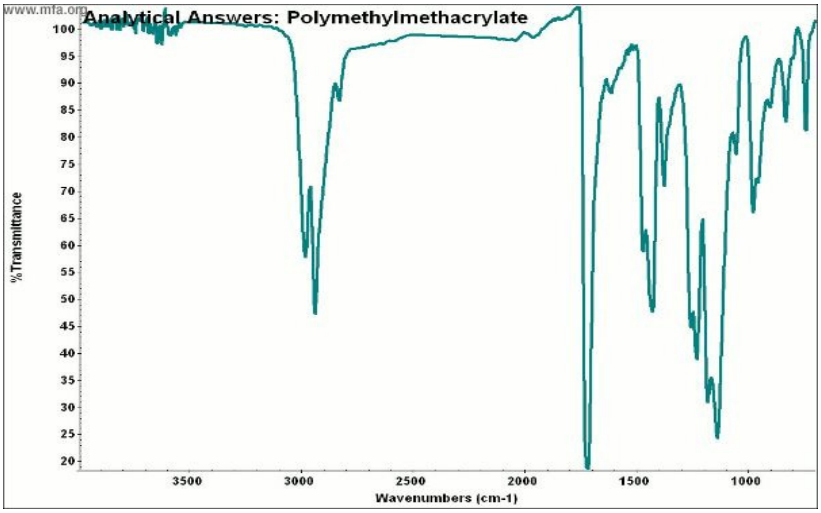

Figure 3.21 – IR spectrum of poly(methyl methacrylate).[22]

Each peak specific to PMMA is identified in Figure 3.21. The probable assignments associated with group vibrations present in PMMA are described in the following table.

Table 3.4 – Peak Assignments of PMMA.

Band (cm^{-1})	**Peak assignment**
2995/2950	Ester methyl C-H stretching
2841	$-CH_3$ stretching
1728	C=O stretching vibration
1481/1453/1438	C-H deformations
1389	$-CH_3$ symmetrical deformation
1271-1063	C-O stretching

The quality of the film might be determined only by looking at PMMA spectrum. Hence, the presence of cracks in the polymeric film will be seen immediately. If POE diffusant is added on the top of PMMA matrix, diffusion is instantaneous and a peak at 1109 cm^{-1} characteristic to poly(oxyethylene) appears immediately. From the beginning, its absorbance is huge and it is not increasing in time as happens in case of a real

diffusion process. Hence, in order to be able to evaluate correctly the diffusion process, a careful attention must be accorded from the beginning of experiments.

The diffusion process of linear or cyclic POE oligomers into the PMMA matrix started as soon as the diffusant was added on the top of the film, but it was observed only when POE reached the penetration depth. The peak chosen for diffusion evaluation of poly(oxyethylene) was the ether C-O-C stretching mode at 1109 cm^{-1}, as shown in Figure 3.22. As interdiffusion proceeds, the intensity of this peak absorbance increases in time, while the intensities of the peaks characteristic to poly(methyl methacrylate), for example at 1728 cm^{-1}, decrease in time, until the diffusion process is completed.

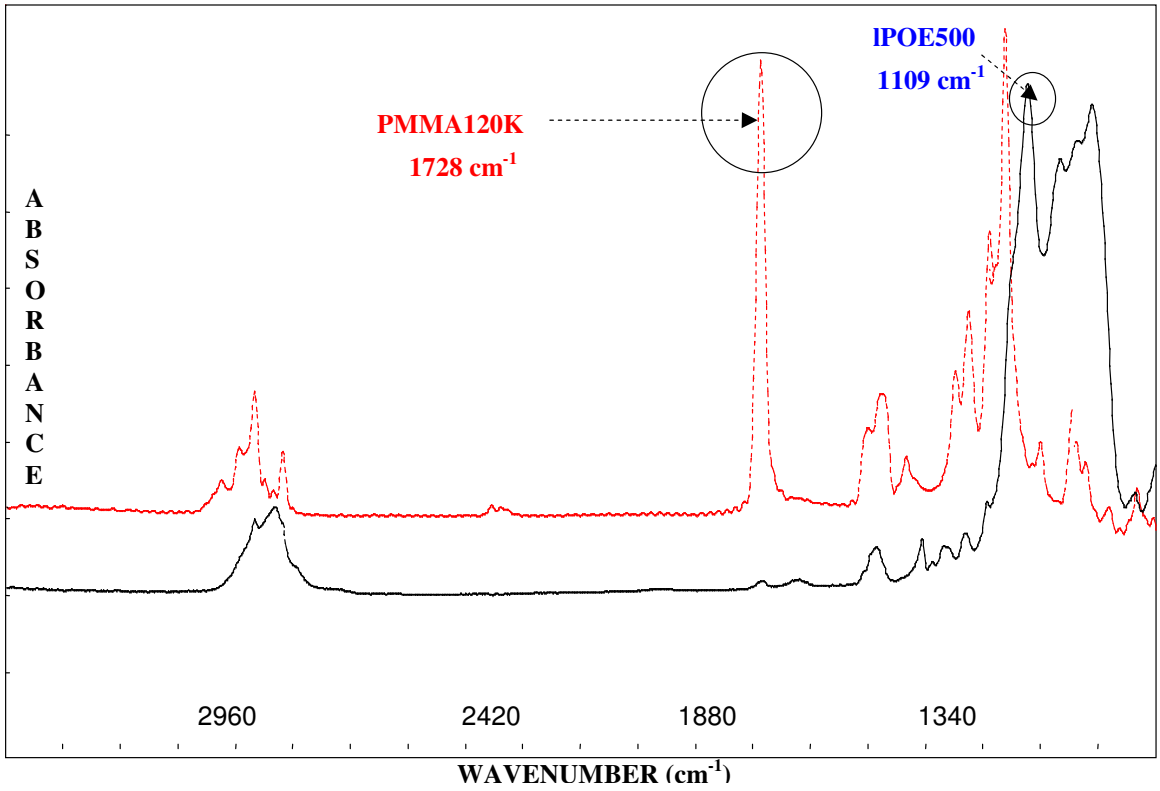

Figure 3.22 – PMMA120K spectrum (top) and lPOE500 spectrum (bottom).

Figure 3.23 represents an example of an interdiffusion experiment conducted at 110 ^{o}C for a PMMA120K/lPOE500 sample. The two peaks selected to evaluate the interdiffusion between PMMA and POE each are shown in Figures 3.24 and Figure 3.25 as a function of time.

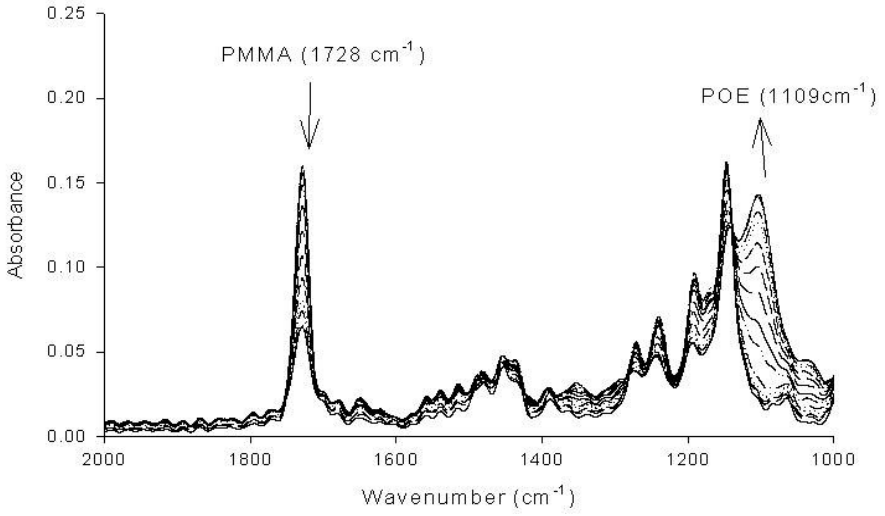

Figure 3.23 – Spectra evolution in time for PMMA120K/lPOE500 interdiffusion system, run at 110 ^{o}C. Peak at 1728 cm^{-1} corresponds to PMMA and peak at 1109 cm^{-1} to POE. Spectra were collected at 1 minute time interval.

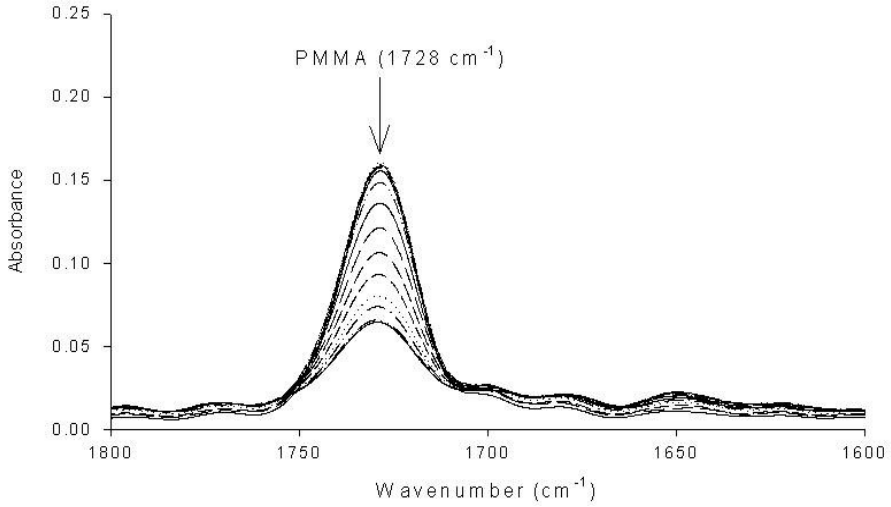

Figure 3.24 – Spectra evolution in time of carbonyl bond vibration at 1728 cm^{-1} characteristic to PMMA, during interdiffusion studies run at 110 ^{o}C between PMMA120K and lPOE500. Peak intensity decreases in time. Spectra were collected at 1 minute time interval.

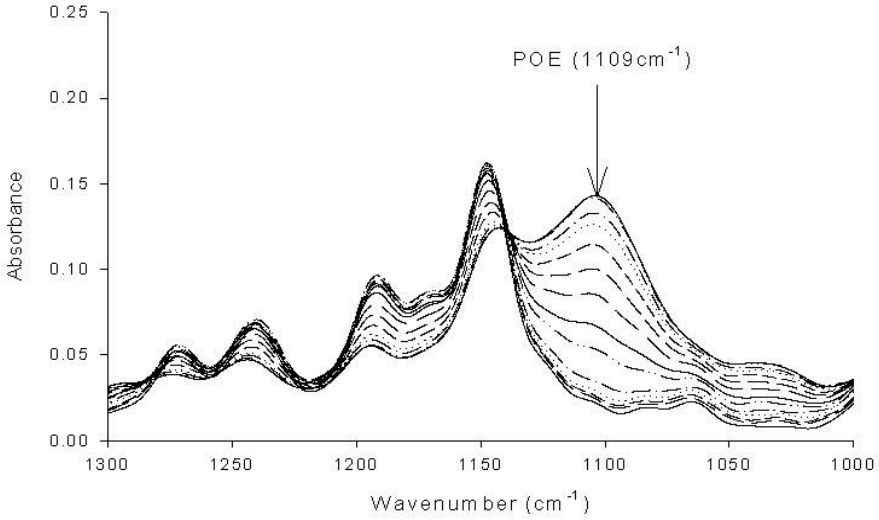

Figure 3.25 – Spectra evolution in time of ether bond stretching at 1109 cm^{-1} characteristic to POE, during interdiffusion studies run at 110 ^{o}C between PMMA120K and lPOE500. Peak intensity increases in time. Spectra were collected at 1 minute time interval.

3.2.7 Spectral deconvolution

Deconvolution is a curve fitting process used to find the best collection of individual peaks whose sum matches the original spectrum of overlapped bands.

To evaluate the interdiffusion from ATR-FTIR spectroscopy, distinguishable infrared bands were identified for the two species involved in this process. In my experimental set-up, IR radiation propagates through the ATR crystal characterized by a high refractive index (n_1 = 2.42) and undergoes total internal reflection at the interface with the PMMA film, because the angle of incidence was higher than the critical angle, which was calculated by using Equation (15) ($\theta_i = 43^o > \theta_c = 38^o$). As discussed before, the PMMA film was coated directly on the crystal and defined as the "rare medium" due to its lower refractive index ($n_2 = 1.492$[3] determined at 589.3 nm, 20 ^oC). At the interface between the crystal and the polymer, an evanescent wave penetrates into the polymer only a short distance (depth of penetration d_p) and some energy is absorbed in this medium due to molecular vibrations. The reflected beam containing absorbance information exits the opposite end of the crystal and it is directed to the detector of the FTIR spectrometer. The attenuated IR beam is recorded as an interferogram that is used to generate an IR spectrum.

The ATR spectrum of PMMA/POE that shows a distinct absorption band at 1109 cm^{-1} specific to the ether C-O-C stretching mode that belongs to POE was used to quantify POE movement into PMMA during the interdiffusion process. At the same time, the intensity of the absorption band at 1728 cm^{-1} due to carbonyl C=O stretching

vibrations characteristic to PMMA changes as a result of dilution of the matrix. The experiments were conducted as a function of time. As interdiffusion advances, the absorbance characteristic to POE at 1109 cm^{-1} increases in time due to oligomer migration into PMMA, and the PMMA-specific absorbance at 1728 cm^{-1} decreases in time due to dilution of this polymer. The POE absorption band at 1109 cm^{-1} was used for quantitative analysis by deconvoluting the spectra to determine the area under this peak. The normalized weight concentration of penetrant specie was calculated from the peak areas by using a calibration curve. The deconvolution program PeakFit v4.12 for Windows provided by SeaSolve Software Inc. is an automated curve fitting program designed to fit the experimental data to a set of calculated Gaussian, Lorentzian, Voigt or Pearson VII peaks. PeakFit offers three autofit options for identifying and fitting peaks, each of these options being capable of finding hidden peaks. The option called "AutoFit Peaks I Residuals" was the most basic one, but the most effective algorithm that could be applied to these studies. The peak widths were varied so that the overall area of the deconcoluted peaks was equal to that of the raw data. To verify the accuracy of the results obtained by using this deconvolution program, fitted parameters were automatically calculated based on goodness of fit criteria at 95% confidence interval. The best fit was obtained with Gaussian peaks and it was considered to be accurate if the R^2 correlation coefficient value was close to 1.0. Figure 3.26 shows a deconvoluted ATR-FTIR spectrum of lPOE500/PMMA120K after 15 minutes difussion time.

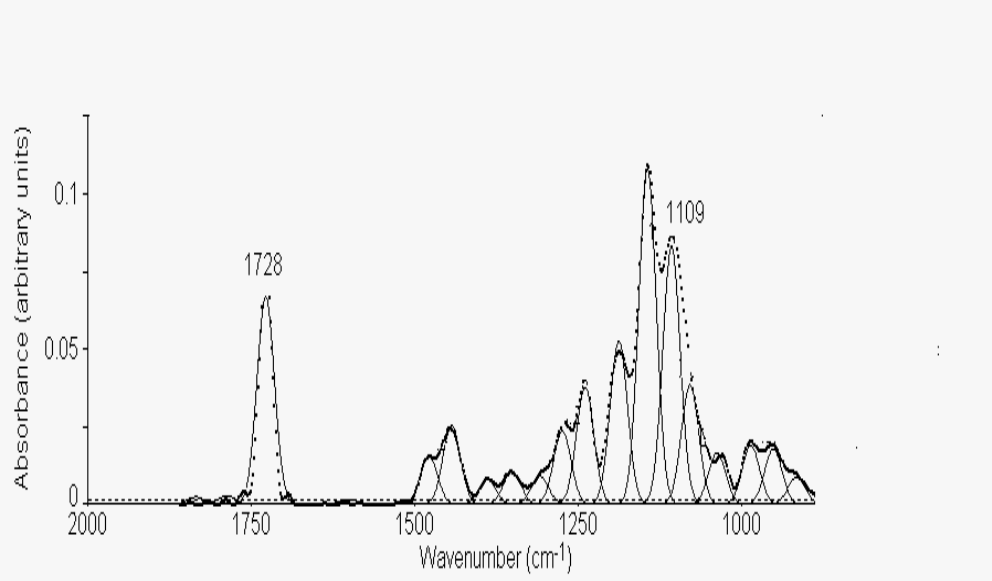

Figure 3.26 - Deconvolution of ATR-FTIR spectrum of lPOE500/PMMA120K after 15 minutes of diffusion at 110 ^{o}C. Absorbance at 1728 cm^{-1} is characteristic to carbonyl bond from PMMA and absorbance at 1109 cm^{-1} to ether bond from POE. Dotted lines correspond to original spectrum and solid lines represent the deconvoluted peaks using Gaussian distribution. The accuracy of the fit is indicated by good statistic values: $R^2 = 0.99$.

The areas under the peaks determined by deconvoluting the raw spectrum were used to calculate the concentration of POE.

3.2.8 Absorbance – concentration calibration curve

The absorbance is proportional with concentration (Beer-Lambert law). To relate the mass fraction of POE to its relative absorbance that increases in time during interdiffusion, a calibration curve was required. Blends of lPOE500 and PMMA120K with known composition, respectively 5%, 10%, 20%, 30%, 40% through 90% POE by weight into PMMA were solvent cast on the ZnSe ATR crystal from 15% solutions in toluene. After the films were prepared by following the same procedure as that used in

obtaining the PMMA films (see Section 3.2.4.), their spectra were collected at room temperature. Figure 3.27 shows the ATR-FTIR spectra of six blends with a specific composition by weight (5%, 20%, 40%, 60%, 70% and 80% lPOE500 into PMMA120K). Even if the studies were conducted at different temperatures, the same calibration curve can be used for all temperature of studies, because the absorbance has not been found to vary with the temperature. From literature, it is known that the refractive index of the polymer might change with temperature, and therefore this can have an influence on the depth of penetration (see Eq.17). If the temperature is increased, the refractive index of the sample might decrease and it is possible that the depth of penetration may become slightly smaller. Thus, a maximum decrease of the sample refractive index of 2% may generate a reduction of 4.5% in the depth of penetration. All these factors will be included in the error assessments.

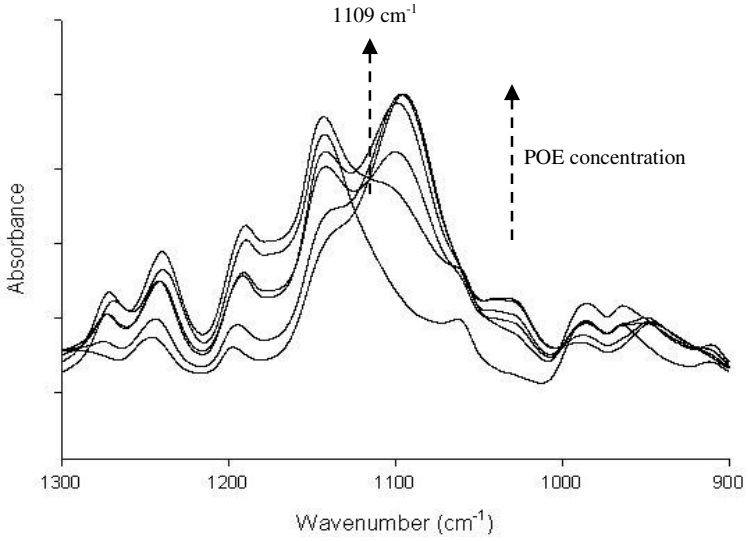

Figure 3.27 – ATR – FTIR spectra of lPOE500/PMMA120K blends of 5%, 20%, 40%, 60%, 80%, 90% POE by weight in PMMA collected at room temperature. The films were cast on ZnSe crystal. The absorbance specific to ether bond stretching at 1109 cm^{-1} of POE component increases with increasing POE concentration.

Due to limited availability of cyclic POE, it was not possible to prepare as many blends as in the case of linear POE, but two blends of cPOE1000/PMMA120K, respectively 25% and 40% POE were prepared and their spectra were collected. It was found almost the same dependence of absorbance versus concentration as in case of linear oligomer blends. Thus, we used the same calibration curve for all our samples.

The areas under the peaks determined by deconvoluting the raw spectra were used to obtain the absorbance – concentration calibration curve, as will be described in the next chapter.

3.2.9 Principal sources of experimental errors

The principal sources of experimental errors in the ATR-FTIR interdiffusion experiments are described below:

a. *Film preparation*, such as inadequate or incomplete removal of solvent. A fast solvent evaporation can create voids or pores in the polymer matrix as "permanent defects" into which penetrant can move quickly at the beginning of a diffusion process. At the same time, a residual solvent present in the film might generate a pathway for fast diffusion.
b. *Bad quality of the film* related with the presence of "cracks", uneven surface of the film or its delamination from the ATR crystal. As discussed here, all these defects can be identified by using microscopy techniques, as well as spectral analysis.

c. *Film thickness measurements*. The error in film thickness measurements does not affect the absorbance values, but it has a direct effect on induction period, which represents the initial time until the penetrant reaches the penetration depth.

d. *ATR crystal imperfections*, such as scratches. The depth of penetration of the IR beam depends on crystal quality. The presence of scratches can influence the IR beam pathway. If any scratches are present on the crystal these errors are minimal if identical set-up is followed for all diffusion studies. Consequently, the errors that might be generated from a variance in depth of penetration will have the same magnitude for each sample pair.

e. *Amount of diffusant* used for interdiffusion studies. If the amount of POE diffusant is not enough, the interdiffusion process slows down or stops before reaching final equilibrium. After each experiment is finished, the POE must still be found on the top of the matrix which is a good indication of sufficient diffusant.

f. *Temperature measurements*. It is well known that the temperature affects the diffusion process. The influence of the errors generated from temperature measurements can be seen especially in the length of the induction period. If the temperature was measured incorrectly, for example the desired temperature was not yet achieved, but the penetrant was already added on the top of the matrix, a longer induction period can be observed.

g. *Spectral deconvolution*. The curve fitting program must be used very cautiously since more than one apparently correct result could be obtained. Different sets of parameters can give equally good results suggesting that the solution is not

unique, but once the parameters were selected carefully the most reasonable results could be obtained. A good indication of the fit accuracy can be obtained by using statistical evaluations, such as the correlation parameter R^2.

A careful error analysis followed by the determination of their magnitudes represents an important aspect of the results validation (see Appendix).

3.3 DIFFERENTIAL SCANNING CALORIMETRY (DSC) MEASUREMENTS

Thermal analyses were conducted on a Seiko SSC/5200 DSC. Blending solutions of lPOE500/PMMA120K with different compositions by weight from 0/100, 5/95, 10/90, 20/80, 30/70 through 100/0 in 15% by weight in toluene were used to prepare films by solvent casting on glass slides. The films were dried at room temperature for few days, followed by drying under vacuum at room temperature (overnight) to eliminate residual solvent. Further, they were peeled from the glass slides and 5-10 mg of each sample was sealed in aluminum crucibles and placed in the DSC furnace under a flux of nitrogen for thermal properties evaluation. Each composition was held for 5 minutes at -120 ^{o}C, heated from this temperature to 150 ^{o}C at a heating rate of 10 ^{o}C/min, held 5 minutes at 150 ^{o}C, cooled to the same starting temperature at 10 ^{o}C/min, and heated again to 150 ^{o}C at 10 ^{o}C/min.

3.4 GRAVIMETRIC STUDIES

Due to limited availability of cyclic POE, only the diffusion of linear POE 500 g/mol into PMMA was studied by both spectroscopic and gravimetric techniques. To conduct the gravimetric experiments, PMMA120K polymeric films were prepared by dissolving poly(methyl methacrylate) into toluene, 15 wt %. The solution was poured into aluminum pans and the films were dried for two days at room temperature under a saturated atmosphere of toluene, followed by drying under vacuum at room temperature for another 24 hours and further drying under vacuum at 60 ^{o}C for another five hours. The films were carefully detached from the aluminum pans and cut into rectangular pieces (13.16 mm x 13.12 mm) by using a knife. The thickness of each polymeric film was measured with a digital micrometer and it was found to be between 200 – 250 μm. Each film was labeled and its weight was determined using a microbalance, Mettler Toledo – MT5 within a precision of ± 1 μg. The set-up used for gravimetric studies is shown in Figure 3.28.

About 10 ml. of linear POE 500 g/mol was poured into a big aluminum pan and heated up for 30 minutes to the desired temperature of study, respectively 60 ^{o}C or 85 ^{o}C. The same temperatures were chosen for gravimetric evaluation as those used for spectroscopic analyses.

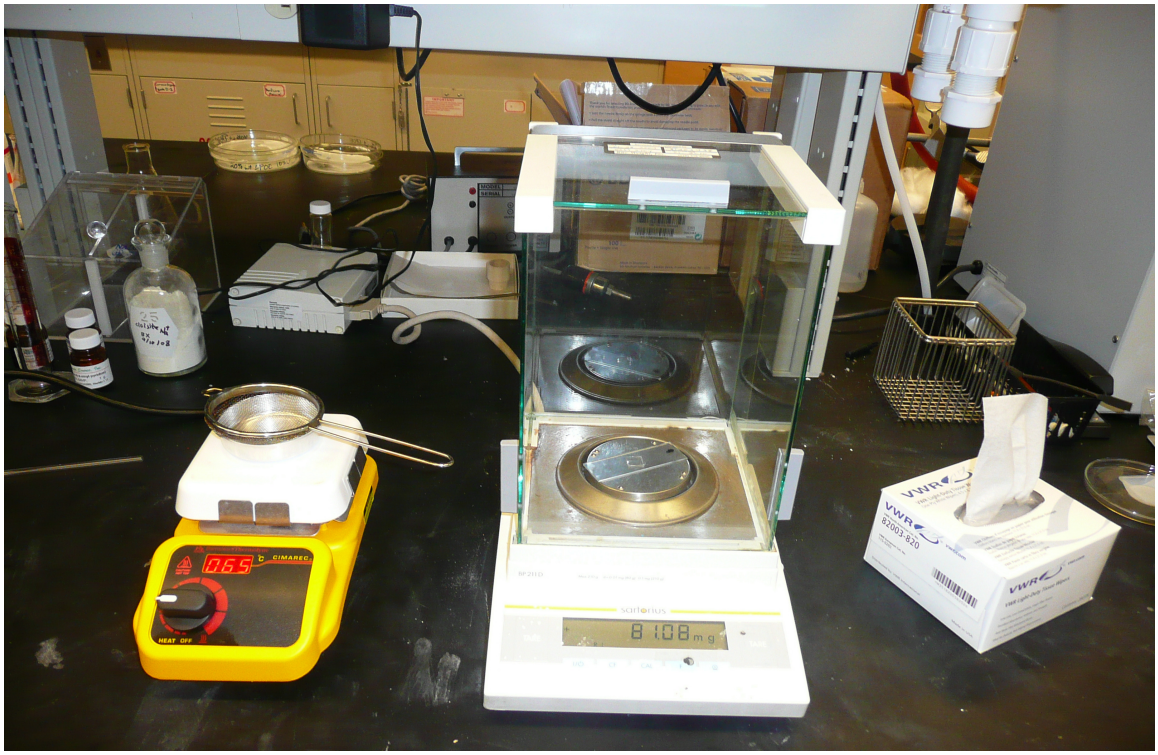

Figure 3.28 – Set-up of gravimetric experiments.

The PMMA films were immersed into the POE heated up to the temperature required for these studies. In order to assure a constant diffusion through both sides of the film, a net (wired lattice) was used when the film was immersed into the penetrant. The diffusion was followed by taking out one film at every 3 minutes and weighing it. It must be noted that the excess of POE was removed by cleaning the films (using wipes) before weighting. While some errors are introduced via this method, their magnitude should be similar for each measurement if the same steps were followed.

The mass of each PMMA film immersed into penetrant increased in time as a result of POE diffusion and the uptake of sorbed diffusant was measured as a function of time. Therefore, the mass uptake was calculated by taking the difference between the mass of film determined at a specific time and the initial mass of the same film measured before

immersing into the penetrant. All the results obtained from gravimetric studies will be discussed later.

3.5 CONCLUSIONS

This chapter is a detailed description of the materials and techniques used in POE/PMMA interdiffusion studies. The discussion was focused more around ATR-FTIR, starting with the experimental set-up, IR spectra collection and curve fitting. Gravimetric studies were performed as a secondary method that can be used to follow the interdiffusion between poly(oxyethylene) and poly(methylmethacrylate) at different temperatures.

3.6 REFERENCES

1. Yu, G. E.; Sinnathamby, P.; Price, C., Preparation of large cyclic poly(oxyethylene)s. *Chemical Communications* **1996**, (1), 31-32.

2. Singla, S.; Zhao, T.; Beckham, H. W., Purification of cyclic polymers prepared from linear precursors by inclusion concentration of linear byproducts with cyclodextrines. *Macromolecules* **2003,** *36*, (18), 6945-6948.

3. *SigmaAldrich*, (Technical Data Sheet).

4. Lumma, D.; Borthwick, M. A.; Falus, P., Equilibrium dynamics in the nondiffusive regime of an entangled polymer blend. *Physical Review Letters* **2001,** *86*, (10), 2042-2045.

5. Gilmore, P. T.; Falabella, R.; Laurence, R. L., Polymer-polymer diffusion - Effect of temperature and molecular weight on macromolecular diffusion in blends of poly(vinyl chloride) and poly(epsilon caprolactone). *Macromolecules* **1980,** *13*, (4), 880-883.

6. Dormidontova, E. E., Influence of end groups on phase behavior and properties of PEO in aqueous solutions. *Macromolecules* **2004,** *37*, (20), 7747-7761.

7. Zdyrko, B.; Varshney, S. K.; Luzinov, I., Effect of molecular weight on synthesis and surface morphology of high-density poly(ethylene glycol) grafted layers. *Langmuir* **2004,** *20*, (16), 6727-6735.

8. Ito, H.; Russell, T. P.; Wignall, G. D., Interactions in mixtures of poly(ethylene oxide) and poly(methyl methacrylate). *Macromolecules* **1987,** *20*, (9), 2213-2220.

9. Koenig, J. L., *Spectroscopy of polymers*. ACS Professional Reference Book: **1990**.

10. Phan, H., *Fundamental Infrared Spectroscopy*. In 1988.

11. Harrick, N. J.; duPre, F. K., *Applied Optics* **1966,** *5*, 1739.

12. Jabbari, E.; Peppas, N. A., Use of FTIR-ATR to study interdiffusion in poly(styrene) and poly(vinyl methyl ether). *Macromolecules* **1993,** *26*, (9), 2175-2186.

13. Born, M.; Wolf, E., *Principles of Optics: Electromagnetic Theory of Propagation, Interference and Diffraction of Light*. Pergamon Press: **1959**.

14. Mirabella, F. M., Strenght of interaction and penetration of infrared radiation for polymer films in internal relection spectroscopy. *Journal of Polymer Science, Part B - Polymer Physics* **1983,** *21*, (11), 2403-2417.

15. Fieldson, G. T.; Barbari, T. A., The use of FTIR-ATR spectroscopy to characterize penetrant diffusion in polymers. *Polymer* **1993,** *34*, (6), 1146-1153.

16. Laot, C.; Marand, E.; Oyama, H. T., Spectroscopic characterization of molecular interdiffusion at a poly(vinyl pyrrolidone) vinyl ester interface. *Polymer* **1999,** *40*, (5), 1095-1108.

17. Technical Data Information. In *Pike Technologies*, http://www.piketech.com.

18. www.piketech.com, PikeTechnologies. *Application Note-0601* **2005**.

19. Harrick, N. J., *Internal Reflection Spectroscopy*. Interscience Publishers: 1967.

20. http://webbook.nist.gov/cgi/cbook/toluene/IR

21. Williams, D.; Flemming, I., *Spectroscopic Methods in Organic Chemistry*. McGraw-Hill Publishing Company Limited, London: **1966**.

22. http://mfa/poly(methylmethacrylate)/IRspectrum

CHAPTER 4

RESULTS

Using ATR-FTIR spectroscopy, interdiffusion of POE into PMMA was followed in situ by observing the spectral changes of the characteristic absorbance peaks of each component as a function of time (as discussed in detail in the previous chapter). In this chapter, it is shown how the absorbance – time data are used to determine the appropriate diffusion model and further applied to obtain an accurate evaluation of this transport phenomenon.

The first section refers to absorbance evolution in time during the interdiffusion between poly(oxyethylene) and poly(methyl methacrylate). Further, an appropriate diffusion model has been determined, allowing determination of the parameters used as metrics for evaluating the diffusion. A detailed description of the penetrant velocity and mutual diffusion (interdiffusion) coefficient is described in this chapter. The results obtained from DSC measurements and gravimetric studies are explained here as well.

4.1 INITIAL VELOCITY ESTIMATION

Once the distinguishable infrared bands used in diffusion evaluation of POE oligomers into the PMMA matrix were identified for both components, their spectral changes in time were followed during the entire diffusion process until equilibrium was reached. As discussed in Chapter 3, the characteristic absorption bands used for quantitative spectral analysis were selected from one of the principal absorptions of the

pure compounds: the stretching of the ether bond at 1109 cm^{-1} for POE and that of the carbonyl bond at 1728 cm^{-1} for PMMA.

At the onset of interdiffusion, the penetrant migrates into the polymeric matrix. No spectral changes are observed until the penetrant reaches the penetration depth. The induction period, when no changes in peak intensities are observed, corresponds to the time taken for the POE to diffuse through the film thickness, d_{PMMA} and reach the penetration depth, d_p. At this point, the spectral changes within the penetration depth appear first at lower wavenumbers, because d_p is larger for low wavenumbers (see Figure 3.7). Table 4.1 contains the calculated values of penetration depth corresponding to the selected characteristic absorbance bands of the two interdiffusing components, determined by using Eq.17.

Table 4.1 - Peak assignments and penetration depth of the peaks chosen for POE/PMMA interdiffusion evaluation.

Component	Peak Assignment	Wavenumber (cm^{-1})	d_p(μm)
POE	C-O-C Stretching mode	1109	2.0
PMMA	C=O Stretching mode	1728	1.3

As discussed in Chapter 3, the penetration depth is a function of the refractive index of the sample and wavelength of the incident IR beam. Hence, during the diffusion process the penetration depth can change as a result of changes that could occur in the refractive index of the sample. The refractive index of PMMA120K found in literature[1] is $n_D^{PMMA120K} = 1.492$ at 20 °C. For 50 °C, the refractive index for 400g/mol linear POE is $n_D^{lPOE400} = 1.456$ at 50 °C, and for 1000g/mol linear POE is $n_D^{lPOE1000} = 1.459$ at 50 °C.[2] Therefore, as POE diffuses into PMMA, the refractive index of the matrix should

decrease with increasing concentration of POE into PMMA until equilibrium is reached. However, the maximum change in the refractive index results in a 4% variation in the penetration depth (see Appendix). At the same time, the refractive index can decrease with increasing temperature.[2] The depth of penetration was estimated to decrease by 4.5% at 110 ^{o}C, 3% at 85 ^{o}C and 2.5% at 60 ^{o}C. These were also taken into consideration when the total magnitude of the errors involved in these studies was estimated (see Appendix).

A schematic representation of POE diffusion into PMMA during the induction period is illustrated in Figure 4.1. As POE diffuses down from the top of the PMMA layer, it starts to migrate into the matrix, but the absorbance peak corresponding to the ether bond at 1109 cm^{-1} will only be observed in the IR spectra when the POE reaches the penetration depth, d_p^{POE}. The time taken for POE to diffuse the distance (d_{PMMA} - d_p^{POE}) is called the POE induction time, t_i^{POE}. The PMMA induction time, t_i^{PMMA} might be determined at the point where the absorbance of the peak corresponding to its carbonyl bond at 1728 cm^{-1} no longer remains constant. At this point the POE reaches the penetration depth characteristic to PMMA, d_p^{PMMA}, and consequently the intensity of the carbonyl bond absorbance will start to decrease.

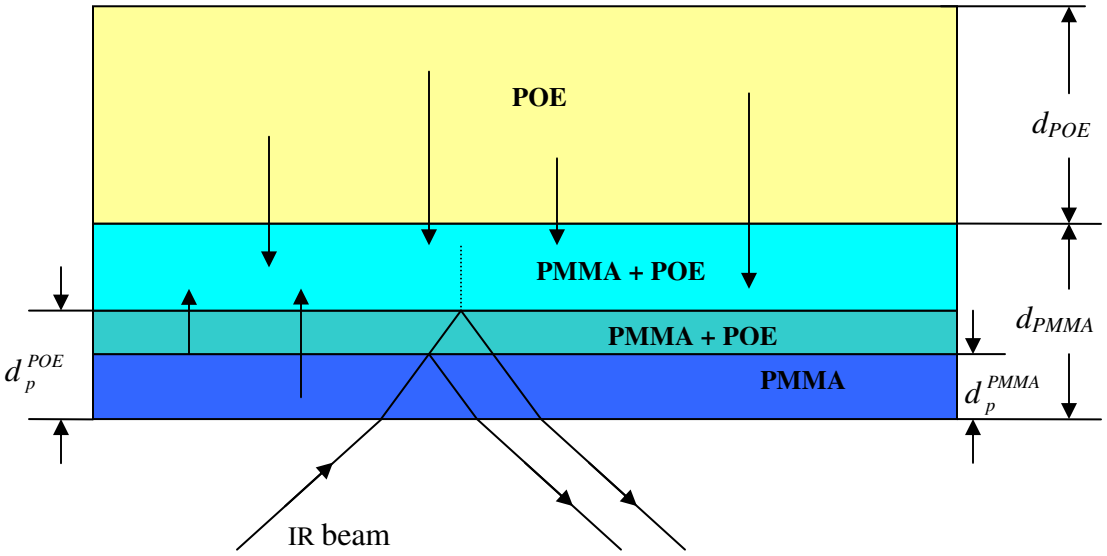

Figure 4.1 - Schematic representation of POE/PMMA interdiffusion system during induction period. Thicknesses of PMMA and POE are symbolized by d_{PMMA} and d_{POE}. The d_p^{PMMA} stands for depth of penetration characteristic to carbonyl bond of PMMA at 1728 cm^{-1}, while d_p^{POE} stands for depth of penetration characteristic to ether bond of POE at 1109 cm^{-1}.

Therefore, by knowing the thickness of poly(methyl methacrylate) from profilometry measurements and calculating the depth of penetration characteristic to the ether bond of POE at 1109 cm^{-1}, the initial velocity of the penetrant can be estimated by using the following equation:

$$v_i = \frac{(d_{PMMA} - d_p^{POE})}{t_i^{POE}} \qquad \text{Eq. 28}$$

where v_i is the initial velocity of the POE calculated as the ratio between the distance traveled by POE from the top of the PMMA film until the d_p^{POE} was reached and the time it took POE to travel this distance.

where: v_i = POE initial velocity (cm/s); d_{PMMA} = PMMA thickness (μm); d_p^{POE} = POE depth of penetration corresponding to the ether bond at 1109 cm^{-1} (μm); t_i^{POE} = POE induction time (s).

The interdiffusion between PMMA/POE pairs was measured at least twice and the results obtained for initial penetrant velocity are presented in Table 4.2.

Table 4.2 – Initial penetrant velocity (v_i) values determined for all interdiffusion studies between POE and PMMA120K. t_{POE}^i is POE induction time.

Oligomer	T (°C)	d_{PMMA} (μm)	t_{POE}^i (min)	$v_i = \frac{d_{PMMA} - d_p^{POE}}{t_{POE}^i}$ (cm/s)	**Average** v_i **x 10^{-6}** (cm/s)
IPOE500	60	58.6	100	**9.43 x 10^{-7}**	0.96 ±0.10
		65.3	110	**9.59 x 10^{-7}**	
IPOE500	85	46.2	48	**1.53 x 10^{-6}**	1.74 ±0.30
		28.8	23	**1.94 x 10^{-6}**	
IPOE500	110	25.2	10	**3.84 x 10^{-6}**	3.91 ±0.39
		96.3	40	**3.93 x 10^{-6}**	
		33.0	13	**3.97 x 10^{-6}**	
cPOE400	110	18.5	4	**6.70 x 10^{-6}**	6.77 ±0.68
		18.0	4	**6.67 x 10^{-6}**	
		106	25	**6.93 x 10^{-6}**	
cPOE1000	110	20.2	8	**3.78 x 10^{-6}**	3.68 ±0.37
		57.5	25	**3.67 x 10^{-6}**	
		44.2	20	**3.58 x 10^{-6}**	

Thus, the penetrant velocity can be easily estimated from thickness measurements and initial induction times. It must be emphasized that thickness must be very carefully

resolved to be able to determine a penetrant velocity. The errors established here include the thickness calculation, variation in the depth of penetration and time measurements.

4.2 ABSORBANCE EVOLUTION IN TIME

As soon as POE reaches the penetration depth, changes in absorbance spectra will be seen. Examples of spectra evolution in time were discussed in Chapter 3 and shown in Figures 3.23 – 3.25. The analytical areas under the peaks were determined by deconvoluting the raw spectra as described in Chapter 3. Thus, the variation in time of ether absorbance band, specifically its increase in peak intensity, is the primary metric used to evaluate interdiffusion. The intensity of the peak at 1728 cm^{-1} characteristic of carbonyl bond stretching present in PMMA decreases as a function of time during interdiffusion process. Figure 4.2 is an example of variation of POE absorbance at 1109 cm^{-1} (analytical area) as a function of interdiffusion time for lPOE500/PMMA120K system at 85 ^{o}C. The induction period of 48 minutes corresponds to POE movement into PMMA matrix until its specific penetration depth estimated at 1109 cm^{-1} is reached. The error bars assigned here include the thickness calculation, variation in penetration depth, time measurements and spectra deconvolution.

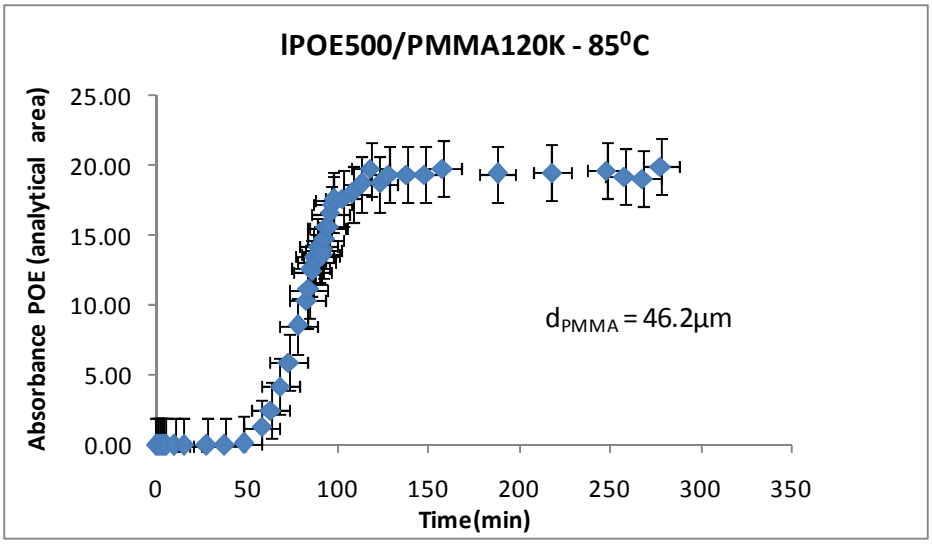

Figure 4.2 - Absorbance as a function of interdiffusion time for lPOE500/PMMA120K sample pair**.** The experiments were performed at 85 ^{o}C. The ether bond vibration of POE at 1109 cm^{-1} was used for analysis. The POE induction time t^{i}_{POE} corresponds to 48 min.

The corresponding time dependency of the PMMA absorbance is shown in Figure 4.3 for the same lPOE500/PMMA120K sample pair at 85 ^{o}C. As expected, in case of the carbonyl peak, the induction period of 55 minutes is present with the exception that it is longer since the matrix is more viscous and the rates of diffusion for POE and PMMA are expected to not be the same. This difference between the induction times of POE and PMMA is more evident at the lower temperatures of study. Also, a shallow penetration depth defines the carbonyl bond of PMMA at 1728 cm^{-1} but this has only a small effect to the induction period.

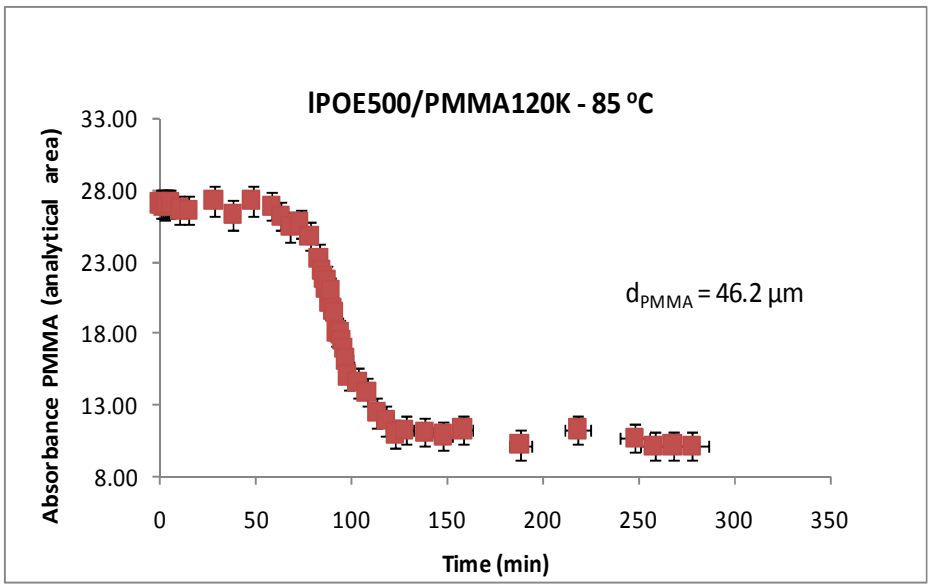

Figure 4.3 - Absorbance as a function of interdiffusion time for lPOE500/PMMA120K sample pair**.** The experiments were performed at 85 °C. The carbonyl bond vibration of PMMA at 1728 cm^{-1} was used for analysis. The PMMA induction time t^{i}_{PMMA} corresponds to 55 min.

Figure 4.4 illustrates the normalized absorbance of POE and PMMA as a function of time for the same system shown above during interdiffusion. The normalized absorbance specific to each component was calculated as followed:

$$A'_{POE} = \frac{A_{POE}(t)}{A_{POE}(t_\infty)} \quad \text{and} \quad A'_{PMMA} = \frac{A_{PMMA}(t)}{A_{PMMA}(t_0)} \qquad \text{Eq. 29}$$

where: A'_{POE} = normalized absorbance of POE; A'_{PMMA} = normalized absorbance of PMMA; $A_{POE}(t)$ = POE absorbance specific to ether bond vibration of POE at 1109 cm^{-1} at each interdiffusion time; $A_{PMMA}(t)$ = PMMA absorbance specific to carbonyl bond vibration of PMMA at 1728 cm^{-1} at each interdiffusion time; $A_{POE}(t_\infty)$ = POE absorbance specific to ether bond vibration of POE at 1109 cm^{-1} at infinitely long interdiffusion times

(equilibrium); $A_{PMMA}(t_0)$ = PMMA absorbance specific to carbonyl bond vibration of PMMA at 1728 cm^{-1} at initial interdiffusion time.

The normalized absorbance specific to ether bond vibration at 1109 cm^{-1} for POE starts to increase in time as soon as the penetration depth of POE reaches. Since the penetrant moves into the matrix, an increase in its absorbance intensity within the penetration depth has been seen until the equilibrium concentration of POE into PMMA has been attained and the diffusion finished. A plateau was observed because the IR spectra were collected for a longer period of time to insure that the equilibrium point was reached. At the same time, the normalized absorbance specific to carbonyl bond vibration at 1728 cm^{-1} for PMMA starts to decrease in time as soon as the penetration depth of PMMA is reached. The dilution of the matrix occurs as a result of penetrant diffusion until the equilibrium concentration of POE/PMMA is reached and the interdiffusion completed. Since the PMMA is still present into the sample, but only diluted with POE, the PMMA plateau is observed at a normalized absorbance value of 0.4 and not at 0.

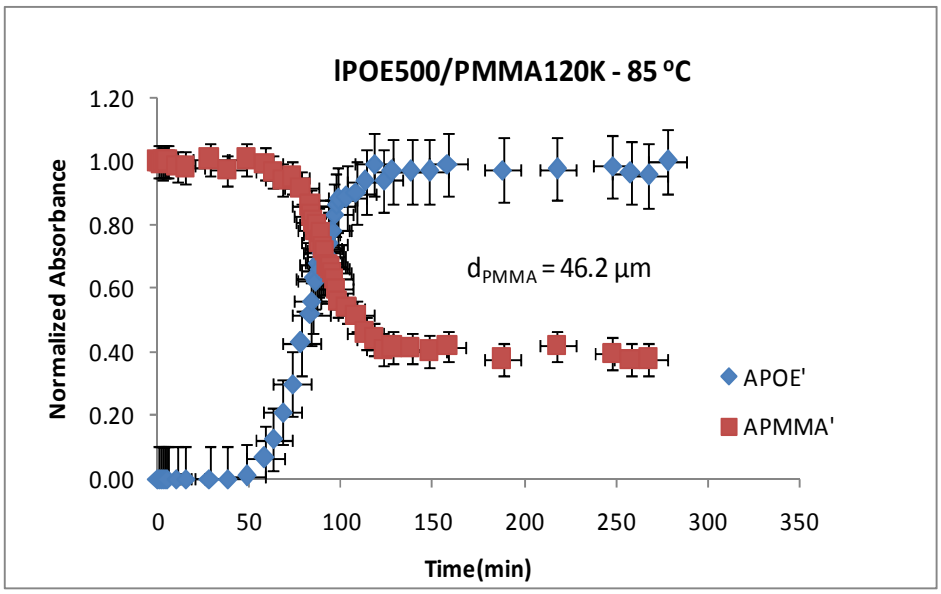

Figure 4.4 – Normalized absorbance as a function of interdiffusion time for lPOE500/PMMA120K sample pair**.** The experiments were performed at 85 °C. The normalized absorbance of POE and PMMA were determined by using Eq.29. The ether bond vibration of POE at 1109 cm^{-1} and the carbonyl bond vibration of PMMA at 1728 cm^{-1} were used for analysis.

As described in Chapter 3, in case of interdiffusion between linear POE, 500 g/mol and PMMA120K the experiments were conducted at different temperatures. Figures 4.5, 4.6 and 4.7 illustrate the absorbance of POE as a function of time at interdiffusion temperatures of 60 °C, 85 °C and 110 °C. The induction period is dependent of the thickness of polymer matrix. Only by looking at the graphs, initially we can conclude that for the same sample pair when the experiments were conducted at different temperatures, diffusion slows down with temperature decrease, which it is in agreement with theory. The slopes of the linear least square regressions can be determined from the plot of absorbance versus time. Therefore, the values of these slopes are smaller at low temperature than at high one.

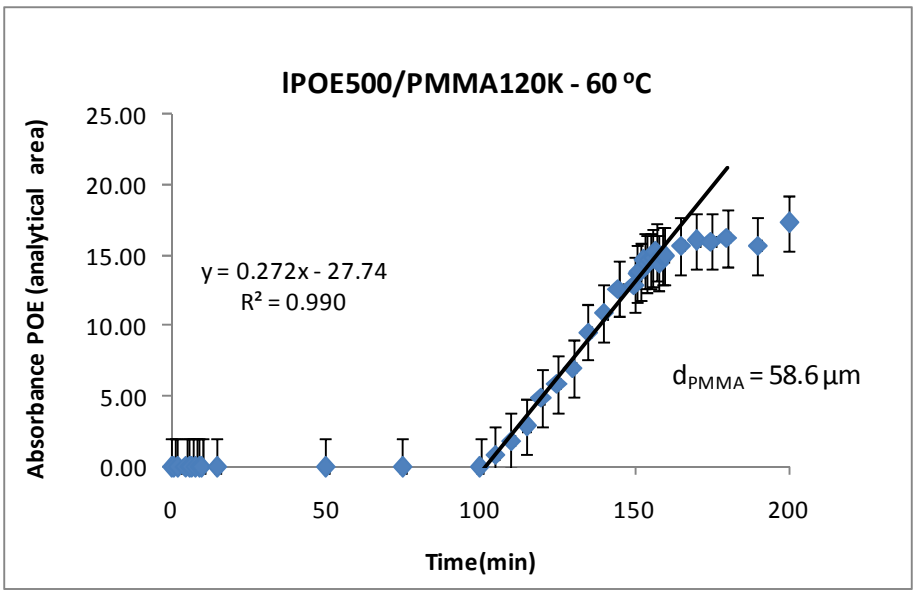

Figure 4.5 - Absorbance as a function of interdiffusion time for lPOE500/PMMA120K sample pair**.** The experiments were conducted at 60 °C. The ether bond vibration of POE at 1109 cm^{-1} was used for analysis.

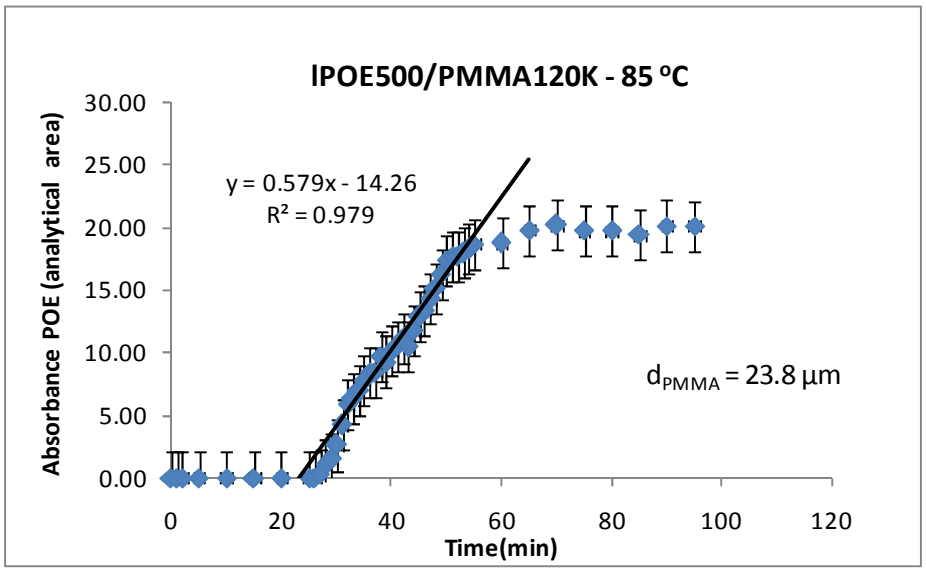

Figure 4.6 - Absorbance as a function of interdiffusion time for lPOE500/PMMA120K sample pair**.** The experiments were performed at 85 °C. The ether bond vibration of POE at 1109 cm^{-1} was used for analysis.

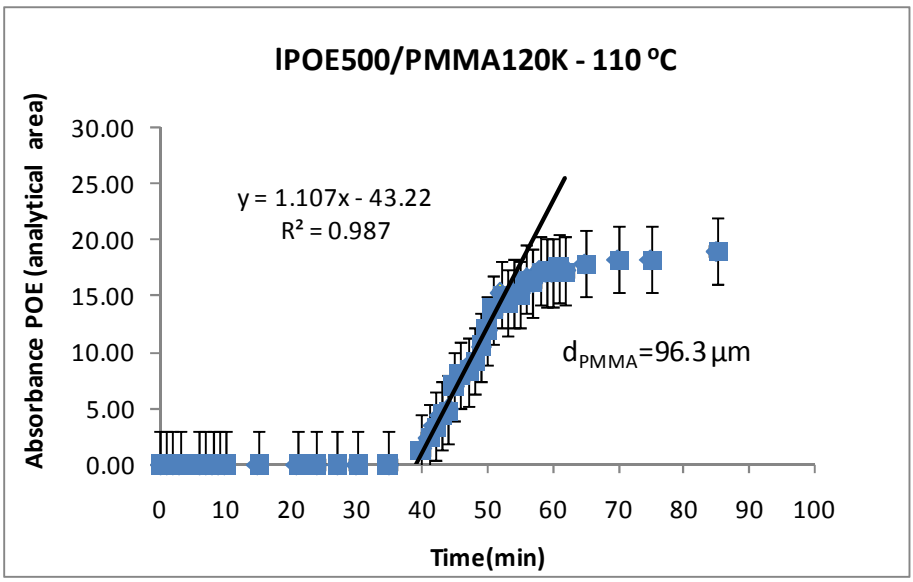

Figure 4.7 - Absorbance as a function of interdiffusion time for lPOE500/PMMA120K sample pair**.** The experiments were conducted at 110 °C. The ether bond vibration of POE at 1109 cm^{-1} was used for analysis.

To compare the diffusion of linear oligomers versus cyclic ones, the variation of absorbance specific to the uptake component is illustrated below (see Figures 4.8, 4.9 and 4.10). Again, a very simple initial evaluation can be accomplished only by looking at the slopes of the linear least square regressions of absorbance versus time. Their values indicate: cPOE400 > cPOE1000 ≅ lPOE500 for interdiffusion at 110 °C. In addition to using the induction period for a given film thickness to determine diffusion rates, the slope at these absorbance – time curves can also be used. So, the penetrant velocity within the depth of penetration can be determined from the value of these slopes. This is expected to be consistent to the initial velocity estimated from the induction time because both constants have the same physical meaning. A detailed discussion follows later in this chapter.

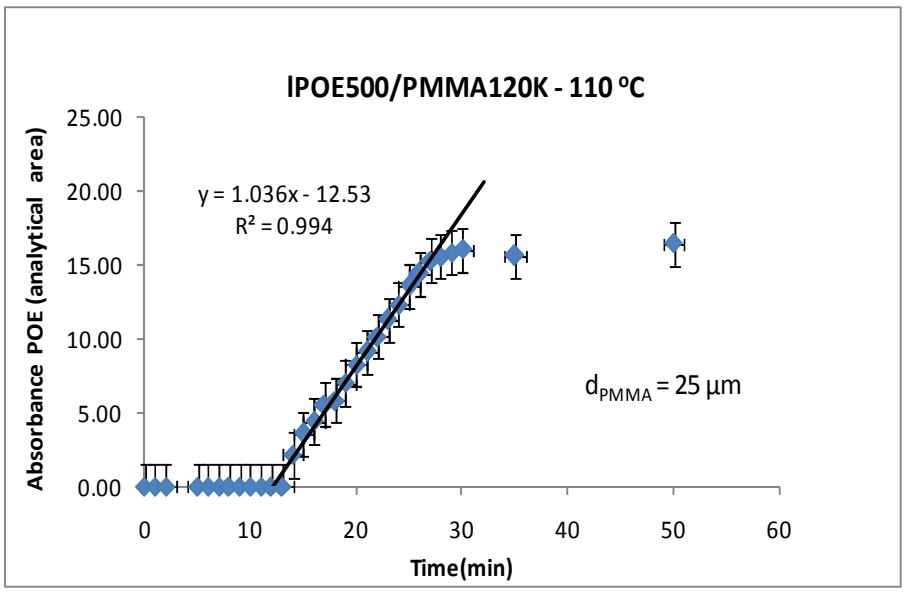

Figure 4.8 - Absorbance as a function of interdiffusion time for lPOE500/PMMA120K sample pair**.** The experiments were conducted at 110 °C. The ether bond vibration of POE at 1109 cm^{-1} was used for analysis.

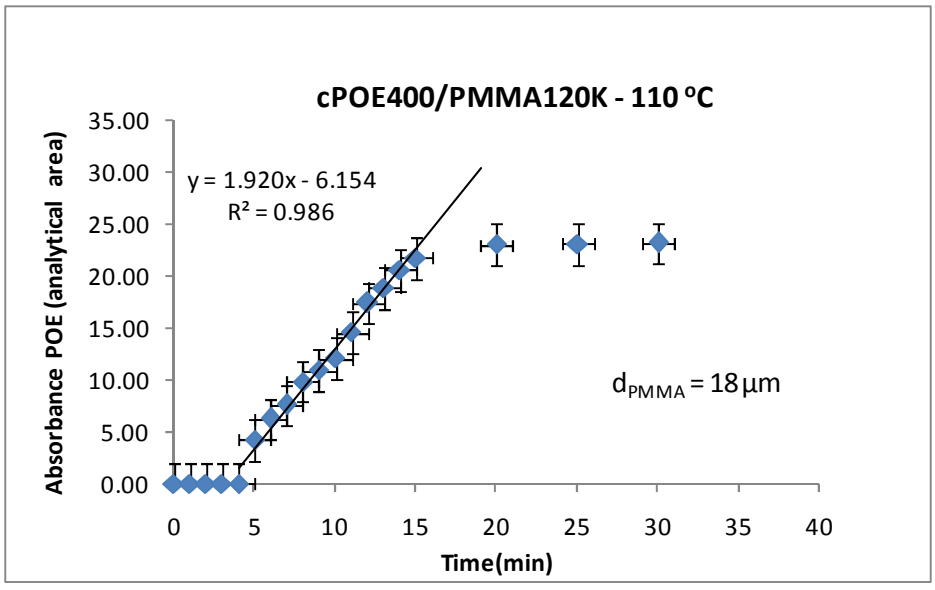

Figure 4.9 - Absorbance as a function of interdiffusion time for cPOE400/PMMA120K sample pair**.** The experiments were performed at 110 °C. The ether bond vibration of POE at 1109 cm^{-1} was used for analysis.

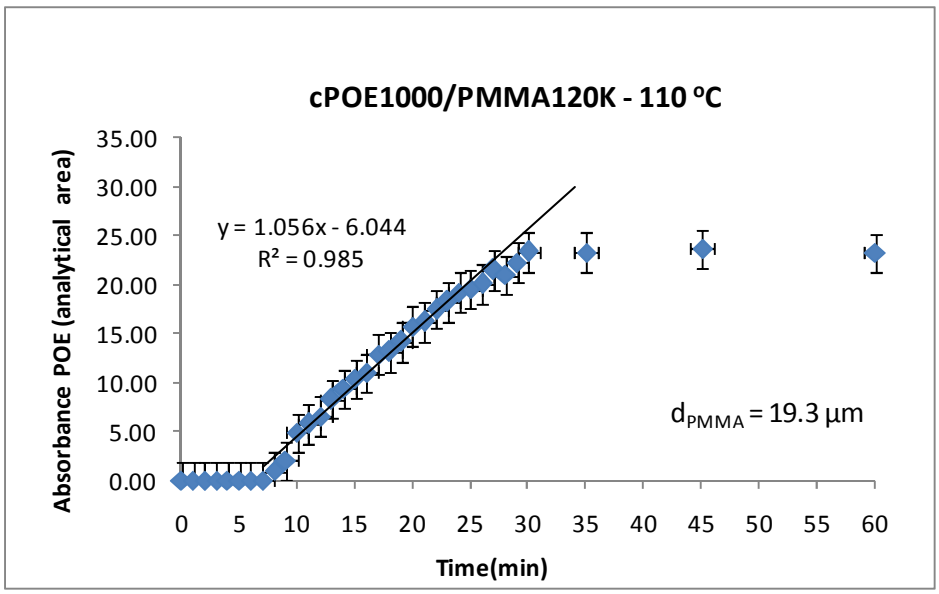

Figure 4.10- Absorbance as a function of interdiffusion time for cPOE1000/PMMA120K sample pair**.** The experiments were conducted at 110 ^{o}C. The ether bond vibration of POE at 1109 cm^{-1} was used for analysis.

Figure 4.11 shows the change in absorbance of POE as a function time, using the same sample pair, cPOE400/PMMA120K at 110 ^{o}C, in which the PMMA film thickness was different. Since the change in absorbance can be seen only within the depth of penetration, the influence of the matrix thickness should affect only the induction period. The linear slopes should be must be similar for the same sample pair measured under identical conditions. This is certainly the case for the cPOE400/PMMA120K data shown in Figure 4.11. The thicker film leads to a longer induction period.

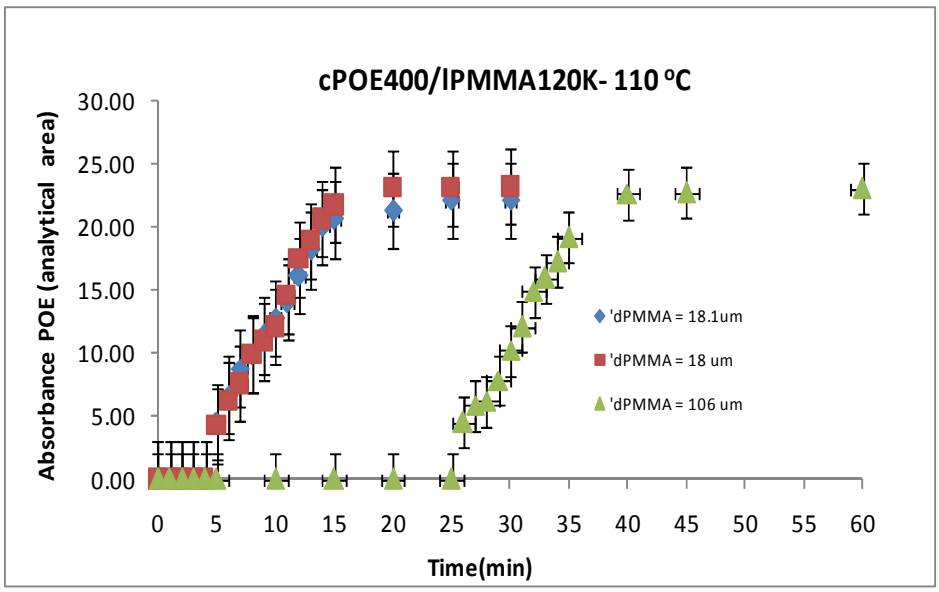

Figure 4.11 - Absorbance as a function of interdiffusion time for cPOE400/PMMA120K sample pairs with different PMMA thickness**.** The experiments were performed at 110 ^{o}C. The ether bond vibration of POE at 1109 cm^{-1} was used for analysis.

4.3 DATA EVALUATION

The absorbance was converted to concentration followed by recognition of the diffusion model. An interface velocity (K_{II}) and an interdiffusion coefficient (D_m) specific to each sample pair were estimated.

4.3.1 Conversion of absorbance to concentration

As described in Chapter 3, a calibration curve (see Figure 4.12) was obtained by measuring different POE/ PMMA blend samples with known concentrations. The errors assigned here come from spectra deconvolution and blends preparations.

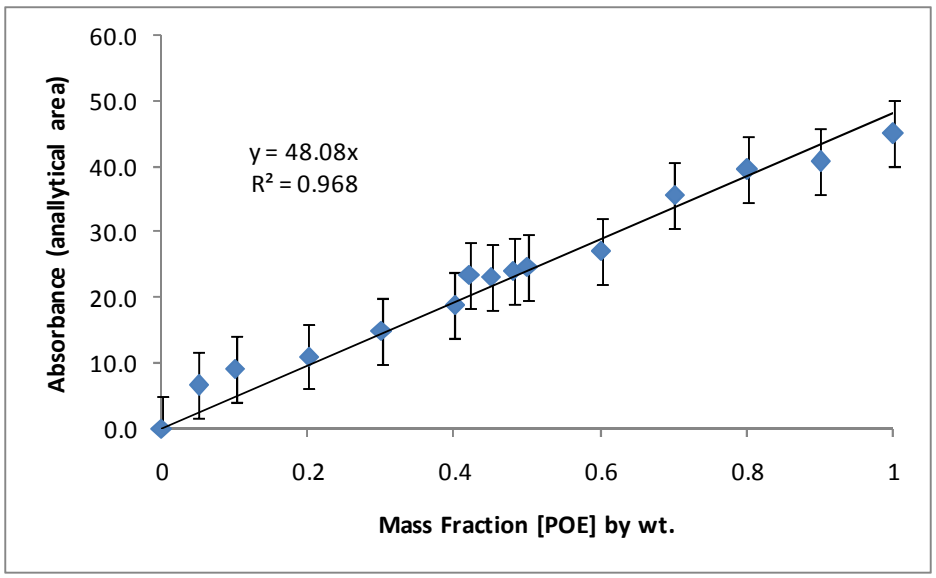

Figure 4.12 – Absorbance – concentration calibration curve**.** The experiments were performed for lPOE500/PMMA120K sample pair. The ether bond vibration of POE at 1109 cm^{-1} was used for analysis.

The calibration curve was determined by deconvoluting the spectra and interpreting the peak for the ether bond of POE at 1109 cm^{-1}. A linear dependence was obtained for the entire range of concentration. Even the linear POE phase separates from PMMA and at a concentration of about 40 wt %, the POE still can be homogenous distributed in the PMMA reach phase which explain the linear dependence of absorbance – concentration obtained here. The absorbance measured for each POE/PMMA sample was converted to POE weight concentration (mass fraction) by applying the following equation derived from the calibration curve:

$$[POE](t) = \frac{A_{POE}(t)}{48.1} \qquad \text{Eq.30}$$

where $[POE](t)$ is the mass fraction of POE within penetration depth at different time and $A_{POE}(t)$ is the POE absorbance specific to the ether bond vibration of POE at 1109 cm^{-1}.

Many research groups have correlated the absorbance obtained by ATR-FTIR spectroscopy with concentration by using a calibration curve.[3, 4] It is demonstrated that the absorbance (A) of diffusant species obtained by the ATR spectroscopy technique can be related to the concentration (c) using the following equation:[5]

$$A = \int_0^L \frac{\varepsilon c I}{I_0} \partial z \qquad \text{Eq.31}$$

where L represents the thickness of the polymeric film.

Eq.31 was obtained by assuming that only weak absorption occurs ATR spectroscopy by combining the Beer-Lambert law with the evanescent field strength Eq.16. It is important to note that when the depth of penetration is small compared with the film thickness (d_{PMMA}), the use of such absorbance-concentration calibration curves is possible. This is called "thick-film approximation"[6] and the requirements which must be met are:[5]

$$\frac{4}{d_p^2} >> \frac{\pi^2}{4 d_{PMMA}} \qquad 32$$

and

$$1 >> \exp(-2\frac{d_{PMMA}}{d_p}) \qquad 33$$

In all samples studied here the conditions described above are met, and the calibration curve was used for further analysis. For example, for the thinnest PMMA film, d_{PMMA} = 18 µm, the requirements described above are met as follows: $1 > 0.1$ and $1 >> 1.5 \times 10^{-8}$.

The mass fraction of penetrant versus interdiffusion time for cPOE1000/PMMA120K at 110 °C is illustrated in Figure 4.13. After an induction period, the POE concentration increases until equilibrium is obtained. When the equilibrium concentration is reached, a plateau is observed as no more POE penetrates into PMMA. This concentration, called the "concentration at long diffusion time" or "concentration at infinity" has been determined to 47% ± 2% by wt for cyclic POE 1000 g/mol. To ensure that equilibrium was reached and no cracks were created in the films during the entire experiment, the absorbance spectra were measured many hours after the intensities appeared to stop changing.

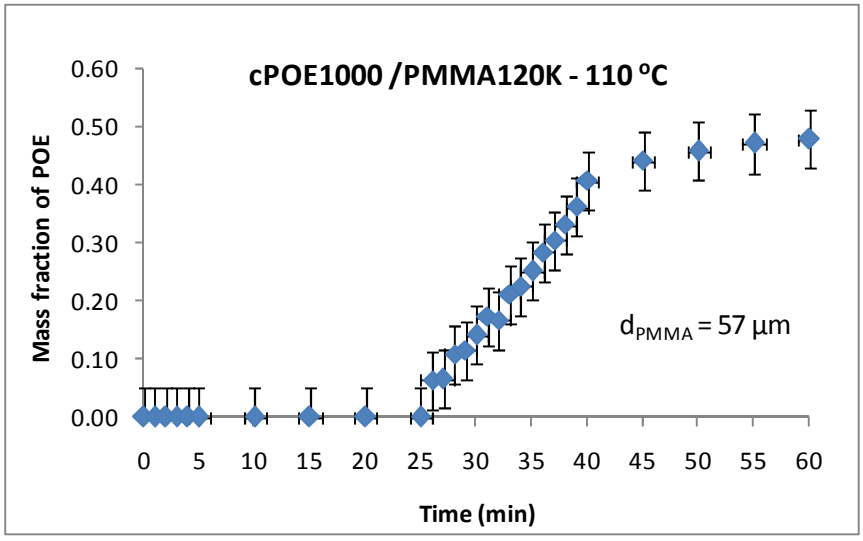

Figure 4.13 – Mass fraction of cPOE1000 into PMMA120K versus interdiffusion time at 110 °C.

For a better comparison between the two sample pairs with different film thicknesses, the induction time can be eliminated and the time zero is considered the time characteristic to change in concentration. Then, by representing graphic the changes in concentration of the diffusant species as a function of interdiffusion time, the diffusion rates could be initially estimated from the slope of the linear least square regressions of this curve. For example, in Figure 4.14 are shown data for mass fraction of lPOE500 and cPOE400 into PMMA120K versus interdiffusion time at 110 °C. The two sample pairs contain the same polymeric matrix PMMA120K, but the penetrant has a different topology (lPOE500 and cPOE400). From the gradients of these slope it is clear that the cyclic diffusant moves faster than the linear one. Also, this comparison demonstrates that linear POE is less miscible than cyclic POE into PMMA120K because the equilibrium concentration has been determined to be 35% ± 3% by wt for linear POE.

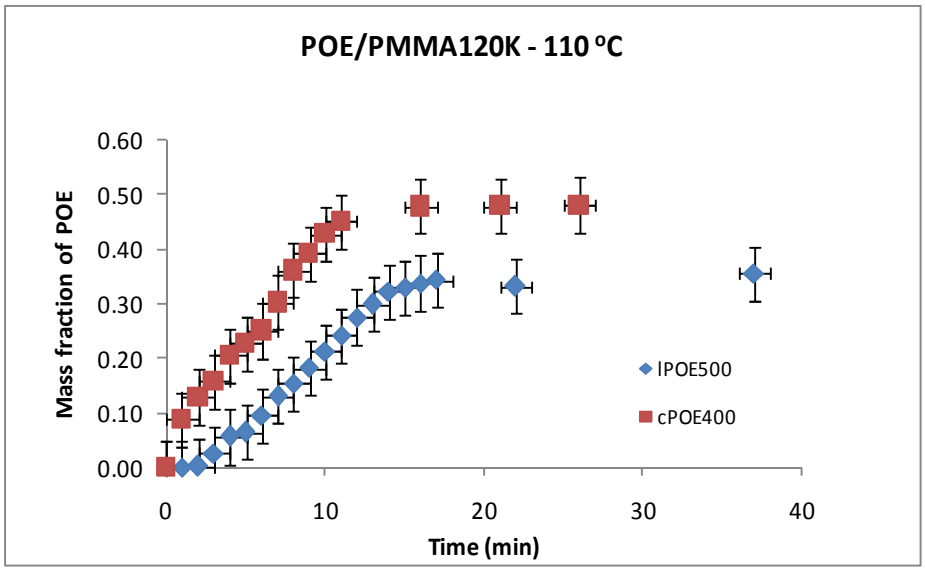

Figure 4.14 - Mass fraction of lPOE500 and cPOE400 into PMMA120K versus interdiffusion time at 110 °C. For a better comparison between the two sample pairs with different thickness, the induction time was eliminated.

The results obtained from ATR-FTIR spectroscopy are supported by DSC data. Figure 4.15 represents the DSC thermogram for poly(methyl methacrylate) (PMMA, 120,000 g/mol) and Figure 4.16 shows the DSC thermogram for linear poly(oxyethylene) (lPOE, 500 g/mol). The glass transition temperatures of PMMA120K, T_g = 105 ± 2 °C and of lPOE500, T_g = -70 ± 2 °C were determined from the second heating curve. Since the poly(oxyethylene) is a semicrystalline polymer, a melting point specific to the crystalline phase of lPOE500 was determined at 12 ± 2 °C. The DSC thermogram for cyclic poly(oxyethylene) (cPOE, 1000 g/mol) is illustrated in Figure 4.17. The glass transition of cPOE1000 was determined at T_g = -54 ± 2 °C and the melting temperature at T_m = 33 ± 2 °C.

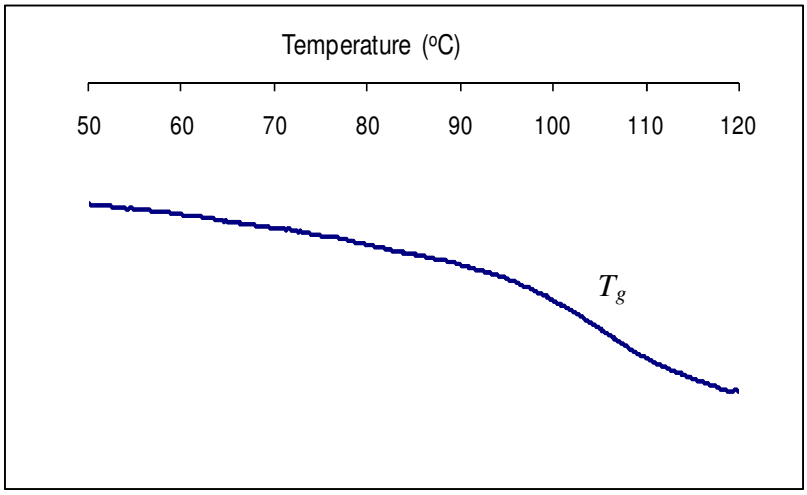

Figure 4.15 – DSC thermogram for poly(methyl methacrylate) (PMMA, 120 kg/mol). T_g = 105 ± 2 °C was determined from the second heating curve.

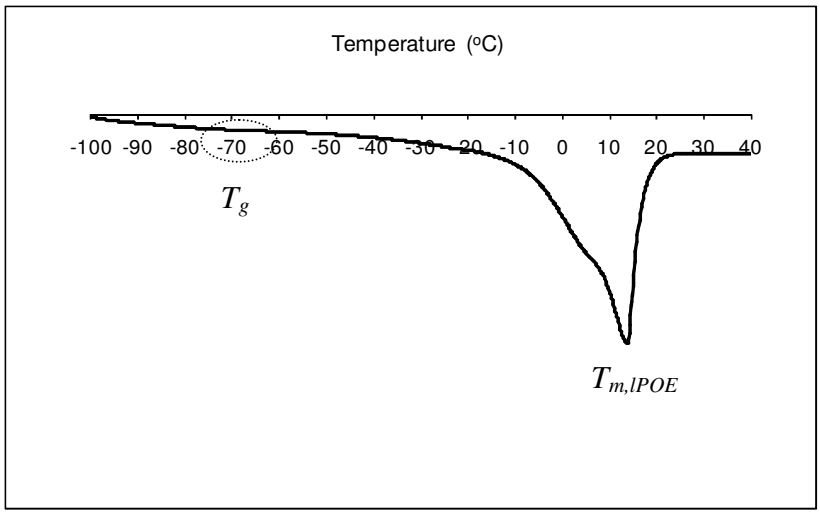

Figure 4.16 – DSC thermogram for linear poly(oxyethylene) (lPOE, 500 g/mol). T_g = -70 ± 2 °C and T_m = 12 ± 2 °C were determined from the second heating curve.

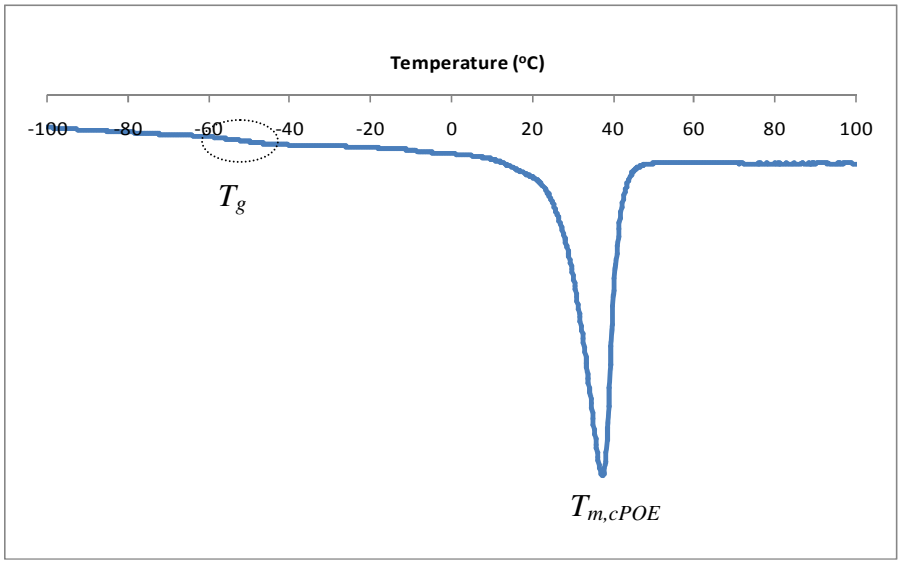

Figure 4.17 – DSC thermogram for cyclic poly(oxyethylene) (cPOE, 1000 g/mol). T_g = -54 ± 2 °C and T_m = 33 ± 2 °C were determined from the second heating curve.

The glass transition temperatures of lPOE500/PMMA120K blends were determined from the second heating curve, as it is shown in Figure 4.18. A careful

examination of DSC thermograms shows that two broad glass transition temperatures were resolved in POE/PMMA blends.

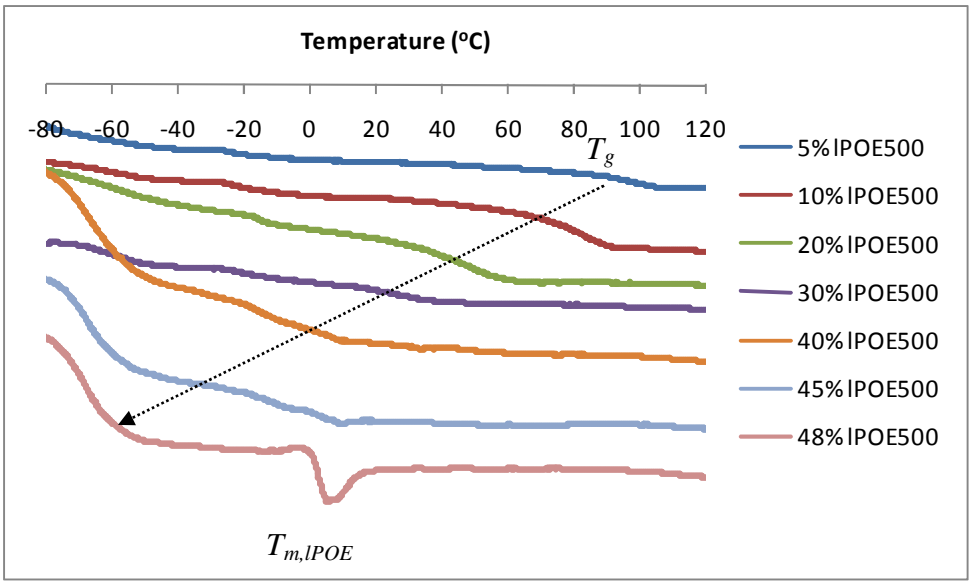

Figure 4.18 – DSC thermograms for blends of linear poly(oxyethylene) (500 g/mol) and poly(methyl methacrylate) (120,000 g/mol). T_g decreases with increasing POE concentration.

These can be interpreted as distinct glass transitions of the two components and it is expected that T_g belonging to POE component to increase with enhancing the concentration of this component into the blend, while the other one, corresponding to PMMA component to drop off. Then, in case of POE/PMMA blends the "rule of thumb that two transitions indicate immiscibility" was found to be incorrect and these can be explained by the self-concentration model of Lodge and McLeish. According to this model, each T_g belongs to a "local environment of a given component being rich in that component due to chain connectivity".[7]

The same procedure was used to determine the glass transitions of the blends made from cyclic POE 1000 g/mol and PMMA 120,000 g/mol. The DSC thermograms of the blends containing the following compositions: 0/100, 10/90, 25/75, 40/60, 50/50, 55/45 and 100/0 by weight cPOE1000 in PMMA120K are shown in Figure 4.19. Same as in case of linear blends two broad glass transitions were resolved in these blends, too.

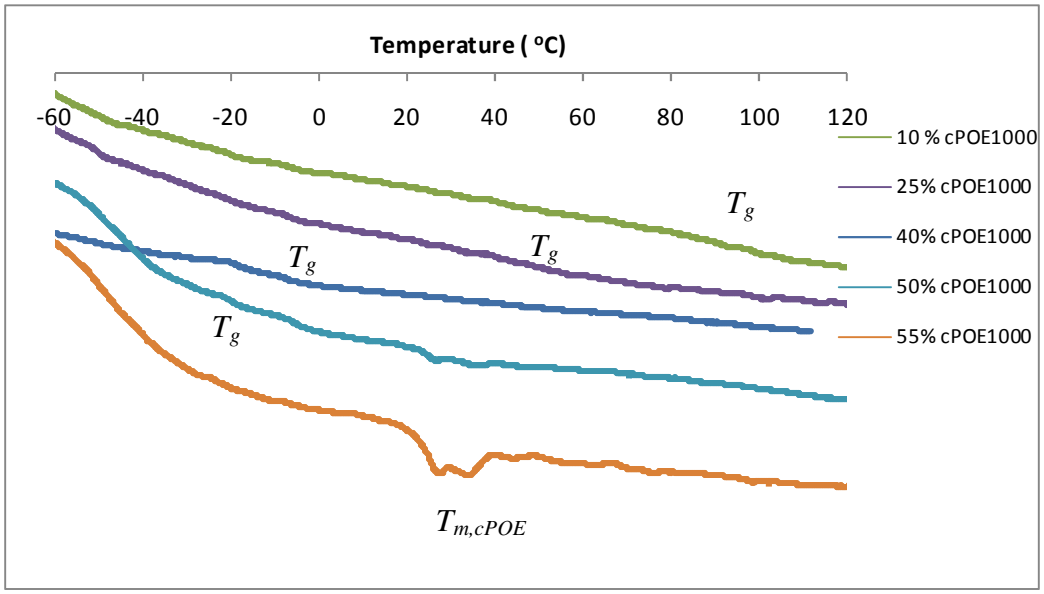

Figure 4.19 – DSC thermograms for blends of cyclic poly(oxyethylene) (1,000g/mol) and poly(methyl methacrylate) (120,000 g/mol). T_g decreases with increasing cPOE1000 concentration.

A simple analysis of all the thermograms shows a reduction in T_g (specific to PMMA rich component) of the POE/PMMA blends with increasing POE content until phase separation can be observed and the melting point (T_m) of POE component becomes visible. This behavior observed in POE/PMMA systems can be explained by considering the change in T_g of the system as the result of plasticizing effect of the POE. Above a certain content of POE into PMMA, it was very hard to measure T_g due to melting peak

specific to crystalline phase of POE component. The semicrystalline blends of 40 % wt linear POE started to exhibit melting of POE crystallites around 12 ^{o}C, while blends of 50 % wt cyclic POE into PMMA started to show a melting of POE crystallites around 33 ^{o}C. Then, this is a good indication of higher miscibility of cyclic POE into PMMA versus linear ones, which is in good agreement with ATR-FTIR spectroscopy results.

Even though Flory-Huggins χ interaction parameter is very small and slightly negative ($\chi_{PEO/dPMMA} = -2.1x10^{-3}$) without temperature dependence in the range of 80 ^{o}C – 160 ^{o}C, many studies of PMMA/POE blends have indicated miscibility in the melt.[8, 9] It is well known that miscibility between blend components might be interpreted by Fox equation[9]. The measured values of T_g specific to "PMMA rich environment" of the blends up to 45% in case of linear POE and 55% in case of cyclic POE are in agreement with those calculated from Fox equation:

$$\frac{1}{T_g} = \frac{w_{PMMA}}{T_g^{PMMA}} + \frac{w_{POE}}{T_g^{POE}} \qquad \text{Eq. 34}$$

where: T_g = glass transition temperature of POE/PMMA blend; T_g^{PMMA} = glass transition temperature of PMMA determined by DSC = 105 ^{o}C ± 2 ^{o}C; $T_g^{lPOE500}$ = glass transition temperature of lPOE determined by DSC = - 70 ^{o}C ± 2 ^{o}C; $T_g^{cPOE1000}$ = glass transition temperature of cPOE determined by DSC = - 54 ^{o}C ± 2 ^{o}C; w_{PMMA} = weight (mass) fraction of PMMA; w_{POE} = weight (mass) fraction of POE.

The values of T_g attained from DSC measurements, as well as these predicted by the Fox equation are shown in Figures 4.20 and 4.21.

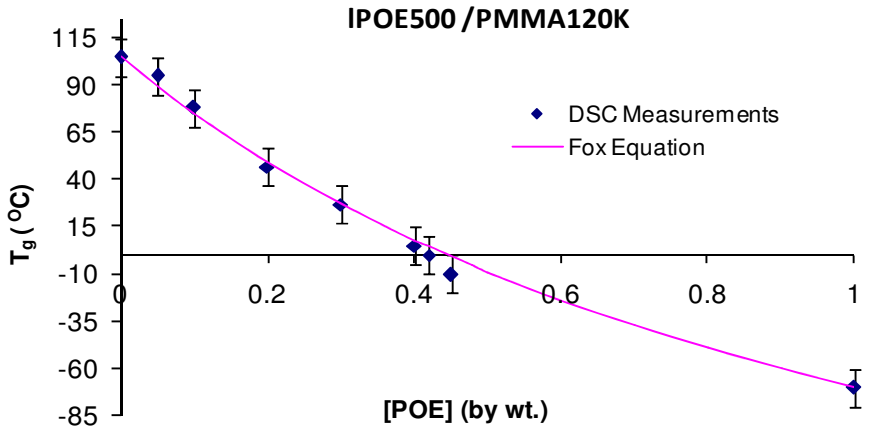

Figure 4.20 - T_g of lPOE500/PMMA120K blend as a function of mass fraction of lPOE500. The dots represent experimental values of T_g obtained by DSC experiments. The solid line is predicted by the Fox equation.

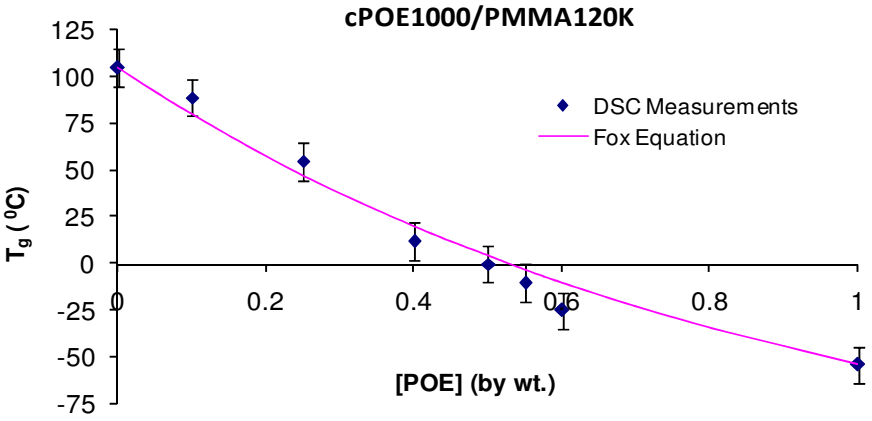

Figure 4.21 - T_g of cPOE1000/PMMA120K blend as a function of mass fraction of cPOE1000. The dots represent experimental values of T_g obtained by DSC experiments. The solid line is predicted by the Fox equation.

4.3.2 Identification of diffusion model

As discussed in Chapter 2, the appropriate diffusion model can be identified by a diffusional exponent *n*. The value of *n* is determined from the slope of log – log plots of normalized mass fraction of penetrant versus time, according to Eq.3.[10] Hence, in the equation below describes the systems studied here:

$$\log[POE]^{'}(t) = \log\frac{[POE](t)}{[POE]_{eq}} = n\log t + \log k \qquad \text{Eq.35}$$

Whilst the slope gives *n* which is a good indication of diffusion model, *k*, which is related to interface velocity (K_{II}) and/or interdiffusion coefficient (D_m) can be computed from the intercept. As explained in Chapter 2, for a planar system (diffusion of penetrant through a polymeric film) *n* has the following physical significance:[10]

i. *Fickian* diffusion (n = 0.5). Since the matrix relaxes much faster than the penetrant diffusion, the interdiffusion should be characterized by D_m. This case is met when the temperature of study is above glass transition temperature of the matrix.

ii. *Case II* diffusion (n = 1). The interdiffusion should be characterized by K_{II}. In this case the interface moves much faster than the matrix relaxes, because the matrix is in the glassy state.

iii. *Anomalous* diffusion *(n* = 0.5 - 1). This case is met when the rates of penetrant diffusion and matrix relaxation are comparable. The interdiffusion should be characterized by D_m and K_{II}.

Examples of the plots used for diffusion model identification and for diffusion constant computation are shown below. The graphs illustrated in Figures 4.22, 4.23 and 4.24 are specific to the interdiffusion studies of lPOE500/PMMA120K sample pairs conducted at different temperature. From the values of *n*, it can be concluded that the diffusion mechanism changes with increasing temperature. At 60 ^{o}C diffusion of linear POE into PMMA follows *Case II* path, while at 85 ^{o}C and 110 ^{o}C the mechanism is *anomalous*. Even if the matrix at 110 ^{o}C is in the glassy state, the diffusion mechanism was found to not be 100 % Fickian because at this temperature we were only 5 ^{o}C above T_g = 105 ± 2 ^{o}C of PMMA. When the interdiffusion between cyclic POE and PMMA at 110 ^{o}C was studied (see Figure 4.25, 4.26), the mechanism was identified as an *anomalous* one. If this is compared with the diffusion of linear POE into PMMA at the same temperature, it must be noted that the values of *n* are closer to *Fickian* behavior than *Case II*.

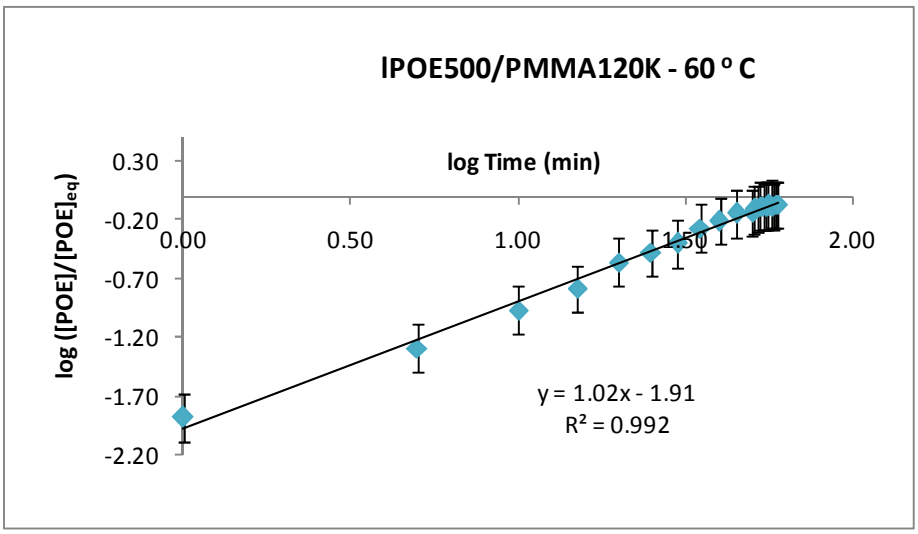

Figure 4.22 - log – log plot of normalized POE mass fraction versus time for lPOE500/ PMMA120K sample pair. Experiments were performed at 60 °C. Diffusional exponent *n* was determined from the slope of the curve. The value obtained for *n* = 1.02 is an indication *Case II* diffusion.

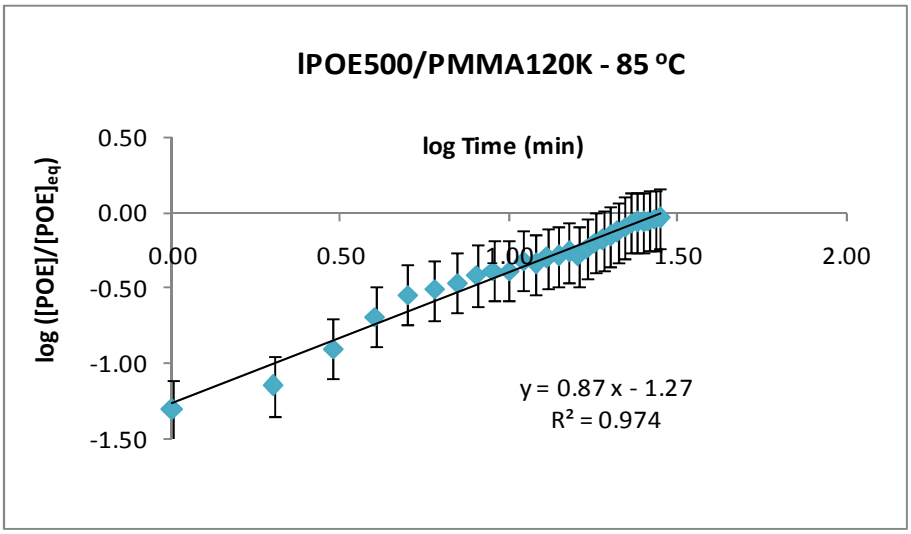

Figure 4.23 - log – log plot of normalized POE mass fraction versus time for lPOE500/ PMMA120K sample pair. Experiments were collected at 85 °C. Diffusional exponent *n* was determined from the slope of the curve. The value obtained for *n* = 0.88 is an indication of *anomalous* diffusion.

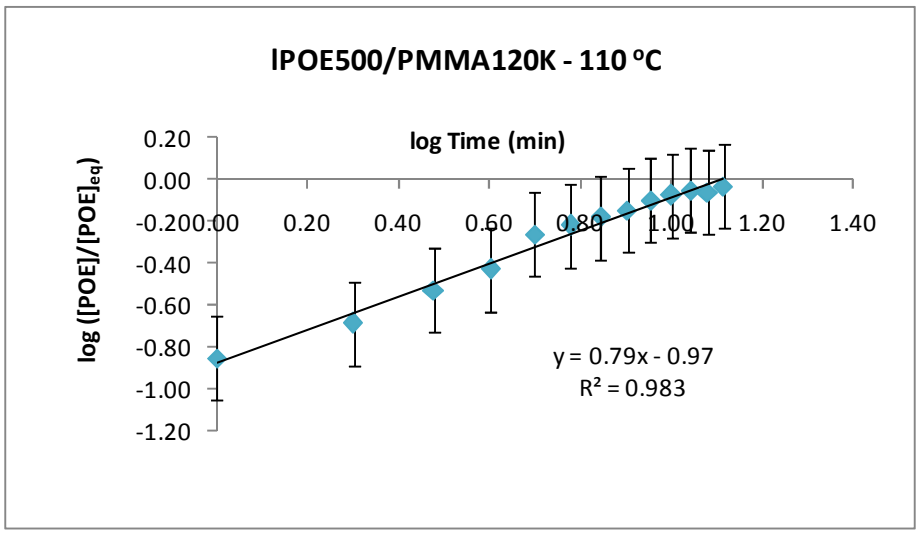

Figure 4.24 - log – log plot of normalized POE mass fraction versus time for lPOE500/ PMMA120K sample pair. Experiments were performed at 110 °C. Diffusional exponent *n* was determined from the slope of the curve. The value obtained for $n = 0.79$ is an indication of *anomalous* diffusion.

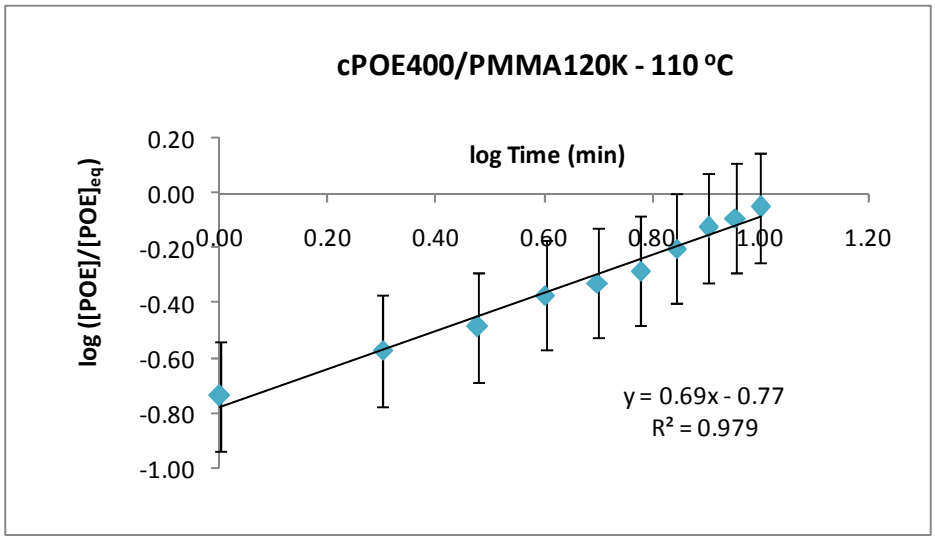

Figure 4.25 - log – log plot of normalized POE mass fraction versus time for cPOE400/ PMMA120K sample pair. Experiments were performed at 110 °C. Diffusional exponent *n* was determined from the slope of the curve. The value obtained for $n = 0.69$ is an indication of *anomalous* diffusion.

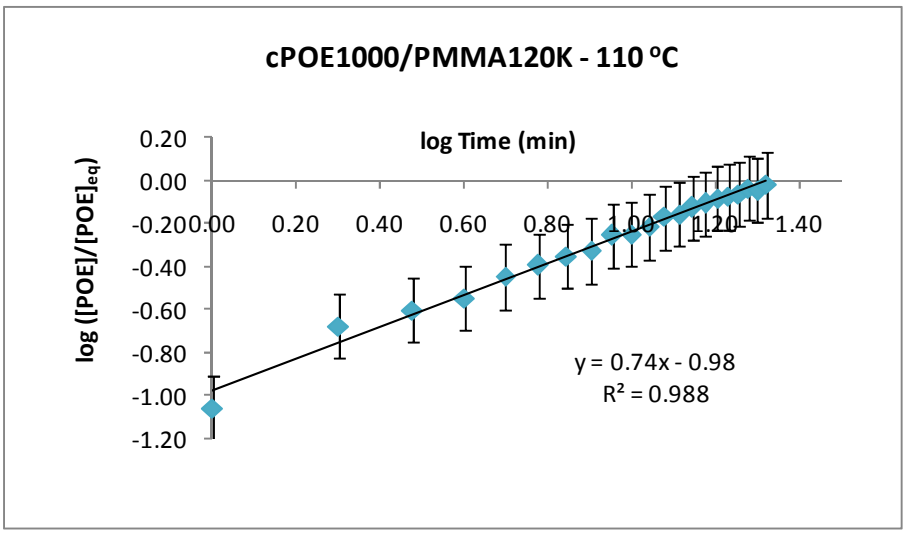

Figure 4.26 - log – log plot of normalized POE mass fraction versus time for cPOE1000/ PMMA120K sample pair. Experiments were performed at 110 °C. Diffusional exponent *n* was determined from the slope of the curve. The value obtained for $n = 0.74$ is an indication of *anomalous* diffusion.

Hence, the observed values of *n* lay between 0.5 and 1 for all sample pairs studied here. The values of *n* and *k* determined for all POE/PMMA systems are summarized in Table 4.3.

A very good interpretation of diffusion behavior can be obtained from *k* values and an initial conclusion can be drawn. As temperature increases, the movement of linear POE into PMMA becomes faster:

$$k_{lPOE500}^{60^oC} < k_{lPOE500}^{85^oC} < k_{lPOE500}^{110^oC} \qquad 36$$

Further, at the same temperature the diffusion of cyclic POE into PMMA is faster and almost double than that for analogous linear specie. At the same time, by increasing molecular weight of cyclic POE, the diffusion becomes slower:

$$k_{lPOE500}^{110^oC} \cong k_{cPOE1000}^{110^oC} < k_{cPOE400}^{110^oC} \quad (37)$$

With $n \neq 0.5$ for all systems observed, the diffusion cannot be evaluated by using only a *Fickian* or *Case II* model. An example of simulating these two models by using the data for one lPOE500/PMMA120K sample at 110 ^oC is illustrated in Figure 4.27. Then, these simulations were performed using the equations specific for these two limiting cases, *Fickian* (Eq. 2) and *Case II* (Eq. 4). As can be seen, none of these models fully explain the experimental data. Even if the diffusion is expected to follow a *Fickian* mechanism at temperatures above the T_g of the matrix and a *Case II* for penetrants moving in a glassy matrix, majority of our studies indicated an anomalous behavior. For the studies conducted at 60 ^oC and 85 ^oC, the matrix changed continuously during the experiments from the glassy to the rubbery state as a result plasticization effect. This explains the deviation from *Case II* especially for 85 ^oC, when the T_g dropped very quickly below 85 ^oC. Then, the mechanism should become *Fickian*. Even for the studies conducted above T_g of the matrix, the diffusion was anomalous. It must be noted that these experiments were performed at 110 ^oC, only 5 ^oC above initial T_g = 105 ^oC of the PMMA. Then at this temperature, the chains are in the rubbery state but still very close to the glassy state which can explain the anomalous behavior.

Table 4.3 - Diffusional exponent *n* and constant *k* values determined for all POE/PMMA120K samples from log – log plots of normalized mass fraction of penetrant versus time, according to Eq.3.

Nr. of Experiments	$\log[POE]'(t) = \log \frac{[POE](t)}{[POE]_{eq}} = n \log t + \log k$			Diffusion Type
	n **Diffusional exponent**	***log k***	***k***	
lPOE500 - 60 °C				
1	1.02	-1.91	0.012	Case II
2	1.05	-2.01	0.010	
Average	**1.03**	**-1.96**	**0.011**	
Stdev	0.02	0.07	0.002	
lPOE500 - 85 °C				
1	0.93	-1.43	0.037	Anomalous
2	0.87	-1.27	0.053	
Average	**0.90**	**-1.35**	**0.045**	
Stdev	0.04	0.11	0.012	
lPOE500 -110 °C				
1	0.79	-0.97	0.106	Anomalous
2	0.74	-0.96	0.110	
3	0.78	-0.97	0.106	
Average	**0.77**	**-0.97**	**0.107**	
Stdev	0.02	0.01	0.002	
cPOE400 -110 °C				
1	0.63	-0.70	0.199	Anomalous
2	0.69	-0.77	0.170	
3	0.65	-0.77	0.170	
Average	**0.66**	**-0.75**	**0.180**	
Stdev	0.03	0.04	0.017	
cPOE1000 -110 °C				
1	0.74	-0.98	0.106	Anomalous
2	0.73	-1.00	0.100	
3	0.70	-0.94	0.114	
Average	**0.72**	**-0.97**	**0.106**	
Stdev	0.02	0.03	0.007	

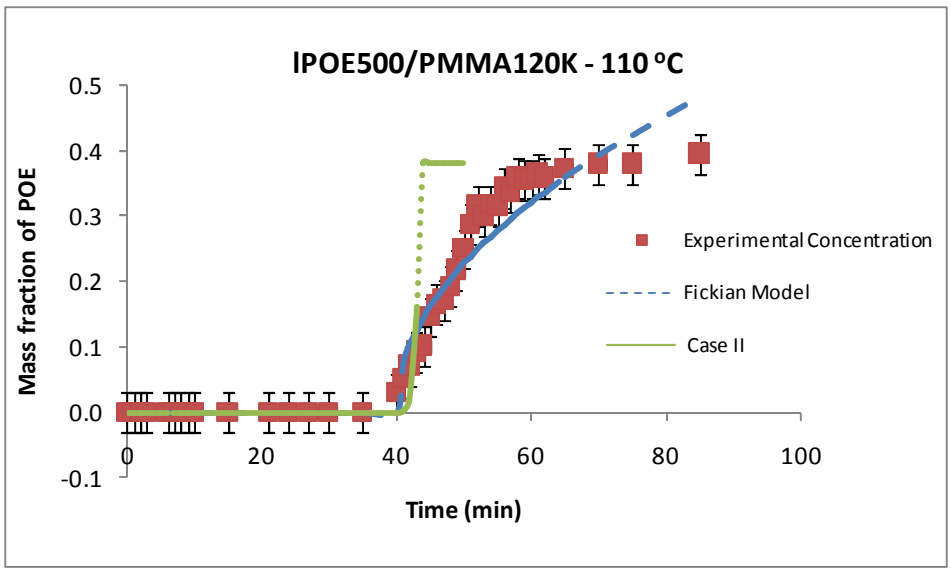

Figure 4.27 – POE concentration versus time for lPOE500/PMMA120K interdiffusion system. Experiments were run at 110 °C. Simulation of the two limiting cases, *Fickian* and *Case II* diffusion are represented here.

Therefore, it is clear that the POE/PMMA interdiffusion cannot be accurately predicted by using either a *Fickian* or *Case II* diffusion model. Then, the best interpretation of these phenomena is by using a combination of these two limiting diffusion cases.

4.4 DETERMINATION OF INTERDIFFUSION CONSTANTS

To characterize the POE/PMMA interdiffusion process an interface velocity called also penetrant velocity, K_{II} was calculated by using *Case II* model and a mutual diffusion coefficient, D_m, was obtained by using *Fickian* diffusion.

4.4.1 Penetrant Velocity (Interface velocity) K_{II}

Case II diffusion represents a process independent of concentration profile, but dependent on matrix relaxation. It can be explained by the fact that POE which can be considered the "faster diffusing component" penetrates into the "slower component" defined by PMMA.[3] The interface is considered to remain "sharp" and moves into the polymer matrix at a constant rate characterized by K_{II}. The travel of interface is equal with the initial penetrant velocity that was calculated from the PMMA film thickness and induction time.

Another way to determine the penetrant velocity (K_{II}) is from the slope of an absorbance versus time plot. The IR absorbance peak characteristic to POE at 1109 cm^{-1} was used to calculate this value (see Figure 4.5 – 4.10). Therefore, the following equation can be expressed:

$$K_{II} = k_{abs} d_p \qquad \text{Eq.38}$$

where: k_{abs} = slope of POE absorbance at 1109 cm^{-1} versus time; d_p = depth of penetration specific at 1109 cm^{-1}.

The interface velocity determined by using Eq.38 should agree with the initial penetrant velocity determined by using Eq.28. A comparison between the initial velocity (v_i) and interface velocity (K_{II}) for all POE/PMMA samples is given in Table 4.4.

Table 4.4 - Initial velocity (v_i) and Interface velocity (K_{II}) determined by using Eq.28 and Eq.38 for all POE/PMMA samples.

Nr. of Experiment	Induction time (min)	Thickness (um)	Thickness-dp (um)	Initial Velocity (v_i) (cm/s)	k_{abs} (Slope) A_{POE} vs. Time	K_{II} (cm/s)
lPOE500 - 60 °C						
1	100	58.6	56.6	9.43E-07	0.275	9.17E-07
2	110	65.3	63.3	9.59E-07	0.281	9.37E-07
		Average		**9.51E-07**		**9.27E-07**
		Stdev		1.11E-08		1.41E-08
lPOE500 - 85 °C						
1	35	39.2	37.2	1.77E-06	0.581	1.94E-06
2	23	28.8	26.8	1.94E-06	0.579	1.93E-06
		Average		**1.85E-06**		**1.93E-06**
		Stdev		1.18E-07		4.71E-09
lPOE500 - 110 °C						
1	10	25.0	23.0	3.84E-06	1.116	3.72E-06
2	40	96.3	94.3	3.93E-06	1.107	3.69E-06
3	13	33.0	31.0	3.97E-06	1.080	3.60E-06
		Average		**3.91E-06**		**3.67E-06**
		Stdev		6.88E-08		6.24E-08
cPOE400 - 110 °C						
1	4	18.1	16.1	6.70E-06	1.970	6.57E-06
2	4	18.0	16.0	6.67E-06	1.920	6.40E-06
3	25	106.0	104.0	6.93E-06	1.901	6.34E-06
		Average		**6.77E-06**		**6.43E-06**
		Stdev		1.46E-07		1.19E-07
cPOE110 - 110 °C						
1	8	20.2	18.2	3.78E-06	1.005	3.35E-06
2	25	57.0	55.0	3.67E-06	1.009	3.36E-06
3	20	45.0	43.0	3.58E-06	1.010	3.37E-06
		Average		**3.68E-06**		**3.36E-06**
		Stdev		9.94E-08		8.82E-09

By increasing the temperature of studies for the same sample pair, lPOE500/PMMA120K, the slope increases. By increasing molecular weight of the penetrant, but keeping the temperature constant, the slope decreases. If a comparison between penetrants having different topology is made, cyclic oligomers move faster than linear analogous under the same conditions. Hence, some relationships defining the diffusion of linear and cyclic POE into PMMA have been established:

$$v_{i\,lPOE500}^{60^oC} \cong K_{IIlPOE500}^{60^OC} < v_{i\,lPOE500}^{85^oC} \cong K_{IIlPOE500}^{85^oC} < v_{i\,lPOE500}^{110^oC} \cong K_{IIlPOE500}^{110^oC} \quad 39$$

$$K_{II\,cPOE400}^{110^oC} \cong 1.8K_{II\,lPOE500}^{110^oC} \cong 1.8K_{II\,cPOE1000}^{110^oC} \quad 40$$

The values obtained for initial velocity and interface velocity for the same sample pairs are in good agreement. This is true even though the PMMA film thickness was different for different samples. Since the interdiffusion between POE and PMMA can be characterized as anomalous, an interdiffusion coefficient must be determined further in order to describe the *Fickian* part of this model.

4.4.2 Interdiffusion Coefficient (D_m)

The interdiffusion coefficient D_m can be obtained by fitting the normalized absorbance-time or concentration-time data to the *Fickian* model described by following equation:[5]

$$\frac{A_{POE}(t)}{A_{eq}} = \frac{[POE](t)}{[POE]_{eq}} = 1 - \frac{4}{\pi}\sum_{n=0}^{\infty}\frac{(-1)^n}{2n+1}\exp\left[\frac{-D_m(2n+1)^2\pi^2 t}{4L^2}\right] \qquad \text{Eq.41}$$

where: $A_{POE}(t)$ = POE absorbance at 1109 cm^{-1} as a function of interdiffusion time within penetration depth; A_{eq} = POE absorbance at 1109 cm^{-1} at equilibrium; *[POE](t)* = POE concentration (mass fraction) as a function of time during interdiffusion between

POE/PMMA determined by using a absorbance – concentration calibration curve; $[POE]_{eq}$ = POE concentration (mass fraction) at equilibrium; n = index of summation; L = thickness of the polymeric film.

Eq.41 is analogous with a mass uptake equation used in gravimetric studies[6] with the exception that for diffusion followed by ATR-FTIR spectroscopy only one surface of polymeric film is exposed to the penetrant, because the other one is attached to the ATR crystal. This equation is the simplified form of ATR-FTIR model applied for the case of a "thick film approximation" (if the conditions 32 and 33 are met). It was derived from *Fickian* diffusion described by Eq.2 and Beer – Lambert law described by Eq.31. If the concentration of penetrant is maintained constant above the depth of penetration, Eq. 41 can be integrated over the depth of penetration. In the studies presented here, this condition is met because the initial velocities were found to be equal with the penetrant velocities determined from the slopes and we can consider that the penetrant moves through the matrix at a constant rate. Therefore, under these conditions, the solution of Eq.41 within the depth of penetration (d_p = depth of penetration at 1109 cm^{-1}) has the following expression:

$$\ln[1-\frac{A_{POE}(t)}{A_{eq}}]=\ln(\frac{4}{\pi})-\frac{D_m\pi^2}{4d_p^2}t \qquad \text{Eq.42}$$

Hence, interdiffusion coefficient can be extracted from the slope of natural logarithm of (1-normalized absorbance) plotted against interdiffusion time. Examples of these plots obtained from interdiffusion studies conducted at same temperature, but using penetrants with different topologies are illustrated in Figures 4.28, 4.29 and 4.30. Cyclic POE (400

g/mol) moves faster than linear POE (500 g/mol), which travels at almost the same diffusion rate as cyclic POE with higher molecular weight (1000 g/mol).

The slope obtained from these graphs, recorded as k_2, has the same physical significance as the intercept (k) (see Table 4.3) determined by plotting log - log of normalized mass fraction against time. The mutual diffusion coefficient is calculated as:

$$D_m = k_2 \frac{4d_p^2}{\pi^2} \qquad \text{Eq.43}$$

The values of interdiffusion coefficient, D_m calculated from all sample pairs are shown in Table 4.5. To compare the slopes (k_2) and intercepts (k) used in D_m computation are included in this table.

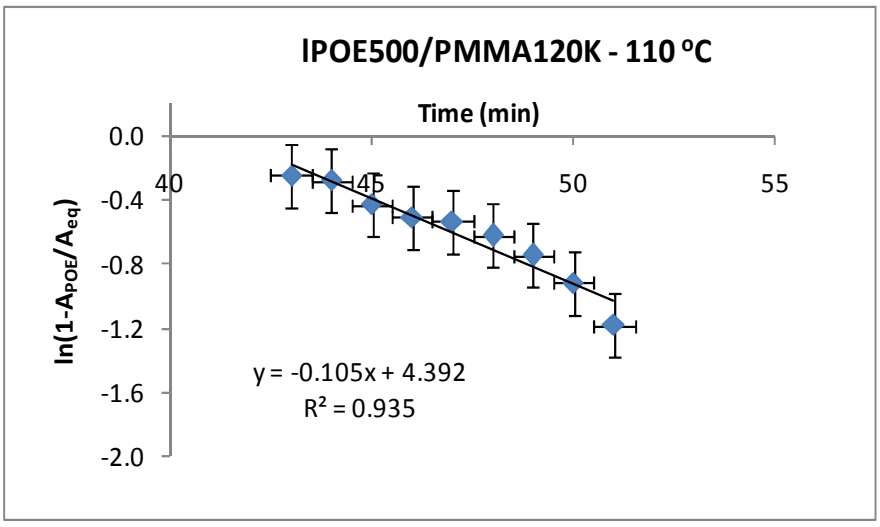

Figure 4.28 - ln ($1-A_{POE}/A_{eq}$) versus time for lPOE500/PMMA120K at 110 °C. Diffusion coefficient, D_m was determined from the slope of the curve (k_2).

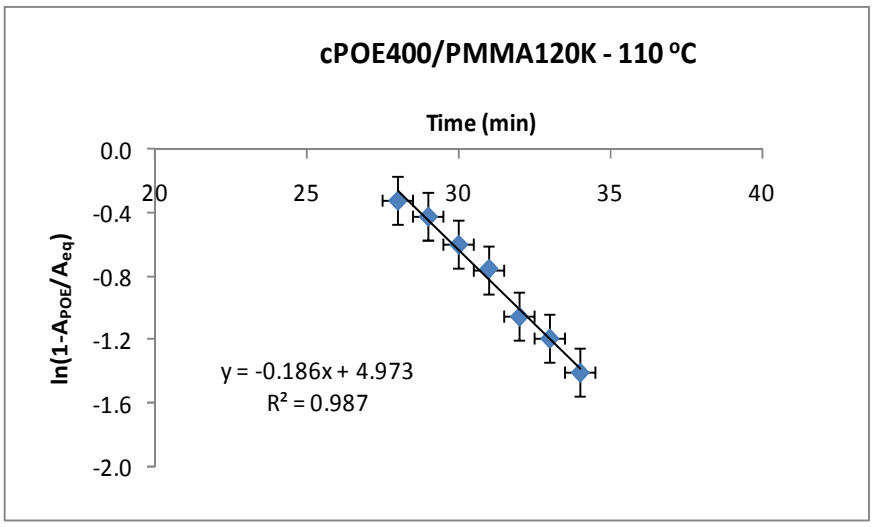

Figure 4.29 - ln $(1\text{-}A_{POE}/A_{eq})$ versus time for cPOE400/PMMA120K at 110 °C. Diffusion coefficient, D_m was determined from the slope of the curve (k_2).

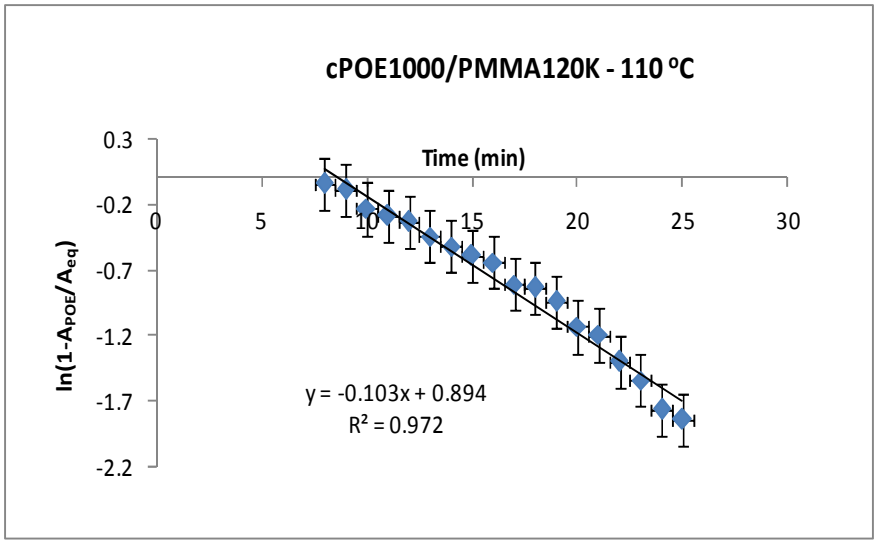

Figure 4.30 - ln $(1\text{-}A_{POE}/A_{eq})$ versus time for cPOE1000/PMMA120K at 110 °C. Diffusion coefficient, D_m was determined from the slope of the curve (k_2).

Since some experiments were conducted at the same temperature, a direct comparison can be made without time-temperature corrections. As may be anticipated, D_m decreases as the molecular weight of poly(oxyethylene) increases and increases with higher temperatures. Also, it can be seen that for almost the same molecular weight, the cyclic

POE diffuses faster than the linear one. The full details of the effects of temperature, topology and molecular weight are discussed in the next chapter.

As shown for penetrant velocity, the same relationships can be drawn for interdiffusion coefficients:

$$D_{m\,lPOE500}^{60^oC} < D_{m\,lPOE500}^{85^oC} < D_{m\,lPOE500}^{110^oC} \quad 46$$

$$D_{m\,cPOE400}^{110^oC} \cong 1.8 D_{mI\,lPOE500}^{110^oC} \cong 1.8 D_{m\,cPOE1000}^{110^oC} \quad 47$$

Table 4.5 - Interdiffusion coefficients (D_m) determined by applying Eq. 43. The mutual diffusion coefficient is calculated from the slope of ln (1-normalized absorbance) plotted against interdiffusion time.

Nr. of Experiment	Thickness	k	k_2	D_m
	(um)	Intercept	ln (1-A_{POE}/A_{eq})	(cm^2/s)
lPOE500 - 60 °C				
1	58.6	0.012	0.013	3.52E-12
2	65.3	0.010	0.012	3.25E-12
	Average	0.011		**3.38E-12**
	Stdev	0.002		1.91E-13
lPOE500 - 85 °C				
1	39.2	0.037	0.046	1.24E-11
2	28.8	0.053	0.050	1.35E-11
	Average	0.045		**1.30E-11**
	Stdev	0.012		7.65E-13
lPOE500 - 110 °C				
1	25.0	0.106	0.103	2.79E-11
2	96.3	0.110	0.105	2.84E-11
3	33.0	0.106	0.110	2.97E-11
	Average	0.107		**2.86E-11**
	Stdev	0.002		9.30E-13
cPOE400 - 110 °C				
1	18.1	0.199	0.191	5.17E-11
2	18.0	0.170	0.190	5.14E-11
3	106.0	0.170	0.186	5.03E-11
	Average	0.180		**5.11E-11**
	Stdev	0.017		7.16E-13
cPOE110 - 110 °C				
1	20.2	0.106	0.103	2.79E-11
2	57.0	0.100	0.107	2.89E-11
3	45.0	0.114	0.109	2.95E-11
	Average	0.106		**2.88E-11**
	Stdev	0.007		8.26E-13

The magnitude of the errors for the interdiffusion coefficients was determined by following the method of Jabbari and Peppas in a diffusion study of PVME into PS.[3] The maximum uncertainty in PMMA film thickness, depth of penetration, refractive index, wavelength of IR radiation and area of deconvoluted peaks gave a maximum compound error of 20% (see Appendix).

4.4.3 Combination of *Fickian* and *Case II* models

The average values of interface velocity K_{II} and mutual diffusion coefficient D_m obtained for all POE/PMMA120K samples including, the errors, are summarized in Table 4.6.

Table 4.6 – Average values of interface velocity (K_{II}) and interdiffusion coefficient (D_m)

Diffusant	MW (g/mol)	Temperature (°C)	K_{II} (cm/sec)	D_m (cm^2/sec)
linear POE				
lPOE500	500	60	$9.27 \pm 0.19 \times 10^{-7}$	$3.38 \pm 0.68 \times 10^{-12}$
		85	$1.93 \pm 0.39 \times 10^{-6}$	$1.30 \pm 0.26 \times 10^{-11}$
		110	$3.67 \pm 0.73 \times 10^{-6}$	$2.86 \pm 0.54 \times 10^{-11}$
cyclic POE				
cPOE400	400	110	$6.43 \pm 1.29 \times 10^{-6}$	$5.11 \pm 1.02 \times 10^{-11}$
cPOE1000	1000	110	$3.36 \pm 0.67 \times 10^{-6}$	$2.88 \pm 0.57 \times 10^{-11}$

It must be emphasized that the interdiffusion constants shown in Table 4.6 were acquired by assuming only *Case II* diffusion in determining K_{II} and only *Fickian* diffusion in resolving D_m. The best way to describe the anomalous behavior of POE/PMMA interdiffusion process is by using a combination of *Fickian* and *Case II* models.

Hence, by following Jabarri and Peppas[3] approach the next steps were applied to attain the diffusion parameters for the best fit of the experimental data:

a. Predict *Fickian* POE concentration values over interdiffusion time by using the ATR diffusion equation for thick film approximation (Eq.41) until they are coming adjacent to experimental results. An interdiffusion coefficient, D_m was computed from here.

b. Determine the non-Fickian (*Case II*) component, $[POE]_{II}$ of cumulative POE concentration inside the penetration depth by taking into account the exponential decay of absorbance intensity. Therefore, an interface velocity, K_{II} was resolved from here:

$$[POE]_{II}(t) = [POE]_{\inf} \exp\left[\frac{-2(d_{PMMA} - K_{II}t)}{d_p}\right] \qquad \text{Eq.48}$$

For a better understanding, Figures 4.31 – 4.35 illustrate the model prediction by using a combination of *Fickian*/*Case II* diffusion for all POE/PMMA samples. The plots also include the experimental data, as well as the predictions using only *Fickian* or *Case II* models. By using a *Fickian* or a *Case II* model by itself a good fit to the experimental values may not be obtained. This is in a very good agreement with our results which indicate an anomalous diffusion for POE/PMMA (see Table 4.3).

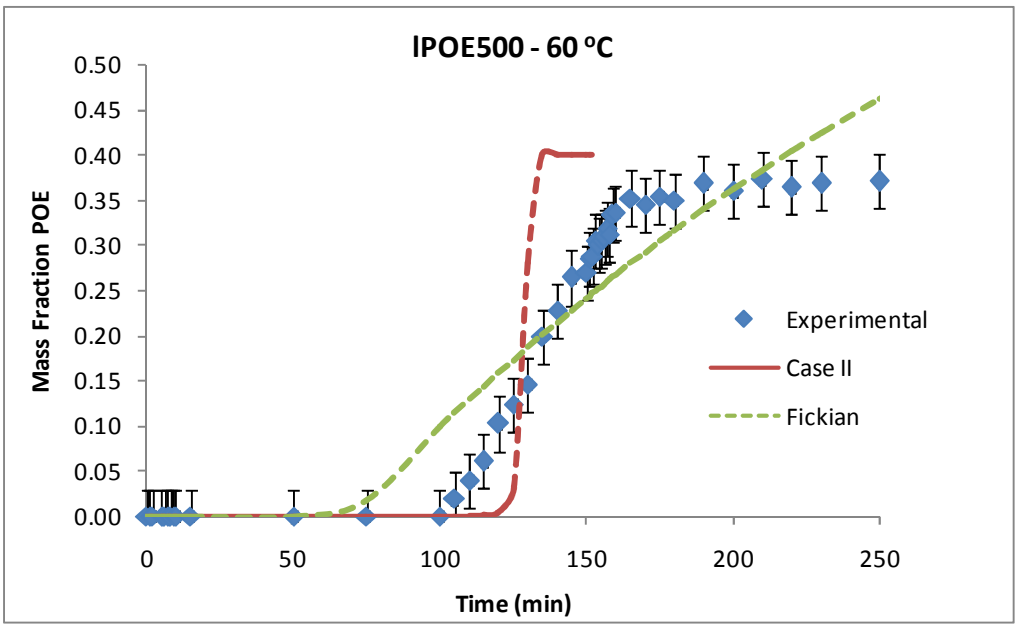

Figure 4.31 – Experimental mass fraction of POE as a function of interdiffusion time and model predictions: *Fickian* and *Case II*. The sample pair studied here was lPOE500/PMMA120K at 60 °C.

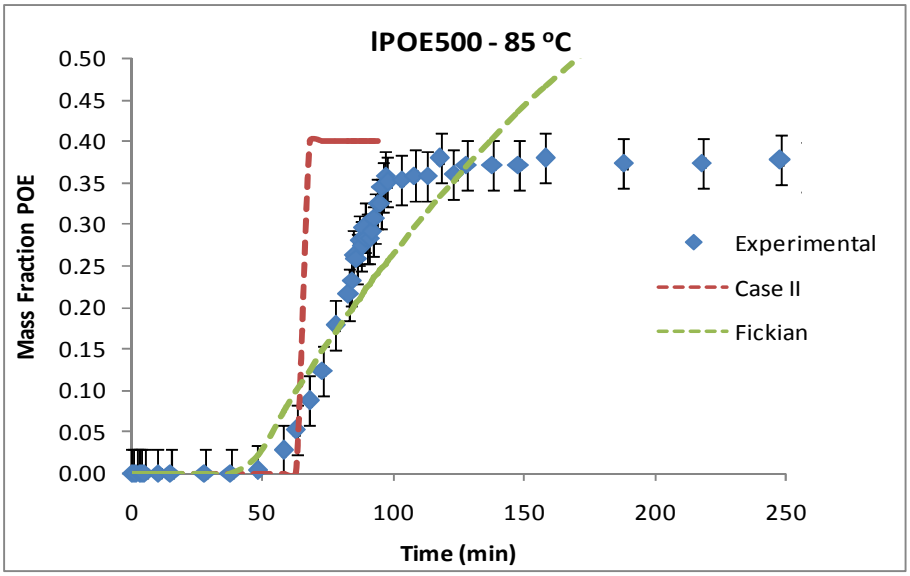

Figure 4.32 – Experimental mass fraction of POE as a function of interdiffusion time and model predictions: *Fickian* and *Case II*. The sample pair studied here was lPOE500/PMMA120K at 85 °C.

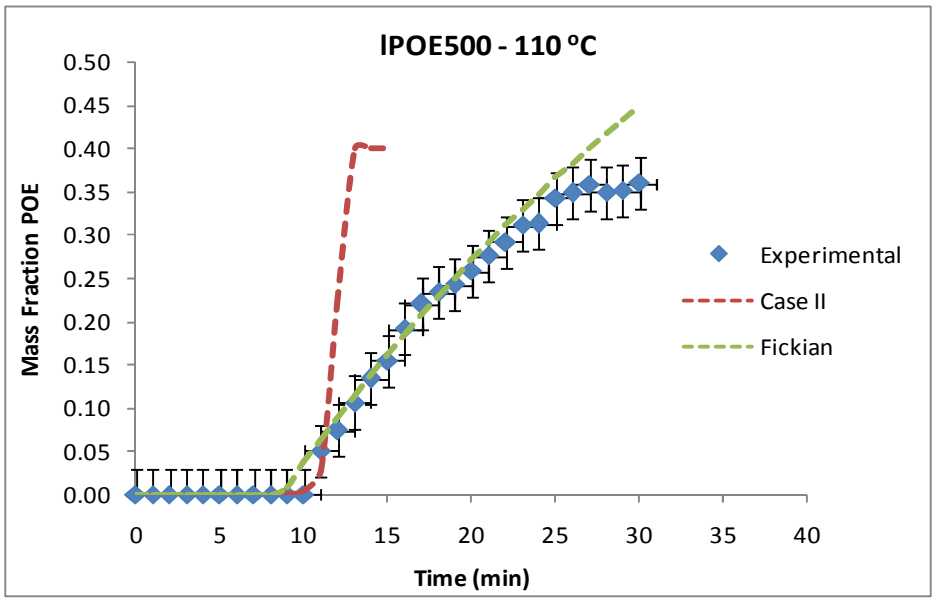

Figure 4.33 – Experimental mass fraction of POE as a function of interdiffusion time and model predictions *Fickian* and *Case II*. The sample pair studied here was lPOE500/PMMA120K at 110 °C.

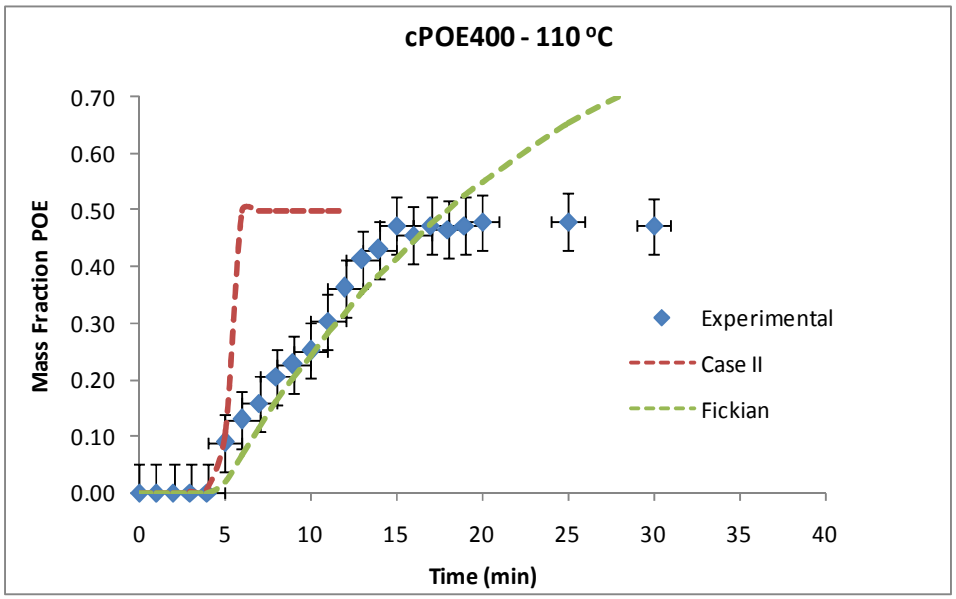

Figure 4.34 – Experimental mass fraction of POE as a function of interdiffusion time and model predictions: *Fickian* and *Case II*. The sample pair studied here was cPOE400/PMMA120K at 110 °C.

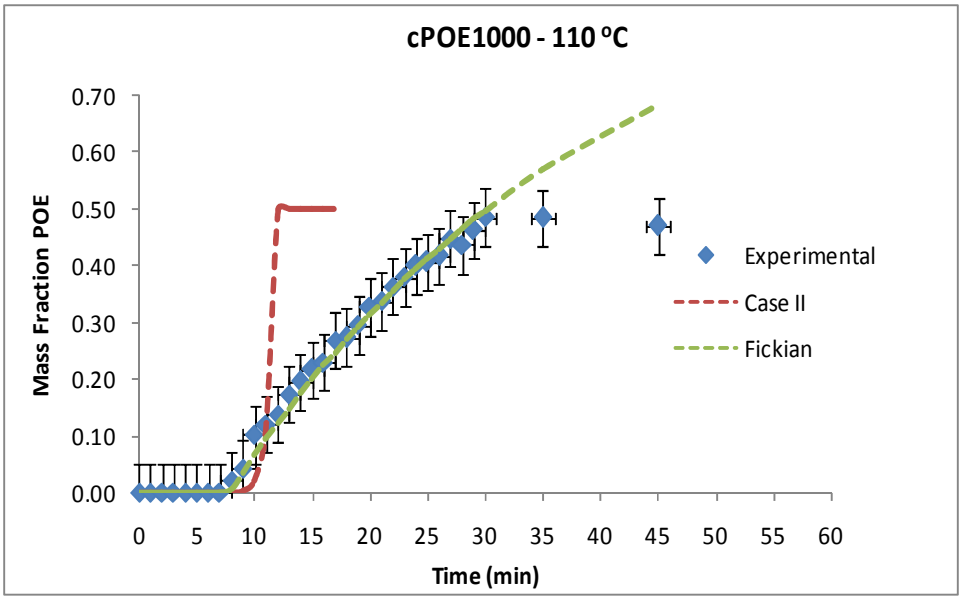

Figure 4.35 – Experimental mass fraction of POE as a function of interdiffusion time and model predictions: *Fickian* and *Case II*. The sample pair studied here was cPOE1000/PMMA120K at 110 °C.

The average values of interdiffusion constants, K_{II} and, respectively D_m determined by using a combination of *Fickian* and *Case II* are presented in Table 4.7.

Table 4.7 – Average values of predicted interface velocity (K_{II}) and interdiffusion coefficient (D_m).

Diffusant	MW (g/mol)	Temperature (°C)	Predicted K_{II} (cm/sec)	Predicted D_m (cm^2/sec)
linear POE				
lPOE500	500	60	7.40×10^{-7}	9.33×10^{-13}
		85	8.70×10^{-7}	1.49×10^{-12}
		110	3.40×10^{-6}	7.50×10^{-12}
cyclic POE				
cPOE400	400	110	5.50×10^{-6}	1.40×10^{-11}
cPOE1000	1000	110	2.80×10^{-6}	8.38×10^{-12}

It must be concluded that the interdiffusion parameters K_{II} and D_m resolved from modeling (see Table 4.7) follow the same path as those obtained from experiments by assuming 100% *Fickian* model for D_m or 100% *Case II* for K_{II} (see Table 4.6). At the same temperature cyclic POE moves faster and closer to a *Fickian* behavior than linear analogous POE. At temperatures lower than the glass transition temperature of the matrix the interdiffusion can be characterized as anomalous, with lower *Fickian* and higher *Case II* component. This was expected because T_g of PMMA drops off during diffusion. Also, same anomalous path, but with higher *Fickian* component was determined at the temperature of study above T_g of the matrix. These predicted results were in good agreement with the diffusion behavior indicated by the n value obtained from the experimental data.

4.5 REFERENCES

1. *SigmaAldrich*, (Technical Data Sheet).

2. Ingham, J. D.; Lawson, D. D., Refractive index-molecular weight relationships for poly(ethylene oxide). *Journal of Polymer Science - Part A: General Papers* **1965,** *3*, (7), 2707-2710.

3. Jabbari, E.; Peppas, N. A., Use of FTIR-ATR to study interdiffusion in poly(styrene) and poly(vinyl methyl ether). *Macromolecules* **1993,** *26*, (9), 2175-2186.

4. Urban, M., *Attenuated Total Reflectance Spectroscopy of Polymers*. American Chemical Society, Washington, DC: 1996.

5. Fieldson, G. T.; Barbari, T. A., The use of FTIR-ATR spectroscopy to characterize penetrant diffusion in polymers. *Polymer* **1993,** *34*, (6), 1146-1153.

6. Guo, J.; Barbari, T. A., A dual mode, local equilibrium relaxation model for small molecule diffusion in glassy polymer. *Macromolecules* **2008,** *41*, (20), 7762-7764.

7. Singla, S.; Beckham, H. W., Miscible blends of cyclic poly(oxyethylene) in linear polystyrene. *Macromolecules* **2008,** *41*, (24), 9784-9792.

8. Martuscelli, E.; Demma, G.; Rossi, E.; Segre, A. L., Evidence of compatibility in the melt for poly(ethylene oxide) poly(methyl methacrylate) blends cy C13 NMR investigations. *Polymer Communications* **1983,** *24*, (9), 266-267.

9. Silva, C. G.; Machado, J. C.; Song, M.; Hourston, D. J., Nanoheterogeneities in PEO/PMMA blends: A modulated DSC approach. *Journal of Applied Polymer Science* **2000,** *77*, (9), 2034-2043.

10. Peppas, N. A.; Brannon-Peppas, L., Water diffusion and sorption in amorphous macromolecular systems. *Journal of Food Engineering* **1994,** *22*, (1-4), 189-210.

CHAPTER 5

DISCUSSIONS

The results collected from diffusion of linear or cyclic poly(oxyethylene) oligomers into poly(methyl methacrylate) using ATR-FTIR spectroscopy indicate that not only the temperature and penetrant molecular weight play a critical role in this process, but also the molecular topology. Interpretation of the data in light of these results is discussed here. Part of the discussion presented in this chapter is a comparison between the current results and the data found in the literature. A predictive scaling for the relationship between the diffusion coefficient of cyclic and linear oligomers is also proposed.

5.1 TEMPERATURE INFLUENCE - DIFFUSION OF LINEAR POE OLIGOMERS INTO PMMA

The temperature dependence on the interdiffusion between linear poly(oxyethylene) oligomers and poly(methyl methacrylate) was evaluated by carrying out repeatable diffusion experiments at several temperatures. The molecular weight of POE diffusant was 500 g/mol, while the molecular weight of the PMMA matrix was 120 kg/mol for all samples. In all the studies presented here, the POE oligomers are in liquid state because they are above their glass transition temperature (T_{gPOE} = -70 ± 2 ^{o}C). In the study conducted at 110 ^{o}C, PMMA was in the rubbery phase, (T_{gPMMA} = 105 ± 2 ^{o}C). The other two interdiffusion studies were initiated at temperatures below T_g of

PMMA120K. However, if the temperatures were maintained at 60 °C or 85 °C until interdiffusion was completed, the glass transition temperature of the matrix drops during POE penetration below the experimental temperature. DSC data show that POE acts as a plasticizer for PMMA resulting in a decrease of the glass transition of the lPOE500/PMMA120K sample to 5 ± 2 °C for 40 wt % POE in PMMA. Only 10 wt % POE in PMMA drops the initial T_g of PMMA to 78 ± 2 °C, whilst 20 wt % POE in decreases the T_g to ~ 47 °C. Thus, for the interdiffusion studies at 85 °C, the matrix became rubbery as soon as ~ 9 wt % POE moved into PMMA. For the studies performed at 60 °C, ~ 17 wt % POE into PMMA reduces the glass transition temperature of the matrix to ~ 58 °C. Many research groups have observed identical changes in the glass transition temperature of PMMA/POE blends.[1,2]

Variation in T_g during the interdiffusion process can have a huge impact on transport behavior. In majority of the cases it was found that POE/PMMA diffusion follows an anomalous path, which is a combination between *Fickian* and *Case II* mechanisms (see Table 4.3). As discussed in Chapter 2, an anomalous mechanism is observed when changes in the glass transition temperature of a material take place during diffusion. This is in an excellent agreement with our observations. As the temperature is decreased, the diffusional exponent (n) increases, which is an indication of more non-Fickian behavior.

This conclusion is supported by the gravimetric studies conducted at 60 °C and 85 °C. The amount of POE penetrant was calculated with the following formula:

$$\Delta m_{POE}(t) = m_{PMMA+POE}(t) - m_{PMMA}(t_0) \qquad \text{Eq.51}$$

where: $\Delta m_{POE}(t) =$ mass of POE penetrating into PMMA film as a function of time; $m_{PMMA+POE}(t) =$ mass of PMMA/POE system as a function of time and $m_{PMMA}(t_0) =$ mass of PMMA film at time zero (initial time) before immersing into POE solution.

The results calculated from a gravimetric study conducted at 60 ^{o}C are shown in Table 5.1. As expected, the amount of POE into PMMA increases in time. The experiments were stopped before reaching equilibrium because the films became flexible and more as a result of troublesome to handle reduced glass transition temperature. Above 16 wt % POE into PMMA, the plasticized PMMA goes into its rubbery phase, which is consistent with DSC measurements.

Table 5.1 – Results obtained from a gravimetric experiment performed at 60 ^{o}C using lPOE500/PMMA120K sample pair.

Measurement	Temperature	Time	$m_i = m_{PMMA}$	$m_f(t) = m_{POE+PMMA}(t)$	$\Delta m(t)$	$\Delta m(t)/m_i$
		(min)	*(mg)*	*(mg)*	*(mg)*	
1	60 ^{o}C	0	98.15	98.15	0.00	0.00
2		5	98.15	101.27	3.12	0.03
3		8	98.80	104.89	6.09	0.06
4		12	85.65	92.31	6.66	0.08
5		15	77.94	86.26	8.32	0.11
6		20	88.98	101.51	12.53	0.14
7		25	84.33	97.98	13.65	0.16

The gravimetric studies at 85 ^{o}C were harder to be performed because the PMMA films go into a rubbery state faster than at 60 ^{o}C. Still, repeatable measurements were carried out at both temperatures. Figure 5.1 illustrates a comparison between gravimetric studies conducted at 60 ^{o}C and 85 ^{o}C. Only by a simple inspection of the graphs, it can be seen that the diffusion rate is higher with increasing the temperature of study.

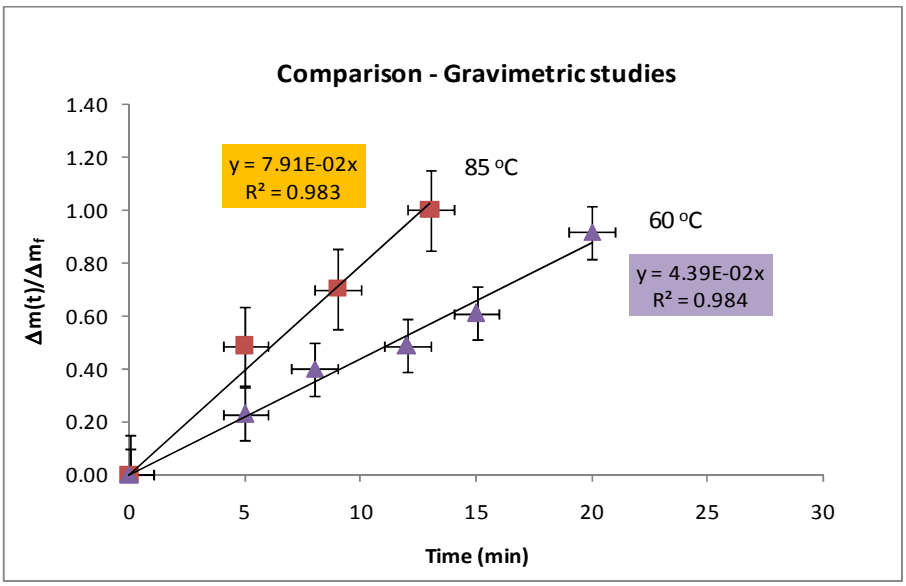

Figure 5.1 – Comparison of normalized mass of POE as a function of interdiffusion time for studies done at 60 °C and 85 °C. The sample studied here was lPOE500/PMMA120K. The thicknesses of the films were 220 ± 2µm.

Following the same algorithm as that used for the ATR-FTIR data, the diffusional exponent (*n*) and the intercept (*k*) were determined from a plot of log $\Delta m_{POE}(t)/m_i$ versus log time (See Figures 5.2 and 5.3).

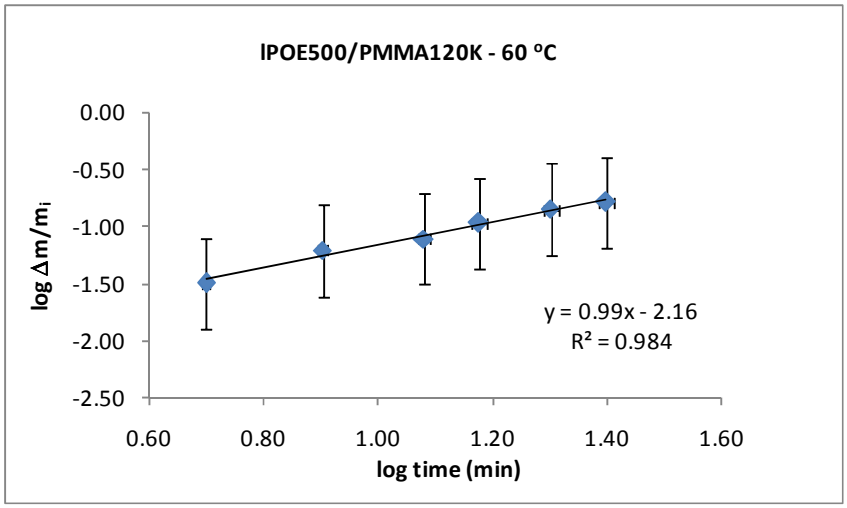

Figure 5.2 – log – log plot of normalized POE mass versus time for lPOE500/ PMMA120K at 60 °C. Diffusional exponent *n* was determined from the slope of the curve. The value obtained for $n = 0.99$ is an indication of *Case II* diffusion.

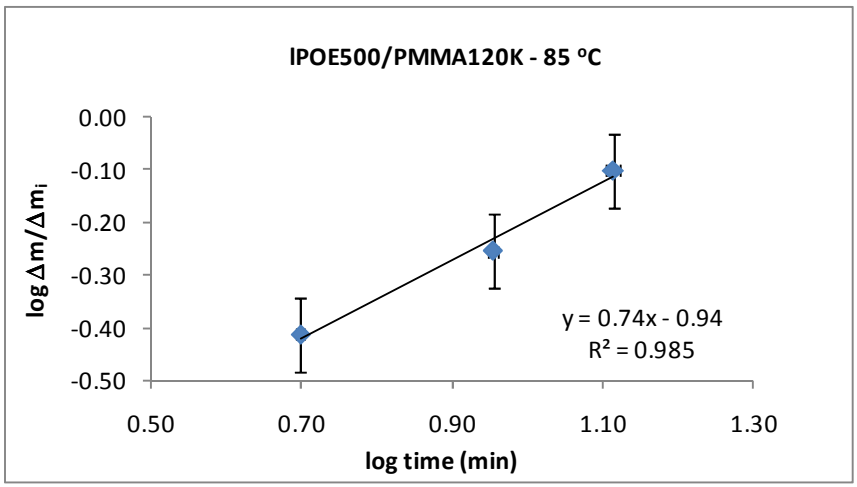

Figure 5.3 – log – log plot of normalized POE mass versus time for lPOE500/ PMMA120K at 85 ^{o}C. Diffusional exponent *n* was determined from the slope of the curve. The value obtained, *n* = 0.74, is an indication of *anomalous* diffusion.

Table 5.2 is a summary of the values obtained for *n* and *k* from gravimetric measurements which are in good agreement with those achieved from spectroscopic investigations. The values of *n* and *k* determined from ATR data can be found in Table 4.3 which is a description of the diffusion type for all POE/PMMA120K samples.

Table 5.2 – Diffusional exponent *n* and constant *k* determined for all lPOE500/PMMA120K samples by gravimetric studies.

Nr. of experiments -Gravimetry-	n Diffusional Exponent	log k	k	Diffusion Type
lPOE500 - 60 °C				
1	0.81	-1.93	0.012	Anomalous
2	0.82	-1.85	0.014	
3	0.81	-1.79	0.016	
4	1.00	-2.16	0.007	
Average	**0.86**	**-1.93**	**0.012**	
Stdev	0.09	0.16	0.004	
lPOE500 - 85 °C				
1	0.74	-0.94	0.115	Anomalous
2	0.63	-0.83	0.148	
Average	**0.68**	**-0.88**	**0.132**	
Stdev	0.08	0.08	0.023	

The diffusion of POE into PMMA follows an anomalous path and the behavior becomes more non-Fickian and slower with a decrease in temperature. Some differences between these two methods are seen in the values of *n* and *k*, but the relative differences are the same.

An interface velocity was determined from the gravimetric studies conducted at 60 ^{o}C by assuming *Case II* diffusion. The values of the intercept (*k*) tabulated in Table 5.3 were entered in the following equation:

$$k = \frac{2K_{II}}{(\frac{d_{PMMA}}{2})} \qquad \text{Eq.52}$$

The thickness of the PMMA film must be divided by 2 because the penetrant diffuses into the matrix through both sides and the diffusion front meets at the center of the slab. The K_{II} values obtained from repeatable experiments are presented in Table 5.3.

Table 5.3 - Interface velocity, K_{II}, for all lPOE500/PMMA120K samples at 60 ^{o}C by gravimetric studies.

Nr. of Experiments	Thickness (um)	*k* Intercept	K_{II} (cm/s)
lPOE500 - 60 ^{o}C			
1	200	0.012	9.81E-07
2	230	0.014	1.37E-06
3	200	0.016	1.35E-06
4	220	0.007	6.30E-07
	Average	0.012	1.08E-06
	Stdev	0.004	3.51E-07

The average values of the interface velocity and mutual diffusion coefficient obtained for the systems studied at 60 ^{o}C, 85 ^{o}C and 110 ^{o}C using ATR-FTIR spectroscopy and sorption kinetics are summarized in Table 5.4. As can be seen, the average value of interface velocity, K_{II} determined from gravimetric studies performed at 60 ^{o}C was in good agreement with that determined from spectroscopy studies. It is evident that K_{II} and D_m increases with increasing temperature of study.

Table 5.4 - Average of interface velocities (K_{II}) and mutual diffusion coefficients (D_m) obtained from experimental data assuming *Case II* or *Fickian* model. The studies were performed at 60 ^{o}C, 85 ^{o}C at 110 ^{o}C. The linear POE penetrant MW was 500 g/mol and PMMA matrix MW was 120 kg/mol.

Diffusant	MW (g/mol)	T (^{o}C)	Gravim - K_{II} (cm/sec)	ATR/FTIR - K_{II} (cm/sec)	ATR/FTIR - D_m (cm^2/sec)
lPOE500	500	60	(10.83 ± 3.51) x 10^{-7}	(9.27 ± 0.19) x 10^{-7}	(3.38 ± 0.68) x 10^{-12}
		85		(1.93 ± 0.39) x 10^{-6}	(1.30 ± 0.26) x 10^{-11}
		110		(3.67 ± 0.73) x 10^{-6}	(2.86 ± 0.54) x 10^{-11}

The mutual diffusion coefficients, D_m obtained at different temperature were fit with an Arrhenius type equation:

$$D_m = D_0 \exp(\frac{-E_a}{RT}) \qquad \text{Eq.53}$$

where: E_a = activation energy of diffusion (J/mol); T = temperature (K); R = 8.31J/molK; D_0 = pre-exponential factor (cm^2/s).

By plotting the natural logarithm of D_m versus reciprocal of temperature, the activation energy can be calculated from the slope and the pre-exponential factor from the intercept (see Figure 5.4).

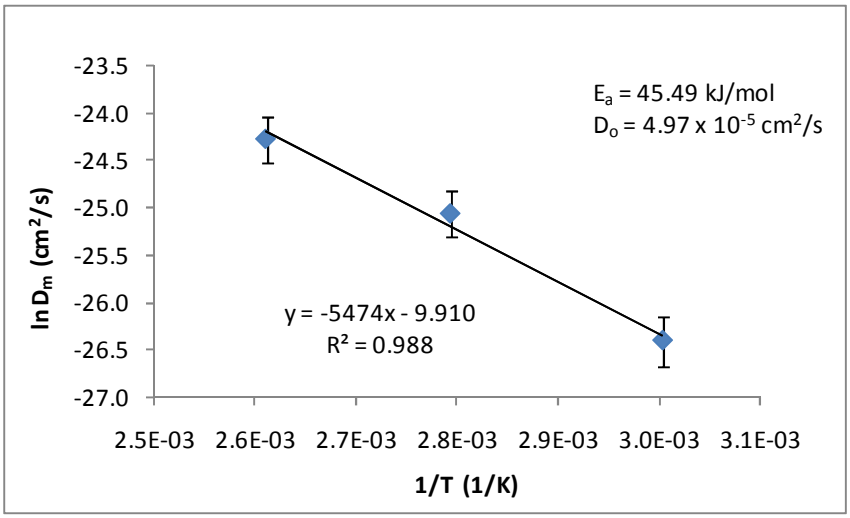

Figure 5.4 – Determination of activation energy of diffusion for lPOE500/PMMA120K by using Arrhenius equation.

The results obtained are shown below:

$$E_a = 45 \text{ kJ/mol} \qquad \text{Eq.54}$$

$$D_0 = 5 \times 10^{-5} \text{ cm}^2/\text{s}$$

The value of activation energy is reasonably comparable with data from the literature. The activation energy of 45 kJ/mol is close to some values reported for similar interdiffusion pairs, such as 49 kJ/mol for polyvinyl chloride/poly(caprolactone)[3] and 62 kJ/mol for a vinyl ester diffusion into poly(vinyl pyrrolidone).[4]

A very limited discussion about possible diffusion mechanisms of the POE/PMMA samples can be provided here. It is expected that PMMA120K follows a reptation mechanism since the molecular weight is above its critical entanglement molecular weight, while linear poly(oxyethylene) follows a Rouse mechanism due to its

comparatively low molecular weight. As discussed in Chapter 2, different models have been proposed to relate D_m with D_s. Despite conflicting results reported by different groups, which indicate that existing models do not uniformly account for experimental results, it is recognized that for low molecular weight penetrants, the interdiffusion behavior above T_g is initially dominated by the penetrant or fast component rather than the polymeric matrix or slow component.[5] In the POE-PMMA sample pairs studied here, the interdiffusing species have very different mobilities since the glass transition of PMMA is much higher than that of POE. Consequently, models such as that described by Eq. 10 cannot be used to obtain a correlation between self-diffusion coefficients of pure components and interdiffusion coefficient. In addition, when penetrants act as plasticizers, a large variation of glass transition temperature with composition is observed,[6] making even more difficult to predict D_m from pure – component D_s values using existing models.

Because in the present systems the molecular weight of PMMA exceeds the entanglement molecular weight, then for the study conducted at 110 ^{o}C ($T > T_g$), the interdiffusion process is expected to be mainly controlled by the motion of POE. Further, as for any miscible blends[2] the value of the mutual diffusion coefficient is expected to be higher than the self-diffusion coefficient of PMMA and lower than the D_s of POE. The Hartley-Crank model[7] can be used to obtain the correlation between the mutual diffusion and self-diffusion coefficients only if both components have similar mobility. Under these circumstances, the Hartley-Crank model might not be a good model to be used here, because POE and PMMA have very different dynamics at a given temperature.

Table 5.5 represents a summary of some interdiffusion coefficients reported in the literature for similar systems. These data represent only a small portion of many diffusion studies conducted by ATR-FTIR spectroscopy found in the literature, but are the most relevant materials to the POE/PMMA study reported here.

Table 5.5 - Summary of the most relevant interdiffusion studies published in literature. The mutual diffusion coefficient (D_m) is reported in cm^2/s.

Matrix (MW)	Penetrant (MW)	Temperature	Technique	D_m (cm^2/s)	Ref. N°
Silicone	Urea	20 ^{0}C	ATR-FTIR	$5.2x10^{-9}$	8
PAN (150K)	H_2O	23 ^{0}C		$1.1x10^{-10}$	9
PVP (1,100K)	VE oligomer (690)	80 ^{0}C		VE Peaks: $5.3 - 8.6x10^{-9}$ PVP Peaks: $2.2 - 2.6x10^{-9}$	4
PVP (1,100K)		90 ^{0}C		VE Peaks: $9.3 - 14x10^{-9}$ PVP Peaks: $4.9 - 5.0x10^{-9}$	
PVP (1,100K)		100 ^{0}C		VE Peaks: $2.1 - 2.2x10^{-8}$ PVP Peaks: $1.4 - 1.5x10^{-8}$	
PS(100K) T_g = 100 ^{0}C	PVME (99K) T_g = -24 ^{0}C	105 ^{0}C		$1.5x10^{-12}$	5
PVP (12K) T_g = 128 ^{0}C	PEG (400)	80 ^{0}C	Optical Wedge Microinterferometry	$10^{-8} - 10^{-7}$	10
PVP (2.5K)	PEG (400, 600, 1000)	100 ^{0}C		PEG(400) - $5x10^{-7}$ PEG(600) - $2x10^{-7}$ PEG(1000) - $5x10^{-8}$	
dPMMA (115K) T_g = 123 ^{0}C	PEG (640) T_g = -19 ^{0}C	26 ^{0}C	Neutron Reflectivity	PEG interface - $3.2x10^{-16}$ PMMA interface - $4.2x10^{-16}$	11
PS (2.9K)	PVME (99K)	112 ^{0}C	Modified Optical Schlieren	$1.1x10^{-9}$	12

The research reported by Jabbari and Peppas[5] is one of the best interdiffusion studies using ATR-FTIR spectroscopy presented in the literature. It can be compared directly to our data. They studied PS100K, which behaves similar to PMMA120K because of their comparable physical properties, such as M_e and T_g. The results obtained from their studies were explained in terms of fast mode theory. Diffusion between PVME and PS at 105 ^oC, which was above the glass transition temperature of PS, was dominated by the fast component, PVME. As discussed above, the same trend was found for POE into PMMA.

Data obtained from PVP/PEG interdiffusion studies[10] using the same penetrant gave values of D_m which are larger than that we measured for POE into PMMA. This is most likely explained by the use of a different matrix (PVP versus PMMA) causing different interactions and chain mobilities. Since the molecular weight of PVP is below its entanglement molecular weight it would be expected to relax by Rouse mechanism.

A direct comparison in systems can be made with data published by Bucknall et al.[11] The interdiffusion coefficients are orders of magnitude lower than ours (10^{-16} cm^2/s versus 10^{-12} cm^2/s), which can be explained by measurements at a different temperature (26 ^oC) in addition to use of a deuterated matrix. In this case the PMMA is almost 80 ^oC below its T_g causing a reduced mobility compared with the current system. When the polymers are below T_g, the free volume effects become very important in diffusion and highly asymmetric diffusion profiles can be observed.[13] Also, if the interdiffusion studies are done below T_g of the matrix, the diffusion might be dominated by the slow PMMA component.[5,7,14] The values of D_m obtained by Bucknall et al. are close to the self-

diffusion coefficient of PMMA120K ($D_s^{dPMMA127K}$ = 4.94 x 10^{-16} cm^2/s),[15] indicating that in this case the diffusion process might be explained by slow mode theory. Also, it is well known that the deuteration plays an important role in slowing down the diffusion behavior.[5,14] In the studies conducted by Jabbari and Peppas,[14] the mutual diffusion coefficients determined in case of PVP/dPS system were ~ 3 times smaller versus PVP/hPS. If the values of E_a = 45 kJ/mol and D_0 = 5 x 10^{-5} cm^2/s obtained from these studies are used, an interdiffusion coefficient of 7.1 x 10^{-13} cm^2/s at 26 ^oC is predicted, which is 3 order of magnitude smaller that D_m = 4.2 x 10^{-16} cm^2/s obtained by Bucknall et al.[11]

By comparing the value of D_m between PS and PVME at 112 ^oC obtained by Ye et al.,[12] it is found that D_m determined in our study at 110 ^oC is about 1 order of magnitude lower than theirs. This faster diffusion observed in the study mentioned above can be explained by a lower molecular weight of the matrix which implies a lower glass transition temperature ($T_{g,\ PS2.9K}$ = 70 ^oC)[5] and therefore, higher mobility of the matrix.

5.2 MOLECULAR WEIGHT INFLUENCE - DIFFUSION OF CYCLIC POE OLIGOMERS INTO PMMA

The diffusion between cyclic poly(oxyethylene) oligomers with different molecular weight and poly(methyl methacrylate) was measured at 110 ^oC. As before, the molecular weight of PMMA was 120 kg/mol, while the molecular weight of cPOE 400 g/mol and

1000 g/mol. The average values of interface velocity (K_{II}) and mutual diffusion coefficient (D_m) obtained from these studies are summarized in Table 5.6.

Table 5.6 - Average of interface velocity (K_{II}) and interdiffusion coefficients (D_m) for cyclic POE – PMMA120K at 110 °C.

Diffusant	MW (g/mol)	T (°C)	K_{II} (cm/sec)	D_m (cm^2/sec)
cPOE400	400	110	(6.43 ± 1.29) x 10^{-6}	(5.11 ± 1.02) x 10^{-11}
cPOE1000	1000	110	(3.36 ± 0.67) x 10^{-6}	(2.88 ± 0.57) x 10^{-11}
Ratio cPOE400/cPOE1000			1.9	1.8

Although the cyclic oligomers have a different topology compared to the linear species, the same trend is observed as for linear ones.[5,10,16] As shown in Figures 5.5 and 5.6, K_{II} and D_m decrease with increasing molecular weight of cPOE diffusants.

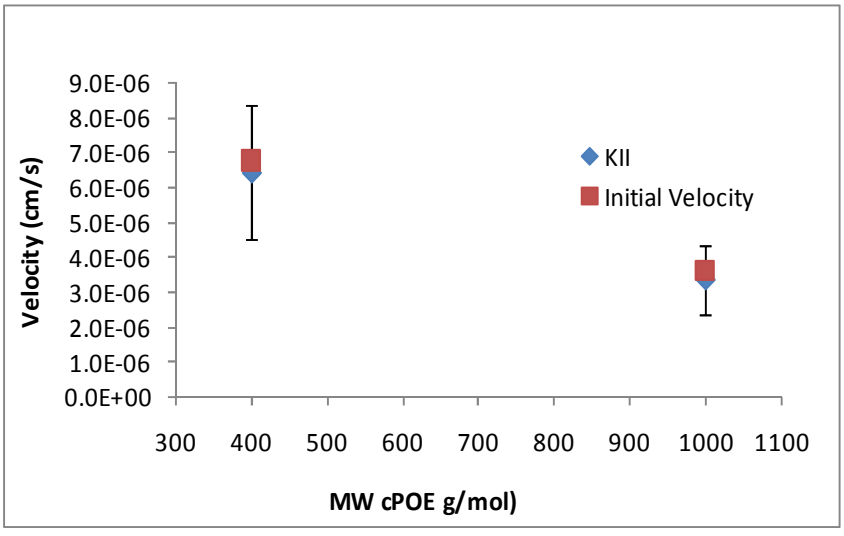

Figure 5.5 – Initial velocity (v_i) and interface velocity (K_{II}) of cyclic POE into PMMA120K as a function of penetrant MW. The studies were conducted at 110 °C.

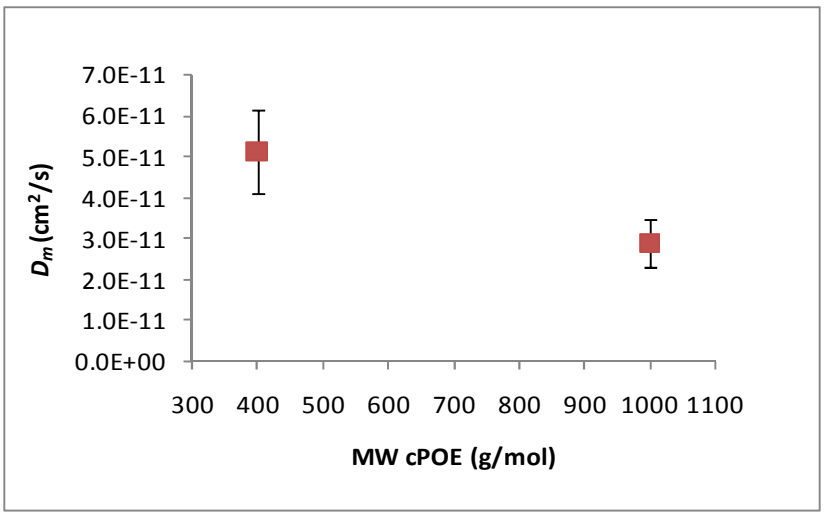

Figure 5.6 – Interdiffusion coefficient (D_m) versus penetrant MW for cyclic POE into PMMA120K at 110 °C.

The ratio between diffusion constants of the cyclic POEs is almost equal with 2, which is expected since the ratio between their molecular weights is 2.5 (400 g/mol versus 1000 g/mol). The equilibrium concentration of cyclic POE in PMMA120K of 47 ± 3 wt% is resolved from ATR-FTIR measurements, which is consistent with DSC data. As can be seen from DSC thermograms shown in Figure 4.19, the glass transition temperature of the blend follows the Fox equation up to 50 wt % cPOE1000 in PMMA120K. A direct comparison between cyclic POE/PMMA blends and linear ones shows an enhanced miscibility of 1.4 times cyclic over linear.

Cates and Deutsch predicted that blends of chemically identical cyclic/linear polymers should have a negative value of Flory-Huggins interaction parameter χ which is an indication of good miscibility.[17] They suggested a possible miscibility of dissimilar ring/linear combinations, even in cases where similar linear/linear combinations are immiscible. MacKnight et al.[17] evaluated the topological effects on blend miscibility by looking at linear or cyclic polycarbonate (PC) blended with linear polystyrene (PS) and

the results indicated that χ is smaller for cyclic PC/linear PS blends than for linear/linear combinations. These results were explained in terms of topological repulsion between rings validating Cates & Deutsch theory.

Both cyclic POE oligomers have their MW below M_e (See Chapter 3) and might be assumed to follow a Rouse mechanism as predicted in theory for linear oligomers with low molecular weight.

Some studies on self-diffusion of cyclic oligomers and polymers have been reported in literature, but only few experimental studies on diffusion of these species into linear matrices were found.[18-20] All of those were discussed in Chapter 2. Whilst the majority of these studies followed the interdiffusion of high molecular weight cyclic polymers in the entanglement regime, the cyclic (POEs) in our studies have a very low molecular weight (below M_e) which might behave differently from the bigger cycles.

In case of dynamics of entangled rings in linear entangled melts, the mechanism proposed by Klein[19] is dependent on the ring size. A more detailed discussion related to the influence of topology to diffusion process follows in the next section.

5.3 TOPOLOGY INFLUENCE - DIFFUSION OF CYCLIC POE OLIGOMERS VERSUS LINEAR INTO PMMA

A direct comparison between the diffusion of cyclic versus linear poly(oxyethylene) oligomers into poly(methyl methacrylate) measured 110 ^{o}C by using

ATR-FTIR spectroscopy technique is shown below. The interdiffusion parameters, K_{II} and D_m, obtained from these studies are summarized in Table 5.7.

Table 5.7 - Average of interface velocity (K_{II}) and interdiffusion coefficients (D_m) for linear and cyclic POE – PMMA120K at 110 ^{o}C.

Diffusant	MW (g/mol)	T (^{o}C)	K_{II} (cm/sec)	D_m (cm^2/sec)
lPOE500	500	110	$(3.67 \pm 0.73) \times 10^{-6}$	$(2.86 \pm 0.54) \times 10^{-11}$
cPOE400	400	110	$(6.43 \pm 1.29) \times 10^{-6}$	$(5.11 \pm 1.02) \times 10^{-11}$
cPOE1000	1000	110	$(3.36 \pm 0.67) \times 10^{-6}$	$(2.88 \pm 0.57) \times 10^{-11}$
Ratio cPOE400/lPOE500			1.8	1.8
Ratio cPOE1000/lPOE500			0.9	1.0

It can be seen that cPOE400 moves 1.8 times faster than lPOE500. Cyclic POE 1000 g/mol and linear 500 g/mol move at almost the same rate, even though the cyclic is double in MW than the linear. For better visualization, the interdiffusion constants are plotted as a function of penetrant molecular weight in Figures 5.7 and 5.8.

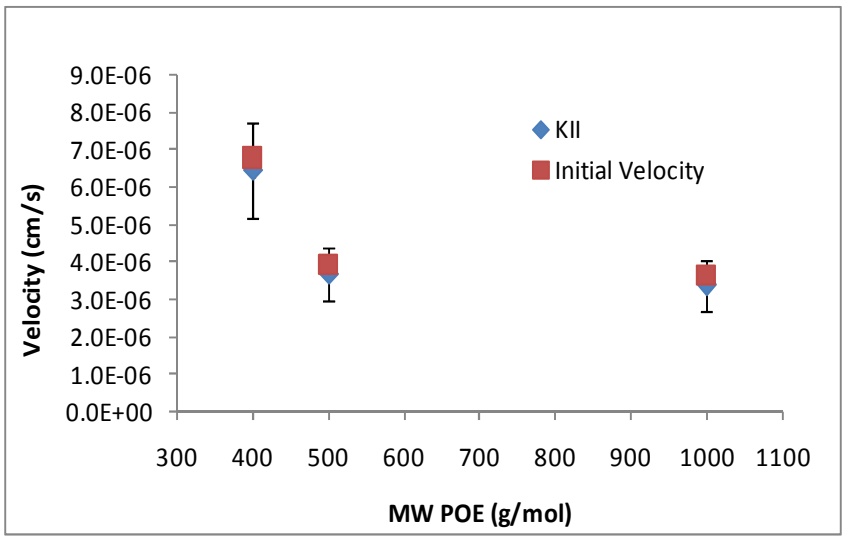

Figure 5.7 – Initial velocity (v_i) and interface velocity (K_{II}) as a function of penetrant MW at 110 °C for diffusion of linear and cyclic POE oligomers into PMMA120K.

.

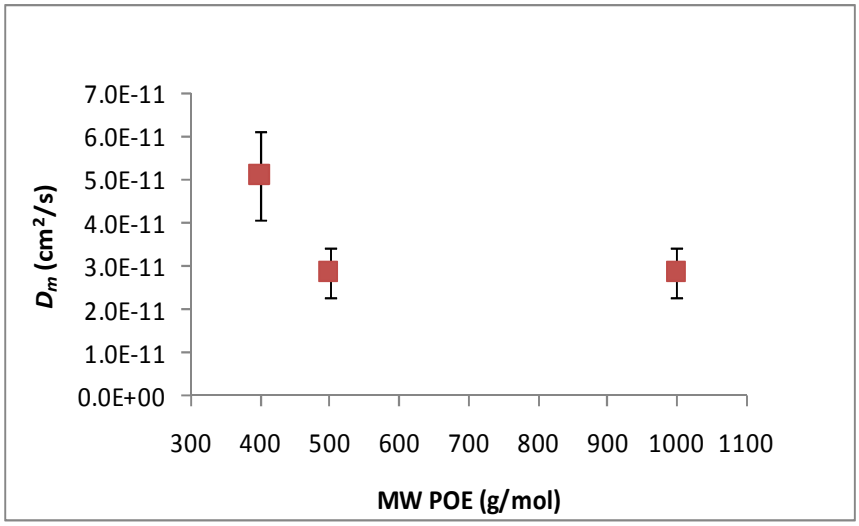

Figure 5.8 – Interdiffusion coefficient (D_m) versus penetrant MW at 110 °C for diffusion of cyclic POE oligomers into PMMA120K.

Diffusional exponents (n) calculated for linear and cyclic POE/PMMA interdiffusing sample pairs revealed anomalous diffusion. This can be explained by the small difference of only 5 °C between the temperature of studies and the initial glass

transition temperature of the matrix. It might be possible that at the beginning of the experiments, the matrix was not fully relaxed and the mechanism was closer to *Case II*. As soon as the POE moves into PMMA, the T_g of the samples drops off and the mechanism starts to be *Fickian*. A smaller value of *n*, closer to 0.5 was found for rings, especially for cPOE400/PMMA120K (see Table 4.3). Thus, under identical conditions the cyclic species behaves more *Fickian* than the linear ones.

An additional approach that can be used to compare the data between these interdiffusing sample pairs with different penetrant topology is to look at interfacial thickness.[4] Since the penetrant enters the matrix only from one side[4] (ATR-FTIR spectroscopy studies), the equation to compute the interface thickness must be modified from the original one derived by Crank.[21] For these particular cases, if there are not other constraints, the equation should be:[4]

$$d_{\text{int}\,erf} = \sqrt{2D_m t} \qquad \text{Eq.55}$$

where d_{interf} represents the interfacial thickness and t is the interdiffusion time. It must be emphasized that this is a slight comparison since this equation was developed to be applied to a symmetrical profile and for the case of infinity diffusion. However, if the thickness of the interface is plotted versus interdiffusion time, it can be observed (see Figure 5.9) that the slope of cPOE400/PMMA120K is 1.7 times larger than that specific to lPOE500/PMMA120K or cPOE1000/PMMA120K system. Of course, that it is expected since the diffusion process follows the same path: cPOE400 > cPOE1000 ≅ lPOE500.

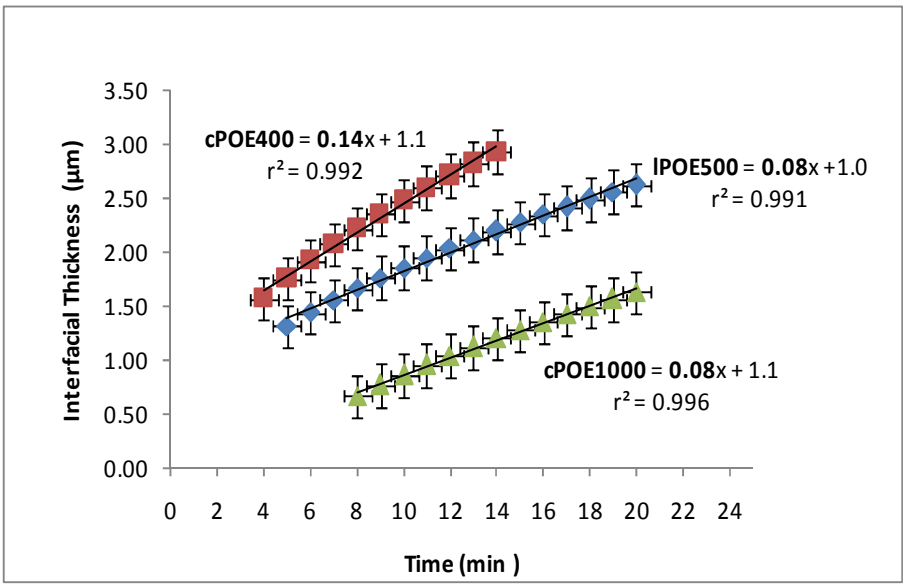

Figure 5.9 – Interfacial thickness (d_{interf}) versus interdiffusion time (t). The studies were conducted at 110 ^{o}C for diffusion of linear (500g/mol) and cyclic POE oligomers (400g/mol, 1000 g/mol) into PMMA120K. For a good comparison, the data for cPOE1000 was shifted down with 1 µm.

As discussed above, there have only been a few experimental studies reported in the literature on diffusion of rings.[18,19] Matsushita et al. compared the diffusion of cyclic and linear high molecular weight polystyrene (PS) and showed that cyclic polymers diffuse 2.2 times faster than linear chains. The conclusions obtained by Matsushita et al. were in good agreement with the prediction of Klein[19] ($D_{cyclic} \cong 2D_{linear}$) for diffusion of small entangled rings in linear matrix. From our studies we came with the same conclusion that the cyclic POE diffuses 1.8 times faster than linear analogous one, even if the diffusion mechanism of unentangled polymers is different than those that are entangled.

The faster diffusion of cyclic oligomers can be explained in terms of chain dimensions. For the same molecular weight, the cyclic and linear POEs have the same

effective degree of polymerization. The free volume introduced by chain ends of linear POE plays an important role in diffusion.[23] Logically the contribution of free volume to diffusion is expected to be less significantly for cyclic polymers, due to the absence of chain ends. Consequently, cPOE1000 diffuses as the same rate as lPOE500, due to the similarity in chain length. In this case, the cyclic polymer acts as a linear chain with an effective chain length half of the size of the linear one and moves into the matrix by following the same dynamics as linear species. However, the fast diffusion of cyclic POE oligomers versus linear chains with comparable molecular weight into PMMA matrix show to be mainly controlled by chain dimensions.

A lot of research could be found in literature on interdiffusion of linear versus star polymers into same polymeric matrix.[24,25] As discussed in Chapter 2, it is well known that branched polymers move slower than linear chains of the same total value of N due to a different diffusion mechanism explained by reptation of stars through arm retraction. The theories[19,24-28] on diffusion of star polymers with g arms, each containing N monomeric units predict that the diffusion coefficient D_{star} scales exponentially with the number of arms and the relationship between a linear polymer and a star one can be expressed as:[25]

$$\frac{D_{star}}{D_l} = g^{0.5}\left[2 - g + 2^{0.5}(g-1)\right]^{-1} \qquad \text{Eq.56}$$

This dependence was experimentally validated for diffusion of three-arm PS stars in high molecular weight linear matrix.[24]

Figure 5.10 shows the log-log plot of $\frac{D_{star}}{D_l}$ calculated by using Eq.56 versus the number of arms corresponding to star polymers having 3,4… to 50 arms. If we assume that a linear polymer has 1 arm, then $\frac{D_{star}}{D_l} = 1$. By considering that a cyclic polymer has "0 arms", we obtain:

$$\frac{D_{cyclic}}{D_l} = 1.6 \qquad \text{Eq.57}$$

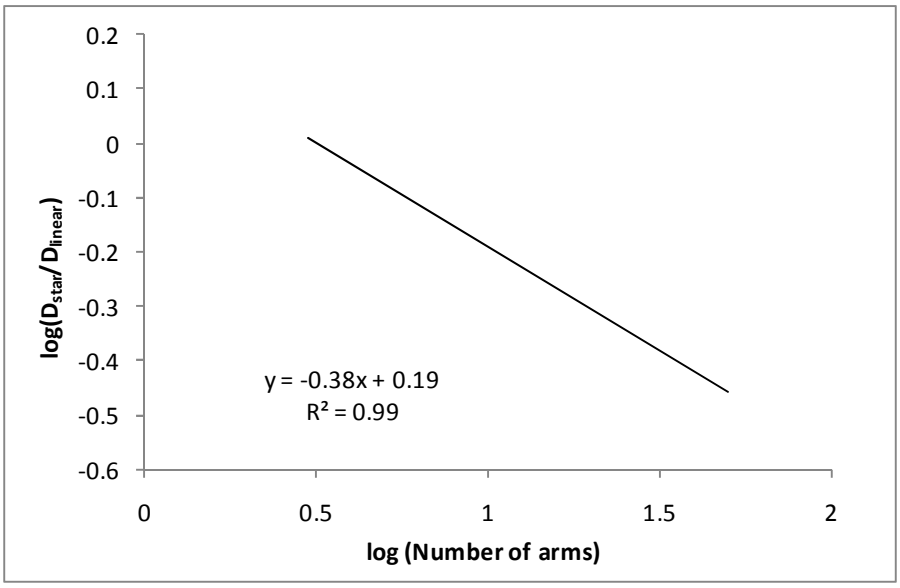

Figure 5.10 - log – log plot of $\frac{D_{cyclic}}{D_l}$ versus the number of arms. The values of $\frac{D_{cyclic}}{D_l}$ corresponding to 3… to 50 arms were calculated by using Eq.56.

Therefore, the prediction of D_{cyclic} using a model derived from star polymers shows that the diffusion of cyclic polymers versus linear corresponding species into a linear matrix is 1.6 times faster. The "star-cyclic" model developed above came in agreement with our studies ($D_{cyclic} \cong 1.8 D_{linear}$) and it might become an appropriate mathematical model if additional factors will be considered for further development.

5.4 REFERENCES

1. Jing, X.; Zhang, S. H.; Runt, J., Broadband dielectric investigation of amorphous poly(methyl metacrylate)/poly(ethylene oxide) blends. *Macromolecules* **2004,** *37*, (21), 8110-8115.

2. Lodge, T. P.; Wood, E.; Haley, J. C., Dynamics of a poly(ethylene oxide) tracer in a poly(methyl methacrylate) matrix: Remarkable decoupling of local and global motions. *Journal of Chemical Physics* **2005,** *122*, (23), 756-763.

3. Gilmore, P. T.; Falabella, R.; Laurence, R. L., Polymer-polymer diffusion - Effect of temperature and molecular weight on macromolecular diffusion in blends of poly(vinyl chloride) and poly(epsilon caprolactone). *Macromolecules* **1980,** *13*, (4), 880-883.

4. Laot, C.; Marand, E.; Oyama, H. T., Spectroscopic characterization of molecular interdiffusion at a poly(vinyl pyrrolidone) vinyl ester interface. *Polymer* **1999,** *40*, (5), 1095-1108.

5. Jabbari, E.; Peppas, N. A., Use of FTIR-ATR to study interdiffusion in poly(styrene) and poly(vinyl methyl ether). *Macromolecules* **1993,** *26*, (9), 2175-2186.

6. Jones, R. A. L.; Klein, J.; Donald, A. M., Mutual diffusion in a miscible polymer blend. *Nature* **1986,** 321, (*6066*), 161-162.

7. Akcasu, A. Z., The "fast" and "slow" mode theories of interdiffusion in polymer mixtures: Resolution of contraversy. *Macromolecular Theory and Simulation* **1997,** 6, (*4*), 679-702.

8. Farinas, K. C.; Doh, L.; Venkatraman, S.; Potts, R. O., Characterization of solute diffusion in a polymer using ATR-FTIR spectroscopy and bulk transport techniques. *Macromolecules* **1994,** *27*, (18), 5220-5222.

9. Fieldson, G. T.; Barbari, T. A., The use of FTIR-ATR spectroscopy to characterize penetrant diffusion in polymers. *Polymer* **1993,** *34*, (6), 1146-1153.

10. Bairamov, D. F.; Chalykh, A. E.; Feldstein, M.; Siegel, R. A., Dissolution and mutual diffusion of poly(N-vinyl pyrrolidone) in short chain poly(ethylene glycol) as observed by optical wedge microinterferometry. *Journal of Applied Polymer Science* **2002,** *85*, (5), 1128-1136.

11. Bucknall, D. G.; Higgins, J. S.; Butler, S. A., Early stages of oligomer-polymer diffusion. *Chemical Engineering Science* **2001,** *56*, (19), 5473-5483.

12. Ye, M.; Composto, R. J.; Stein, R. S., A modified optical schlieren technique for measuring the mutual diffusion coefficient in polymer blends. *Macromolecules* **1990,** *23*, (22), 4830-4834.

13. Shearmur, T. E.; Clough, A. S.; Drew, D. W., Interdiffusion of low molecular weight deuterated polystyrene in poly(methyl methacrylate). *Macromolecules* **1996,** *29*, (22), 7269-7275.

14. Jabbari, E.; Peppas, N. A., Matrix effects on interdiffusion at the polystyrene and poly(vinyl methyl ether) interface. *Macromolecules* **1995,** *28*, (18), 6229-6237.

15. Shearmur, T. E.; Clough, A. S.; Drew, D. W., Interdiffusion of deuterated and protonated poly(methyl methacrylate). *Polymer* **1998,** *39*, (11), 2155-2159.

16. Bairamov, D. F.; Chalykh, A. E.; Feldstein, M.; Siegel, R. A., Impact of molecular weight on miscibility and interdiffusion between poly(N-vinyl pyrrolidone) and poly(ethylene glycol). *Macromolecular Chemistry and Physics* **2002,** *203*, (18), 2674-2685.

17. Nachlis, W. L.; Bendler, J. T.; Kambour, R. P.; MacKnight, W. J., Topological effects on blend miscibility. *Macromolecules* **1995,** 28, (*23*), 7869-7878.

18. Kawaguchi, D.; Masuoka, K.; Takano, A.; Tanaka, K.; Nagamura, T.; Torikai, N.; Dalgliesh, R.; Langridge, S.; Matsushita, Y., Comparison of interdiffusion behavior between cyclic and linear polystyrenes with high molecular weights. *Macromolecules* **2006,** *39*, (16), 5180-5182.

19. Klein, J., Dynamics of entangled linear, branched, and cyclic polymers. *Macromolecules* **1986,** *19*, (1), 105-118.

20. Tead, S. F.; Kramer, E. J.; Hadziioannou, G., Polymer topology and diffusion - A comparison of diffusion in linear and cyclic macromolecules. *Macromolecules* **1992,** *25*, (15), 3942-3947.

21. Crank, J., *The Mathematics of Diffusion, 2nd Ed.* In Oxford University Press: Oxford, U., Ed. **1975**.

22. Nam, S.; Leisen, J.; Breedveld, V., Dynamics of unentangled cyclic and linear poly(oxyethylene) melts. *Polymer* **2008,** *49*, (25), 5467-5473.

23. Nam, S.; Leisen, J.; Breedveld, V.; Beckham, H. W., *Polymer* **2008**.

24. Roovers, J.; Toporowski, P. M., Hydrodynamic studies on model branched polystyrenes. *Journal of Polymer Science - Part B: Polymer Physics* **1980,** *18*, (9), 1907-1917.

25. Sikorski, A.; Romiszowski, P., Motion of star-branched vs. linear polymer: A Monte Carlo study. *Journal of Chemical Physics* **1996,** *104*, (21), 8703-8712.

26. Fetters, L. J.; Lohse, D. J.; Richter, D., Connection between polymer molecular weight, density, chain dimensions, and melt viscoelastic properties. *Macromolecules* **1994,** *27*, (17), 4639-4647.

27. Graessley, W. W., Entangled linear, branched and network polymer systems-molecular theories. *Advances in polymer science* **1982,** *47*, 67-117.

28. Shull, K. R.; Kramer, E. J.; Fetters, L. J., Effect of number of stars on diffusion of star polymers. *Nature* **1990,** *345*, (6278), 790-791.

CHAPTER 6

CONCLUSIONS AND RECOMMENDATIONS FOR FUTURE WORK

6.1 CONCLUSIONS

- (ATR) IR spectroscopy proved to be a powerful technique to investigate the diffusion of low-molecular-weight linear and cyclic poly(oxyethylene) (POE) into entangled poly(methyl methacrylate) (PMMA) at temperatures below and above glass transition temperature of the matrix .
- Linear and cyclic POE diffuse into PMMA by following a non-Fickian diffusion model, which can be explained by a change in mechanism (as penetrant concentration increases in time) due to a decrease in the glass transition temperature of the matrix.
- The values of 0.66 - 1.02 specific to diffusional exponents extracted from the plots of the normalized concentration versus interdiffusion time confirmed the non-Fickian behavior of POE/PMMA interdiffusion explained by the plasticization effect of the matrix.
- It was clear that the POE/PMMA interdiffusion cannot be accurately interpreted by using only one of the two extreme diffusion models, *Fickian* or *Case II*.
- It was proved that the best way to describe the anomalous behavior of these phenomena is by using a combination of the two classical diffusion models.

- The POE moves faster and more Fickian with increasing the temperature from 60°C to 85 °C and 110 °C.
- The equilibrium concentration of cyclic POE into PMMA is 12 ± 2 wt % higher than the linear one.
- An interface velocity, K_{II} = 6.43 ± 1.29 x 10^{-6} cm/s and an interdiffusion coefficient, D_m = 5.11 ± 1.02 x 10^{-11} cm/s^2 describe the diffusion of cyclic POE 400 g/mol into PMMA 120 kg/mol at 110 °C.
- At 110 °C, the linear POE 500 g/mol and cyclic POE 1000 g/mol move into PMMA 120 kg/mol at the same rates of diffusion. An average interface velocity of 3.67 ± 0.73 x 10^{-6} cm/s and an interdiffusion coefficient of 2.86 ± 0.54 x 10^{-11} cm/s^2 describe the diffusion of lPOE500, which are identical within the errors of measurements with the those specific to cPOE1000, K_{II} = 3.36 ± 0.67 x 10^{-6} cm/s and D_m = 2.88 ± 0.57 x 10^{-11} cm/s^2.
    - The results indicated that for the same molecular weight, the cyclic POE moves 1.8 times faster than linear one, which are in reasonable agreement with the limited studies for diffusion of entangled rings into linear matrices.[1,2] Matsushita et al.[1] found that PS rings move 2.2 times faster than the linear one, while Klein[2] predicted a scaling diffusion parameter of 2 ($D_{cyclic} \cong 2D_{linear}$).
    - The cyclic POE acts as a linear chain with an effective chain length half of the size of the linear corresponding one and moves into the matrix by following the same dynamics.

The knowledge gained from this research gives us a deeper understanding of the transport behavior of unentangled polymers into polymer matrices, in particular the influence of topology on diffusion. Such information is expected to be a valuable contribution to applications where migration plays an important role.

6.2 RECOMMENDATIONS FOR FUTURE WORK

- To obtain information related with the influence of matrix molecular weight to the diffusion, further analysis could be done by using a PMMA with a molecular weight that is smaller than its M_e = 10 kg/mol. It can be determined if the diffusion mechanism changes and becomes Fickian.
- Some studies can be done to correlate the self-diffusion with the mutual interdiffusion coefficients.
- Another comparison between linear POE oligomers and cyclic ones diffusing into the same matrix would be by varying the chain ends of the linear species. For example, the interdiffusion of linear poly(oxyethylene)s with hydroxyl chain ends into poly(methyl methacrylate) can be compared with cyclic POE/PMMA.

6.3 REFERENCES

1. Kawaguchi, D.; Masuoka, K.; Takano, A.; Tanaka, K.; Nagamura, T.; Torikai, N.; Dalgliesh, R.; Langridge, S.; Matsushita, Y., Comparison of interdiffusion behavior between cyclic and linear polystyrenes with high molecular weights. *Macromolecules* **2006,** *39*, (16), 5180-5182.

2. Klein, J., Dynamics of entangled linear, branched, and cyclic polymers. *Macromolecules* **1986,** *19*, (1), 105-118.

APPENDIX

ERRORS ANALYSIS

The errors analysis for POE/PMMA interdiffusion studies were done by following Jabbari & Peppas approach.[1] The maximum uncertainty of 20% in the interface velocity, $\varepsilon(K_{II})$, as well as interdiffusion coefficient values, $\varepsilon(D_m)$, includes the following sources of errors:

1. Errors in depth of penetration - $\varepsilon(d_p)$;
2. Errors in the PMMA film thickness - $\varepsilon(d_{PMMA})$;

1. Uncertainty in depth of penetration - $\varepsilon(d_p)$.

As given by Eq.17**,** the penetration depth is a function of the refractive index of the polymer. The errors in the d_p are:

$$\varepsilon(d_p) \approx \frac{\Delta n_2(T)}{n_2} + \frac{\Delta n_2([POE])}{n_2} \qquad \textbf{A.1}$$

where: $\varepsilon(d_p)$ = uncertainty in the penetration depth (d_p); $\Delta n_2(T)$ = uncertainty in the refractive index of polymer as a function of temperature; $\Delta n_2([POE])$ = uncertainty in the refractive index of polymer as a function of POE penetration into PMMA (change in POE concentration). Then the errors in the depth of penetration due to changes in the refractive index of the sample (n_2) are calculated by using the following formula:

$$\varepsilon(d_p) = \frac{\Delta d_p}{d_p} = \frac{1}{\frac{\sin^2 \theta_i}{\left(\frac{n_2}{n_1}\right)^2} - 1} \varepsilon(n_2) \qquad \textbf{A.2}$$

where θ_i is the incident angle of IR beam and n_1 represents the refractive index of the ATR crystal.

It was estimated that the refractive index of PMMA might become smaller than $n_{20}^{D} = 1.492$ with 0.0001 for each ^{o}C difference. Hence, these changes in the refractive index of PMMA might have an influence to d_p, as shown:

110 ^{o}C - $n_{110}^{D} = 1.483$ - d_p decreases with max. 5.5%

85 ^{o}C - $n_{85}^{D} = 1.486$ - d_p decreases with max. 4.5%

60 ^{o}C - $n_{60}^{D} = 1.488$ - d_p decreases with max. 4.0%

The decrease in the refractive index of PMMA as result of POE migration was estimated to be maximum 0.015 at the equilibrium concentration of 47 wt % cyclic POE into PMMA which gives a 4.5 % decrease in d_p. For the linear one, a change in the refractive index of 0.014 at equilibrium concentration of 35 wt % into PMMA might decrease the d_p with maximum 4.5%.

Then, it was estimated a maximum decrease of 5.5 % in the depth of penetration due to changes in the refractive index as a result of temperature changes (see Table A.1).

Table A.1 – Uncertainity in depth of penetration as a result of temperature changes.

Temp	n_2	ε (n_2)	d_p	ε (d_p)
°C		%	μm	%
20	1.492	-	2.02	-
110	1.469	1.5	1.91	5.5
85	1.472	1.4	1.92	4.5
60	1.474	1.2	1.93	4

Also, a maximum decrease of 4.5 % in the depth of penetration was estimated as a result of the changes in the refractive index due to POE diffusing into PMMA (see Table A.2).

Table A.2 – Uncertainity in depth of penetration as a result increase POE concentration in PMMA.

Interdiffusion	n_2	ε (n_2)	d_p	ε (d_p)
		%	μm	%
PMMA120K	1.492	-	2.02	-
POE	1.456	-	-	-
35 wt % lPOE500	1.478	0.9	1.95	4.5
47 wt % cPOE400	1.476	1.1	1.95	4.5

The errors in the values of K_{II} and D_m due to ε(d_p) can be estimated with the following equations:

$$K_{II} \approx d_p \Rightarrow \varepsilon(K_{II}) \approx \varepsilon(d_p) \qquad \textbf{A.3}$$

$$D_m \approx d_p^2 \Rightarrow \varepsilon(D_m) \approx 2\varepsilon(d_p) \qquad \textbf{A.4}$$

Then, by using Equation A.3 and A.4, a maximum uncertainty of 10% in K_{II} and 20% in D_m was estimated.

2. Uncertainty in PMMA film thickness - $\varepsilon(d_{PMMA})$.

A maximum of 10% errors were assigned to film thickness measurements which might contributed to another 10% errors in the values of K_{II}.

All the errors discussed above were estimated to contribute to a relative uncertainty of ~ 20 % reflected in the values of interdiffusion coefficients, D_m and K_{II}.

REFERENCES

1. Jabbari, E.; Peppas, N. A., Use of FTIR-ATR to study interdiffusion in poly(styrene) and poly(vinyl methyl ether). *Macromolecules* **1993,** *26*, (9), 2175-2186.